Norwegian University
of Life Sciences

Master's Thesis 2022 60 ECTS
Faculty of Chemistry, Biotechnology, and Food Science

Effect of different modes of naturalization on expression of barrier-related genes in the murine intestine

Signe Birkeland
Biotechnology –Molecular Biology

Effect of different modes of naturalization on expression of barrier-related genes in the murine intestine

Signe Birkeland

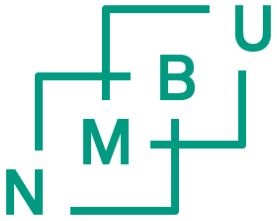

Supervisors

Harald Carlsen

Preben Boysen

Henriette Arnesen

Master's thesis

Faculty of Chemistry, Biotechnology and Food Science

Norwegian University of Life Sciences

May 2022

Effect of different modes of naturalization on expression of barrier-related genes in the murine intestine

https://nmbu.brage.unit.no

ACKNOWLEDGEMENTS

This thesis project was performed during the fall of 2021 to the spring of 2022, at the faculty of Chemistry, Biotechnology and Food Science at the Norwegian University of Life Sciences.

There are several people I would like to thank for a memorable and educational year, and for helping me through this project. I would like to start off by thanking my main supervisor Professor Harald Carlsen for many interesting discussions and all your invaluable feedback. With me being impatient and pessimistic at times, I have really appreciated your patience and never-ending optimism.

Further, I owe a big thanks to my co-supervisor, Dr. Henriette Arnesen, who simultaneously with supervising me finished her PhD and carried a little one to the world. Thank you for everything you have taught me and for being such an inspiration. Further, thank you to my second co-supervisor, Professor Preben Boysen, for being so welcoming and encouraging, and for your enthusiasm for this project.

A warm thank you to Harriet Stendahl for the many hours we spent driving and in the animal lab. I have very much appreciated our conversations and making a new friend. I would also like to thank people at the Immunology Unit at the Faculty of Veterinary Medicine for the help with all things qPCR, and everyone in the Nutrition and Biomedicine research group at the faculty of Chemistry, Biotechnology and Food Science who have lent me some of their time answering my endless questions. Thank you for being so welcoming and making the life of a master's student easier.

Thank you to my family and friends for cheering me on and sharing my excitement for this journey. Lastly, I am forever grateful to Bendik for being my rock.

"I want to tell you a joke about the small intestine, but villi?"

- Anon.

May 2022 – Ås, Norway
Signe Birkeland

ABSTRACT

Background: Non-communicable diseases are frequent in western populations, often characterized by a disturbed intestinal epithelial barrier. The epithelium limits contact between gut microbes and immune cells. A well-known model animal for humans is the house mouse (*Mus musculus*); however, they are housed in strict hygienic conditions far from their natural habitat. Concerns raised about the physiological relevance of lab mouse research gave rise to "naturalized" mice housed in "dirty" environments. The increased microbial exposure led to an immunophenotype more like that of humans.

Aims: We wanted to determine the effect of three different naturalization modes on the murine intestinal epithelial barrier by comparing the expression of barrier- and immune-related genes in intestinal epithelial cells (IECs), evaluate an IEC isolation method, and assess animal welfare and health in naturalized housing.

Methods: Female C57BL/6JRj mice were housed in three different naturalizing pens, containing either feralizing material (farm animal droppings and soil), female wild caught house mice (*M. musculus*), or both. A control group was housed in strictly hygienic animal lab cages. Feces samples were collected, and body weight registered, every two weeks throughout the 10-week experiment. Parasitological analyses were done on fecal samples. Upon euthanization of animals, intestines were dissected out, from which epithelial cells were isolated. The epithelial cell suspension was analyzed by flow cytometry for cell purity assessment. Moreover, RNA was isolated from these cells and analyzed by real-time quantitative polymerase chain reaction to determine relative gene expression levels in epithelial cells using Biomark™ HD from Fluidigm.

Results: The results showed a significant effect of naturalization on relative expression levels of barrier- and immune-related genes in the intestinal epithelium. Differences in expression were both larger, and found in more genes, in cohoused mice compared to lab mice, and in the colon compared to the small intestine (SI). Highest increase was found in genes encoding antimicrobial peptides (colon) and immunosurveillance receptors (SI). Parasite eggs and (oo-)cysts were detected in mice from all three naturalized groups, but especially in wild mice. Feralized mice showed significantly lower body weight development than the other groups. Lastly, immune cell fractions were discovered in the epithelial cell suspensions.

Conclusion: Naturalized housing of mice, particularly wild-mouse cohousing, appeared to positively affect the intestinal barrier, reflected in an increased expression of several barrier- and immune-related genes. The greatest effect was observed in the colon, complying with a larger microbial load. Discovery of parasites strongly vouches for an altered microbiota and may explain the differences observed in some of the genes. However, the relative gene expression levels may have been affected by mRNA from the immune cells discovered in the epithelial cell suspension, and further assessment of IEC isolation should be done in future experiments.

SAMMENDRAG

Bakgrunn: Mange av våre store, ikke-smittsomme sykdommer har høy prevalens i den vestlige verden, ofte preget av en forstyrret tarmepitelbarriere. Epitelet begrenser kontakten mellom tarmmikrober og immunceller. Den mest brukte modellorganismen for mennesker er husmusen (*Mus musculus*), som normalt oppstalles under strenge, hygieniske forhold, langt fra deres naturlige habitat. Det er reist bekymring i hvilken grad en slik ren oppstallingspraksis er relevant i forståelsen av sykdomsutvikling og fysiologi generelt. Denne bekymringen har gitt opphav til å studere "naturaliserte" mus som lever mer i tråd med det miljøet de har utviklet seg i. Tidligere funn viste at denne strategien, med økt mikrobiell eksponering, førte til en immunfenotype mer lik den til mennesker.

Hensikt: Vi ønsket å bestemme effekten av tre ulike naturaliseringsmetoder på tarmbarrieren ved å sammenligne ekspresjonen av barriere- og immunrelaterte gener i tarmepitelceller (IECs), evaluere en IEC-isolasjonsmetode, og vurdere dyrevelferd og helse i naturalisert oppstalling.

Metoder: C57BL/6JRj-hunnmus ble oppstallet i tre ulike naturaliserende binger, som inneholdt enten feraliserende materiale (avføring fra husdyr og jord), viltfangede hunn-husmus (*M. musculus*), eller begge deler. En kontrollgruppe ble plassert i strengt hygieniske bur. Annenhver uke gjennom det 10-ukers lange forsøket ble kroppsvekt registrert og avføringsprøver samlet inn, hvorav det ble gjort parasittologiske analyser. Etter avlivingen av musene ble tarmene dissekert ut, hvorfra IEC-er ble isolert. Epitelcellesuspensjonen ble analysert ved flowcytometri for vurdering av cellerenhet. Videre ble RNA isolert fra disse cellene og analysert ved kvantitativ PCR for å bestemme nivået av relativ genekspresjon i epitelceller ved bruk av Biomark™ HD fra Fluidigm.

Resultater: Resultatene viste en signifikant effekt av naturalisering på relative ekspresjonsnivåer av barriere- og immunrelaterte gener i tarmepitelet. Forskjeller i uttrykk var både større, og funnet i flere gener, hos mus oppstallet med ville mus sammenlignet med labmus, og i tykktarmen sammenlignet med tynntarmen (SI). Høyest økning ble funnet i gener som koder for antimikrobielle peptider (tykktarm) og immunovervåkingsreseptorer (SI). Parasittegg og (oo-)cyster ble påvist i mus fra alle de tre naturaliserte gruppene, men spesielt i ville mus. Feraliserte mus viste signifikant lavere kroppsvektutvikling enn de andre gruppene. Avslutningsvis ble det påvist immuncellefraksjoner i epitelcellesuspensjonene.

Konklusjon: Naturalisert oppstalling av mus, spesielt ved inkludering av villmus, så ut til å positivt påvirke tarmbarrieren, reflektert i økt ekspresjon av flere barriere- og immunrelaterte gener. Den største effekten ble observert i tykktarmen, i samsvar med en større mikrobiell belastning. Oppdagelsen av parasitter støtter antagelsen om en endret mikrobiota og kan forklare forskjellene observert i noen av genene. Imidlertid kan de relative genekspresjonsnivåene ha blitt påvirket av mRNA fra immuncellene oppdaget i epitelcellesuspensjonen, og ytterligere vurdering av IEC-isolasjon bør gjøres i fremtidige eksperimenter.

TABLE OF CONTENTS

LIST OF FIGURES

LIST OF TABLES

ABBREVIATIONS

Ab	Antibody
AhR	Aryl hydrocarbon receptor
AMP	Antimicrobial peptide
ANOVA	Analysis of variance
APC	Antigen precenting cell
B6	C57BL/6
BCR	B cell receptor
beta-ME	Beta-mercaptoethanol
bp	Base pairs
cDNA	Complementary DNA
Cq	Quantitative cycle
CRC	Colorectal cancer
DC	Dendritic cell
DNA	Deoxyribonucleic acid
dNTP	Deoxyribonucleoside triphosphate
dsDNA	Double stranded DNA
dT	Deoxythymine
DTT	Dithiothreitol
E	Efficiency (of primer)
EDTA	Ethylenediaminetetraacetic acid
EEC	Enteroendocrine cell
EtOH	Ethanol
FC	Fold change
FELASA	Federation of European Laboratory Animal Science Associations
FOTS	Forsøksdyrforvatningen tilsyns- og søknadssystem
GALT	Gut-associated lymphoid tissue
gDNA	Genomic DNA
GF	Germ free
GIT	Gastrointestinal tract
GOI	Gene of interest
GTC	Guanidinium thiocyanate
IBD	Inflammatory bowel disease
IC	Intracellular
IEC	Intestinal epithelial cell
IEL	Intraepithelial lymphocyte
IFC	Integrated fluidic circuit
Ig	Immunoglobulin
IgA	Immunoglobulin A
IKK	IκB kinase
IL	Interleukin
ILC	Innate lymphoid cell
ISC	Intestinal stem cell
IVC	Individually ventilated cage
JAM	Junctional adhesion molecule
LI	Large intestine
LP	Lamina propria

LPS	Lipopolysaccharide
M cell	Microfold cell
MAMP	Microbe-associated molecular pattern
MHC	Major histocompatibility complex
MoF	Modes of Feralization
mp	Melt peak
mRNA	messenger RNA
NCD	Noncommunicable disease
NF-κB	Nuclear factor kappa B
NK	Natural killer (cell)
NLR	NOD-like receptor
NMBU	Norwegian University of Life Sciences
NOD	Nucleotide-binding oligomerization domain
NRT	No reverse transcriptase (control)
NTC	No template control
PAMP	Pathogen-associated molecular pattern
PC	Principal component
PCA	Principal component analysis
PRR	Pattern recognizing receptor
qPCR	quantitative polymerase chain reaction
RA	Retinoic acid
REL	Relative expression level
RH	Relative humidity
RIN	RNA integrity number
RNA	Ribonucleic acid
RNS	Reactive nitrogen species
ROS	Reactive oxygen species
rpm	Revolutions per minute
RT	Room temperature
SCFA	Short chain fatty acid
SFB	Segmented filamentous bacteria
SI	Small intestine
sIgA	Secreted immunoglobulin A
SPF	Specific pathogen free
ssDNA	Single stranded DNA
TCR	T cell receptor
Tfh	Follicular helper T cell
TGF-beta	Transforming growth factor beta
Th	Helper T cell
TLR	Toll-like receptor
Tm	Melting temperature
Treg	Regulatory T cell
Trm	Tissue resident memory T cell
Trp	Tryptophan
UiO	University of Oslo
UMN	University of Minnesota

1 INTRODUCTION

1.1 The "big picture"

Humans surround themselves in a vast spectrum of different environments, living in a large variety of geographical areas, with varying diets and hygiene status, in addition to having great genetic variation. Incidences of gut-related noncommunicable (NCD) diseases are increasing, particularly in the western world, including diet-related and autoimmune diseases, allergies, and cancer. Colorectal cancer (CRC) is one of the most common cancer types and one of the leading causes of cancer deaths worldwide (Bray et al., 2018). Inflammatory bowel diseases (IBD, includes Crohn's disease and Ulcerative Colitis) increase the risk of developing CRC, making it even more important to understand the mechanisms behind them. The pathology of chronic inflammatory states of the gut involves disturbances in the gut microbiota and breach of the intestinal barrier (Coleman & Haller, 2021).

1.2 The gastrointestinal tract

The gastrointestinal tract (GIT, Figure 1.1 A) is part of the digestive system through which food and drinks are processed. It stretches from mouth to anus and forms a continuous hollow tube comprising the mouth and throat, esophagus, stomach, small intestine, and large intestine. These segments differ in structure, composition of cell types, and microbial content, all of which is adapted to their function (Barrett, 2014).

1.2.1 Anatomy and physiology of the gut

The intestine is a collective term for the small and large intestines, which are separated from the stomach by the pyloric sphincter. First comes the small intestine (SI), consisting of the duodenum, jejunum, and ileum. The ileocecal sphincter separates the small and large intestines (LI), the latter composed of the ascending, transverse, and descending colon, and the rectum, ending in the internal anal sphincter (Barrett, 2014). The entire GIT is lined by a continuous monolayer of columnar intestinal epithelial cells (IECs) that separates the hollow interior of the intestine, the lumen, from the rest of the body's internal tissues. Thus, the lumen is considered "outside" of the body (Soderholm & Pedicord, 2019). Separated from the epithelium only by a thin basement membrane is the *lamina propria* (LP), consisting of connective tissue in which immune cells, enteric nerves, and blood and lymphatic vessels, are embedded. The lymphatics connected with the gut is referred to as the gut associated lymphoid tissue (GALT) (Mowat & Agace, 2014). Outside the LP is a thin layer of muscle cells (*muscularis mucosae*). This makes up the mucosa layer of the gut wall (Figure 1.1 B). Next comes the submucosa, consisting of connective- and nervous tissue (submucosal plexus), followed by *muscularis propria*, two muscle layers responsible for gut movement and peristalsis. Between them lies the myenteric nerve plexus conveying signals of muscle contraction (Barrett, 2014).

Villi, crypts, and microvilli increase the surface area of the intestinal tract up to 600-fold. A villus is formed by protrusion of IECs into the lumen, while the crypts invaginate in the opposite direction (Figure 1.2). Each IEC has roughly 3000 microvilli on its apical (lumen-facing) surface, that together with the villi and crypts ("crypts of Lieberkühn") allows for efficient nutrient uptake in the SI. The LI has only crypts, as its main functions are water reabsorption and the formation of feces. The IECs form an important barrier to the outside world and is constantly stimulated by the luminal contents, both nutrients and microorganisms (Mowat & Agace, 2014; Volk & Lacy, 2017).

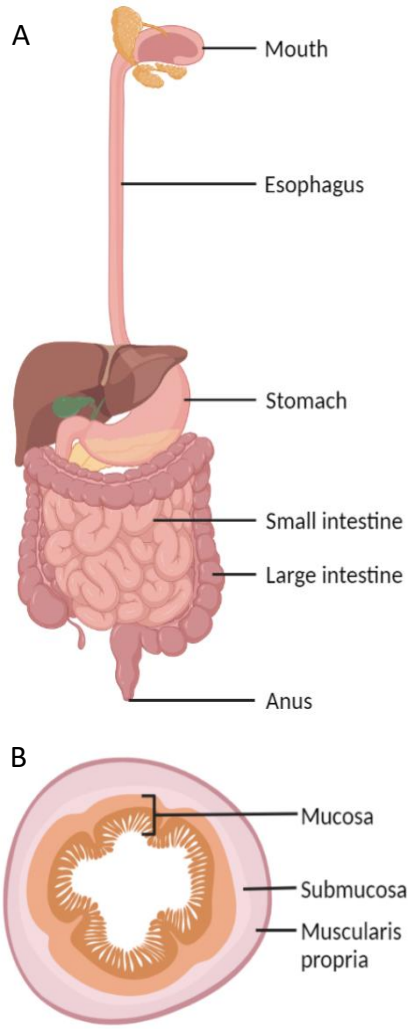

Figure 1.1 - Anatomy of the gastrointestinal tract (GIT). **A**) overview of the GIT, **B**) cross-section of the gut-wall. Created with Biorender.com.

1.2.2 The gut microbiota

In the lumen resides a large microbial population estimated to approximately 40 trillion bacterial cells representing potentially 1000 different species; however, about 150-200 species are estimated to inhabit an average human GIT (Figure 1.2) (Qin et al., 2010; Sender et al., 2016). These bacteria, together with protozoa, fungi, and archaea, make up the gut microbiota. The LI has the highest microbial density of any organ in the body (Allaire et al., 2018; Barrett, 2014; Milani et al., 2017). Most bacteria are commensal organisms, having neutral or beneficial effects on the intestinal tissue. Others are opportunistic pathogens, such as *Escherichia coli*, intruding intestinal tissue if given the opportunity through tissue damage or compositional shifts in the microbiota, for example caused by antibiotic treatments (Allaire et al., 2018; Milani et al., 2017). Demonstrating the symbiosis between the beneficial microbes and the intestinal tissue is when bacteria such as *Bacteroides thetaiotaomicron* in the colon break down non-digestible fibers to short chain fatty acids (SCFA) such as butyrate. Butyrate is the main energy source of colonocytes (Allaire et al., 2018; Barrett, 2014). See section 1.5 for further explanation and more examples.

The colonization of the infant GIT begins at birth, and the gut microbiota composition changes throughout our entire life in response to factors such as delivery mode, genetics, diet, antibiotics, disease, and lifestyle (Avershina et al., 2016; Milani et al., 2017). Although the gut microbiota is subjected to change, most adult humans have developed a stable "normobiota". Interactions between the epithelium, immune cells and microbes are tightly controlled, contributing to the resistance to change of the normobiota. For

example, this involves counteracting compositional shifts caused by "newcomers", because the microbes of the normobiota will compete with them for space and nutrients. Some microbes even produce their own antimicrobial peptide as defense against other microbial species (Allaire et al., 2018).

1.3 The intestinal barrier

The intestinal barrier is essential to confine the gut microbes to the lumen and prevent microbial invasion of internal tissues. It is complex, composed of many different components including the mucus layer(s), cellular junctions tightly connecting the epithelial cells, secretion of antimicrobial peptides (AMPs) and Immunoglobulin A (IgA), innate and adaptive immune cells, and innate microbial receptors such as Toll-like receptors (TLRs) largely expressed by immune cells, and to a lesser degree by IECs (Figure 1.2, section 1.4.1) (Yu & Gao, 2015). Hence, IECs also have important immunological functions themselves. Moreover, intestinal cells produce reactive oxygen species (ROS) and reactive nitrogen species (RNS) that aid in the defense against microbial invasion. The intestinal barrier is part of what is also referred to as "the mucosal immune system", where all the components work together to *prevent* infection. Invasion prevention mechanisms include both active interaction with luminal microbes and preparations for possible microbial encounters by becoming familiar with what resides in the lumen (Parham, 2015).

1.3.1 Epithelial cell types in the gut

At the base of the crypts lie the intestinal stem cells (ISCs) from which seven differentiated intestinal epithelial cell-types emerge (Figure 1.2). While differentiating, they move up towards the tip of the villi in the SI, or the top of the crypt in the LI, and are termed transit amplifying cells. Damage from microbial products and material passing through the gut activates a constant regenerative cycle in IECs (Patankar & Becker, 2020). This *cell turnover* replaces all IECs every 4-5 days (Baulies et al., 2020; van der Flier & Clevers, 2009). A tightly regulated cell death program called anoikis is induced in the dying cell at the villus tip when it is pushed out of the monolayer by the new cells migrating upwards. Anoikis prevents breach of the epithelial barrier because the neighboring cells adhere and form tight junctions with each other from the bottom up in a zipper-like fashion. (Patankar & Becker, 2020). The most common mature IEC is the absorptive enterocyte (colonocyte in the LI), with the main task being absorption of nutrients and water. Residing in the crypt together with the ISCs are the paneth cells, maintaining the correct milieu for the ISCs (the stem cell "niche"), and secretion of AMPs into the lumen (Jasper, 2020; Soderholm & Pedicord, 2019; Volk & Lacy, 2017).

Other important IECs include the enteroendocrine cells (EECs) that secrete digestive hormones, while goblet cells are responsible for the formation of mucus, a gel-like substance consisting of mucin glycoproteins covering the IEC monolayer that protects the gut wall from luminal contents. There is one, relatively loose, layer of mucus in the SI, while the LI additionally has a dense, nearly sterile, inner layer. Less common are the tuft

cells – chemosensory cells involved in parasite defense. Finally, microfold (M) cells overlay Payer's Patches in the SI, or colonic patches/lymphoid follicles in the LI. M-cells are specialized to sample antigens from the lumen and present them to LP-residing immune cells (see section 1.4.2) (Jasper, 2020; Masahata et al., 2014; Soderholm & Pedicord, 2019; Volk & Lacy, 2017).

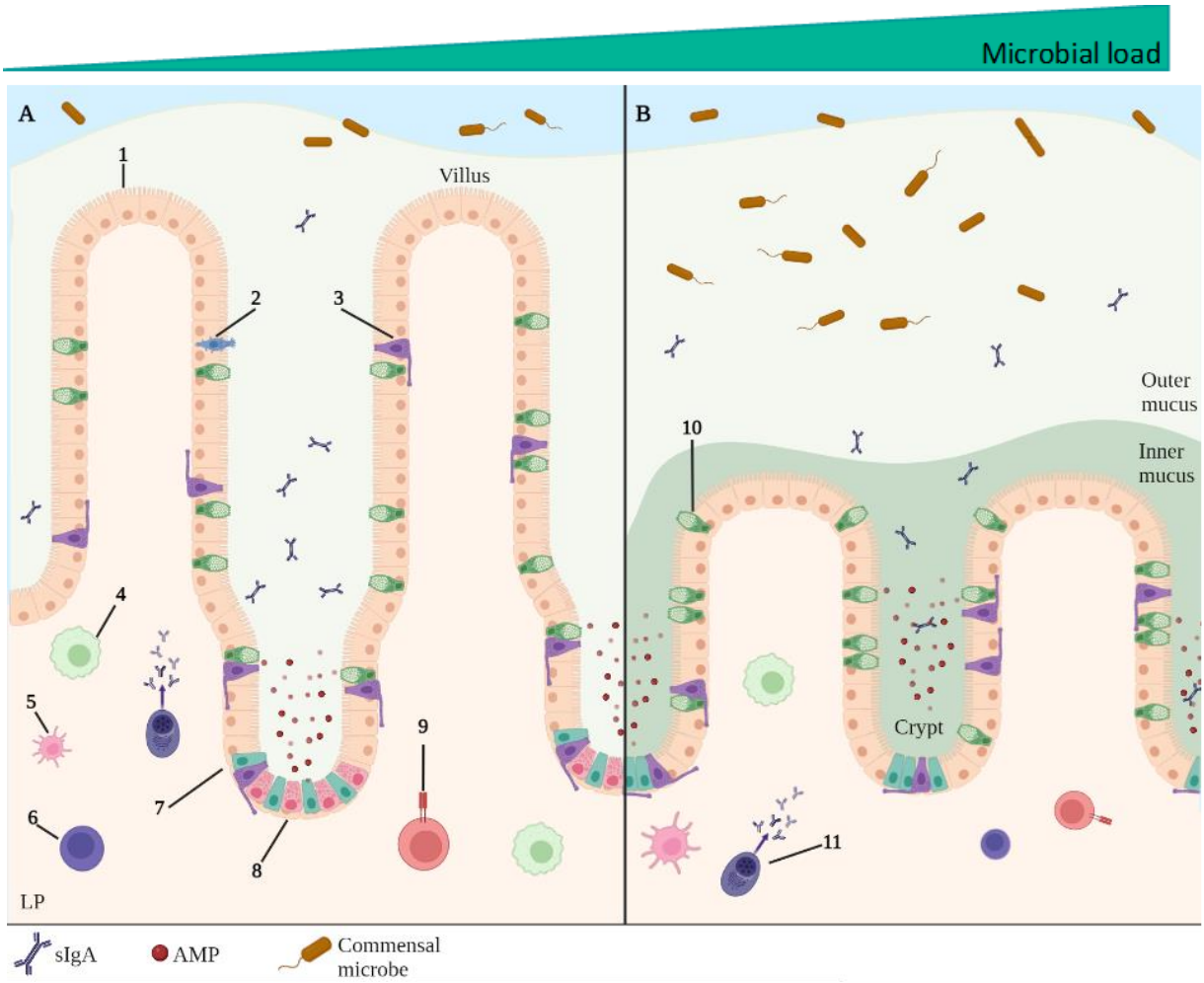

Figure 1.2 - Anatomy of the gut mucosa. **A**) small intestine (SI), **B**) large intestine (LI). 1: enterocyte with microvilli, 2: tuft cell, 3: EEC, 4: macrophage, 5: dendritic cell, 6: B-cell, 7: ISC, 8: paneth cell, 9: T-cell, 10: goblet cell, 11: plasma B-cell. There are two mucus layers in the LI. Also illustrated are the villi, crypts, and LP, as well as AMPs, secreted Immunoglobulin A (sIgA), and commensal microbes. Microbial load increases along the SI and LI in a proximal to distal fashion. Inspired by Allaire et al., 2018. Created with Biorender.com.

1.3.2 The mucus layer

The mucus layer contributes to lubrication of food passing through the GIT, protecting the epithelium against mechanical damage. However, the most important function lies in its ability to restrict microbial access to the epithelium. Mucus structure and composition varies along the length of the GIT, adapted to the requirements of each intestinal segment (Coleman & Haller, 2021). The low density of the small intestinal mucus layer allows for nutrient diffusion, while the inner layer of the LI mucus is dense to keep it (nearly) sterile,

an adaptation to the large microbial load. The thickness allows for filtration of luminal particles by size, keeping large microbial aggregates away (Coleman & Haller, 2021).

Mucus mainly consists of water bound to mucin glycoproteins, and associated proteoglycans, peptides, lipids, and enzymes (Coleman & Haller, 2021). Important mucins include Mucin 2 (Muc2), a secreted glycoprotein that makes up the largest proportion of mucins, and Mucin 3 (Muc3) which is transmembrane and helps anchor the mucus layer to the epithelium. Important mucus-associated proteins are for example IgGFc-binding protein (Fcgbp) and Calcium-activated chloride channel regulator 1 (Clca1) (Allaire et al., 2018; van Putten & Strijbis, 2017). These are suggested as being important for mucus formation and processing/rearrangement (Ehrencrona et al., 2021; Nyström et al., 2019).

Muc2 is produced by goblet cells, secreted as trimeric structures that assemble via disulfide bonds in the endoplasmic reticulum. The structure of Muc2 includes a protein core with mainly O-linked, but also N-linked, glycosylations, with glycosyl chains of galactose, fucose, N-acetylgalactosamine, N-acetylglucosamine, mannose, and sialic acid. The glycosylations make the mucin capable of hydrating and expanding after secretion and is essential for mucus viscosity. Moreover, the pattern of glycosylation varies with the different intestinal regions (Coleman & Haller, 2021). A disrupted mucus layer is associated with gastrointestinal diseases, such as ulcerative-colitis-associated CRC, whose risk increases if mucin glycosylation is impaired (Bergstrom et al., 2016). Moreover, Muc2 deficient mice have been shown to spontaneously develop colitis (Van der Sluis et al., 2006) and CRC (Velcich et al., 2002).

Microbes can attach to the mucins and utilize them as a nutrient source. Thus, the structure and composition of mucus plays a role in the microbial composition. Attachment of commensals is important to hinder pathogens from colonizing, and under normal circumstances the mucus structure and composition is adapted in favor of the normobiota. However, it can be altered in the case of “dysbiosis” (shift in microbial composition away from the normobiota, unfavorable for health and associated with disease states), possibly contributing to pathogenesis. If the inner mucus of the colon is breached, goblet cells at the top of the crypt can secrete large amounts of mucus all at once to try and flush out the invading microbe, and if that does not work the goblet cells residing in the crypt can empty all its stored mucus as a last attempt to keep the intruder at bay (Coleman & Haller, 2021). This massive flush of mucins is signaled via TLR (see section 1.5) (Allaire et al., 2018).

1.3.3 The barrier function of intestinal epithelial cells

A fundamental purpose of IECs, besides nutrient uptake, is to sustain an impenetrable barrier to luminal microorganisms. This is more challenging in the intestines than at other body sites since there is only a single cell layer in the gut that separates the inside of the body from the outside world. It is achieved by elaborate cell-to-cell protein connections, including tight junctions, adherence junctions, gap junctions, and desmosomes. Tight junctions are especially important as they tightly connect the cell membranes of

neighboring IECs to restrict unwanted transport between cells (paracellular transport). Other than small, hydrophobic particles and water, very few molecules are allowed to pass paracellular (Chelakkot et al., 2018). Additionally, tight junctions support formation of cell polarity by limiting specific lipids and proteins to the apical or basolateral surface of the cell. They act as a fence, essential for Na^+-dependent nutrient absorption and other processes in the SI (Otani & Furuse, 2020). The most studied junctional proteins include zonula occludens (such as ZO-1, also known as Tjp1), occludins, claudins, and junctional adhesion molecules (JAMs, e.g., F11r). Occludin and claudin are the membrane integrated tight junction proteins that directly connect the membranes of neighboring cells, while ZO proteins connect occludin and claudin to the cytoskeleton and are important for a strong, integrated barrier structure (Chelakkot et al., 2018). In addition to keeping microbes and other unwanted molecules out of the intercellular space, the junction complexes regulate paracellular flow of fluids and macromolecules. Claudins form small, charge-selective pores, and the flowrate can be adjusted by the number of claudins in the membrane. Studies trying to explain the different models of paracellular passage agree that the junctions are dynamic structures (Otani & Furuse, 2020).

Antimicrobial peptides are secreted from several IECs, but especially from the paneth cells. These include α- and β-defensins, Reg3-proteins such as Reg3γ and -β, and enzymes such as lysozyme (Allaire et al., 2018). Lysozyme kills bacteria by degrading the peptidoglycan in the bacterial cell wall, causing the bacteria to lyse. The Reg3 proteins break down the bacterial cell membrane by forming pores through binding to peptidoglycan and then translocating to the phospholipid bilayer (Mukherjee & Hooper, 2015). α-defensins are restricted to small intestinal expression and disrupt bacterial membranes through pore-formation. β-defensins are expressed both in SI and LI and interrupt the cell wall synthesis in bacteria which leads to lesions and finally lysis of the bacterium (Allaire et al., 2018; Mukherjee & Hooper, 2015). Their secretion is regulated in response to sensing of luminal microbes (Figure 1.3 in section 1.5).

Other barrier-protective responses include production and release of ROS and RNS by epithelial cells. ROS include superoxide ($O_2^{\bullet-}$), hydroxyl radical ($^{\bullet}OH$), hydrogen peroxide (H_2O_2), and hypochlorous acid (HOCl). Two ROS-producing enzymes expressed in the intestinal tract are the NADPH oxidases Nox1 and Duox2, that make superoxide and H_2O_2, respectively. Duox2 is expressed in all intestinal segments but especially in cecum and colon, while Nox1 is mainly expressed in ileum, cecum, and colon. Increased expression of both enzymes is induced by microbial products or inflammatory signaling. RNS are nitric oxide-derived products including peroxynitrite ($ONOO^-$) that forms when NO reacts with $O_2^{\bullet-}$. NO is produced by Nos2/inducible Nos (iNos). ROS and RNS are antimicrobial in that they oxidize lipids and proteins in the membranes of luminal microbes. At constant, high expression levels they cause oxidative stress is which host cells and tissues are damaged, common during inflammation. However, controlled, low, and constitutive expression is necessary for antimicrobial defense (Aviello & Knaus, 2017).

Another protein produced by IECs that interacts with microbes as part of the barrier function includes Lipocalin 2 (Lcn2) (Lu et al., 2019). Lcn2 can directly affect gut microbial composition by inhibiting bacterial growth through inhibition of bacterial iron-uptake and is additionally an established marker of gut inflammation (Singh et al., 2016). It is easily detectable as a protein in feces and has also been correlated with gene expression level in IECs, which are higher in colon than in the SI. Hence, the expression level of Lcn2 indicates the degree of inflammation in the intestinal tissues (Singh et al., 2016). Lcn2 is also an important portion of the toxic components of the neutrophilic granules, which is mostly why its presence increases in feces during inflammation (Eckhardt et al., 2010; Singh et al., 2016).

Serum Amyloid A (Saa) is most known as an acute-phase protein produced by the liver during infection, but isoforms such as Saa1 is also produced in gut epithelium from which it is secreted into the lumen (Eckhardt et al., 2010). Moreover, it has been shown to help activate Th17 cells in response to attachment of segmented filamentous bacteria (SFB) to the epithelium, mainly in ileum (section 1.4.2) (Atarashi et al., 2015; Eckhardt et al., 2010). Hence, it has become of interest in research on antimicrobial defenses and immune stimulation of the gut.

1.4 Immunology in the gut

The immune system's primary responsibility is to protect us from harmful microbes. It is commonly divided in two main categories: the innate and the adaptive immune system. The former is a relatively pre-programmed system that we are born with and is the first responder to an invasion. The innate immune system can react within hours and recognizes general microbial motifs. Hence, it is unspecific to the type of pathogen. The adaptive immune system, on the other hand, is very specific regarding the type of pathogen and the response generally takes several hours up to several days after invasion of a new pathogen, as it is recruited when the innate system is overwhelmed. An important difference between the two is that the cells of the adaptive immune system are known to acquire a memory of previous infections, giving them the ability to react much faster in the event of a secondary infection – also called acquired immunity (Parham, 2015).

The immune response in the gut differs from that in other parts of the body. The default response to microbe invasion is inflammation, working to eliminate the invader. Unfortunately, inflammation also brings collateral damage, involving the killing of host cells and tissue damage. Tissue damage of the single layer of epithelial cells lining the intestinal tract can cause severe invasion by giving more microbes further access to internal tissues via the blood or lymph, leading to systemic infections. Therefore, the default state in the gut is tolerance, involving exclusion and elimination of microbes without inflammatory reactions. As described in section 1.3.3, the IECs themselves play a critical role regarding exclusion, sensing, and control of luminal microbes, but immune cells provide additional protection that becomes especially important when a microbe manages to breach the initial barrier (Parham, 2015).

1.4.1 The role of the innate immune system in the gut

The innate immune system includes all physical barriers such as the skin and the mucus, and innate immune cells such as macrophages, granulocytes, natural killer (NK) cells, and dendritic cells (DCs). Macrophages and neutrophils, a type of granulocyte, eliminate microbes by phagocytosis, killing the bacteria through fusion of phagosomes with lysosomes and other cytotoxic granules. In the intestines, LP-resident macrophages engulf any microbe that manages to pass through the epithelial layer (Parham, 2015). Microbes are generally recognized through special receptors called pattern recognizing receptors (PRR), also widely expressed by IECs. PRRs bind to microbe- and pathogen-associated molecular patterns (MAMPs and PAMPs), conserved molecular structures in both commensal and pathogenic microbes. These are recognized both in the presence and absence of infection, such as MAMPs on commensals in the gut microbiota, and the immune reaction is therefore context dependent (Chu & Mazmanian, 2013; Thaiss et al., 2016). Common PRRs are the membrane-bound Toll-Like Receptors (TLRs) and the cytosolic Nucleotide-binding and Oligomerization Domain (NOD)-Like Receptors (NLRs). Examples of TLR ligands (aka MAMPs) are bacterial lipopolysaccharide (LPS; TLR4), the bacterial protein flagellin (TLR5), bacterial and viral DNA (TLR9), and lipoproteins (TLR2) (Parham, 2015). Another important part of TLR-signaling is how the signal is conveyed throughout the cell, which depends on "adaptor molecules" such as MyD88. MyD88 induces activation of IκB kinase (IKK), an enzyme that phosphorylates IκB, the inhibitory protein of Nuclear Factor kappa B (NF-κB), also known as the "master regulator of inflammation". When NF-κB is released from IκB, it can translocate into the cell nucleus where it binds NF-κB binding sites on promoters of >200 different genes related to inflammation (Alberts et al., 2015; Spehlmann & Eckmann, 2009).

An important distinction between macrophage activation in the gut and elsewhere, is that the intestinal macrophages do not produce the same inflammatory cytokines. Cytokines are signaling molecules inducing specific responses in the target cells and are widely used by all cells of the immune system. They are short-lived and therefore at their highest concentration surrounding the cells that secrete them, confining the immune stimulus relatively locally. Examples of cytokines important in the gut are interleukins (IL) such as IL-1β, IL-10, IL-18, IL-22, and IL-25, and the anti-inflammatory cytokine Transforming Growth Factor beta (TGF-β). Although intestinal macrophages do not secrete many cytokines themselves, their differentiation relies on cytokine signaling from other intestinal cells such as IECs and DCs. IECs can recruit neutrophils and monocytes (blood-circulating macrophage progenitor) through cytokine and chemokine (a type of cytokine that induces "cell movement") signaling in response to binding of MAMPs to PRRs, where the monocytes are induced to differentiate into intestinal macrophage upon entering the LP. Neutrophils are rare in the intestines, but can accumulate quickly during an infection (Parham, 2015). Activation of cytokine production via PRRs such as TLRs happens via NF-κB translocation to nucleus, as explained above. Other important target genes of NF-κB include those encoding AMPs.

Another cell type worth mentioning is the innate lymphoid cells (ILC), grossly divided into three classes (1, 2, and 3). They originate from lymphocytes (see next section), however their effector functions are more like the cells of the innate immune system, quick reacting and relying on cytokine signaling (Saez et al., 2021).

DCs are responsible for monitoring the environment and interact with the immune cells, especially those of the adaptive immune system. Those that reside in the intestine express receptors that bind to chemokines expressed by IECs, particularly those overlaying Peyer's Patches (see next section). These DCs are specialized in secreting IL-10, an anti-inflammatory cytokine, and are responsible for conveying information to the adaptive immune system by leaving the LP through afferent lymph to activate and recruit adaptive immune cells from mesenteric lymphoid nodes (Parham, 2015).

1.4.2 The role of the adaptive immune system in the gut

The adaptive immune system comprises B cells and T cells that recognize specific microbial antigens. An antigen is a part of a microbial component with a specific molecular structure bound by a T cell receptor (TCR) or a B cell receptor (BCR, commonly termed immunoglobulins, Ig). When the BCR is secreted, they are called antibodies (Ab). B cells can express different isotypes of Igs, IgM being the one commonly expressed by naïve B cells that have not yet encountered an antigen. A TCR recognizes antigens that are presented on major histocompatibility complex (MHC) molecules by another cell. There are two classes of MHC molecules expressed by different types of cells: MHC class I that is expressed by all nucleated cells and presents intracellular antigens, while class II is expressed by professional antigen presenting cells (APCs, including DCs, B cells, and macrophages) and present extracellular antigens. T cells with TCRs that bind to MHC class II are called CD4+ helper T (Th) cells, while those binding MHC class I are called CD8+ cytotoxic T cells, and they have different effector functions. When a BCR binds an antigen, it is endocytosed by the B cell so that the antigen can be transferred to an MHC molecule. The binding of a TCR to an antigen-presenting MHC molecule activates the T cell. Hence, B cells can activate CD4+ T cells. Dendritic cells are also major T- and B cell activators. The process of antigen presentation by DCs resembles that of a B cell except that the DCs phagocytose entire extracellular microbes or antigens and further present the antigen on MHC class II to activate a Th cell (Parham, 2015).

There are several subclasses of Th cells: Th1, Th2, Th17, Tfh, and Tregs (regulatory T cell). The Tfh (follicular helper T cell) mainly resides in secondary lymphoid tissue such as mesenteric lymph nodes and are essential for intestinal immunology as they interact with activated B cells and induce them to differentiate into IgA-secreting plasma B cells. IgA is the most abundant type of Ig and are a critical part of the intestinal barrier. IgA produced by LP-residing plasma cells is transported through IECs by transcytosis via the poly-Ig receptor which dimerizes two IgA's to form secreted IgA (sIgA) (Brandtzaeg & Prydz, 1984; Johansen et al., 1999; Parham, 2015). Secreted Abs that bind an antigen can normally recruit other immune cells such as macrophages that can recognize the tail of the Ab (termed the Fc region) through receptor binding, initiating phagocytosis of the

bound microbe and inflammatory responses. However, the main reason sIgA is not inflammatory is that the Fc regions are unavailable when they are in the dimer form. IgA can therefore bind specific microbes and neutralize them, hindering them from tissue invasion and proliferating without inducing an inflammatory reaction. The dimer form also allows for microbe aggregation that makes them more easily flushed away with other luminal contents. Additionally, IgA can bind microbes in the LP and bring them back out into the lumen via the transcytosis mechanism (Parham, 2015).

Further, Tregs are essential anti-inflammatory cells that secrete IL-10, an anti-inflammatory cytokine that suppresses inflammatory responses in other immune cells. They help keep the tolerance state in the intestine, especially important to avoid inflammatory reactions to food- and commensal antigens. Differentiation of a CD4+ Th cell into a Treg is induced by DCs that secrete anti-inflammatory cytokines TGF-β and IL-10 in response to microbial recognition, in addition to secretion of retinoic acid (RA). RA is metabolite of vitamin A (retinol), a critical function of intestinal DCs that seems to form the basis of all DC function mentioned in this section (Agace & Persson, 2012). DC activation is achieved either by stretching an "arm" paracellularly of IECs, sampling luminal contents, or by phagocytosis of microbes/antigens that are transcytosed through M cells. M cells are differentiated IECs overlaying lymphoid follicles called Peyer's Patches in the SI (similar structures are found in the LI). Here, DCs can activate T- and B cells, or travel to mesenteric lymph nodes via the lymph. The site where the adaptive immune cells are presented an antigen is called the induction site, while the site at which they perform their immunological effector function is called the effector site. Specific markers on DCs and IECs help the activated immune cells to return to the site at which the antigen was detected, a process called homing. However, activated immune cells of the mucosa tend to spread throughout the mucosal surfaces, strengthening the defense at all mucosal sites (Parham, 2015).

If intestinal tissue is infected, Th17 cells play an important role in the immune response. Their responses are normally limited by Tregs; however, during infections Tregs can lower their secretion of IL-10. DC secretion of TGF-β and IL-6 (a pro-inflammatory cytokine) induce the differentiation of Th into Th17 (Atarashi et al., 2015; Belkaid & Harrison, 2017). Moreover, Th17 are more prone to become inflammatory from stimulation by certain pathogens than by commensals such as SFBs (Zheng et al., 2020). There are numerous Th17 cells in the gut mucosa, their name derived from their signature cytokine: IL-17, although other important cytokines are secreted by them as well. For example, they secrete IL-22 which induces AMP secretion by IECs. They are also known to help neutrophils respond to invading bacteria and fungi, important for clearance of infection (Atarashi et al., 2015). Microbial sensing by macrophages can induce secretion of IL-1β which stimulates accumulation of Th17 cells. However, this also stimulates other immune cells such as the DCs to produce IL-10, limiting inflammatory responses induced by Th17 in a negative-feedback fashion (Belkaid & Harrison, 2017). Secretion of TGF-β together with inflammatory cytokines promotes CD4+ T cell towards Th17

differentiation, while TGF-β alone induces differentiation into Tregs. An imbalance in the ratio of Th17/Treg is commonly found in IBD patients (Yan et al., 2020).

Th1 and Th2 are also important in responses to infection, and the cytokine environment in the LP determines the differentiation of a Th cell into either one. Th1 responses are commonly against intracellular bacterial and viral infections, while the Th2 response is specialized against helminths. IL-3, -9, and -5 secretion by Th2 cells recruit eosinophils (another granulocyte) and mast cells (also derived from a granulocyte progenitor) that bind the parasite-directed IgE (produced by B cells activated during parasite infection). Binding to IgE activates their effector functions that involve degranulation of cytotoxic granules to injure the parasite and induce cellular and muscular responses to help flush the parasite out of the intestines. An interesting aspect of Th2-mediated responses is that it is also the driver of allergic reactions, and it has been suggested that it is the lack of parasite exposure in the developed world that has driven Th2 immunology to induce allergies (Parham, 2015). Research related to allergies and the "hygiene hypothesis" (section 1.6) often bring up shifts in the "balance" between Th1 and Th2 mediated responses as a factor affecting the risk of allergy development. However, it is likely affected by the combination of both microbial composition, infections by pathogens, and the general balance of all Th cells (Parham, 2015; Scudellari, 2017).

Cytotoxic CD8+ T cells are commonly found as intra epithelial lymphocytes (IELs), involving them lying within the epithelial monolayer between IECs, approximately at every 7-10 IEC (Parham, 2015). Generally, CD8+ T cells in homeostatic environment in the intestine are driven into a memory-cell state, e.g., through stimulation by SCFAs (Zheng et al., 2020). Memory cells have previously been activated by an antigen, differentiated further to keep a repertoire of specific receptors in case of a secondary infection. Normally, these are stored in lymphoid follicles (Parham, 2015). However, tissue resident memory T cells (Trm) have recently become a great interest in research on adaptive immunity in the gut (Nguyen et al., 2019).

1.5 Communication between gut microbes, IECs and immune cells

The following examples further elaborate the forementioned interaction between IECs and the gut microbes and other important barrier-related interactions. Generally, microbial antigens/MAMPs are sensed through PRRs (section 1.4.1), inducing responses such as increased mucus and AMP production (Eshleman & Alenghat, 2021). Expression of the AMP Reg3γ depends on induction by flagellin or LPS (MAMPs) through TLR-MYD88 signaling pathway together with cytokine signaling (IL-22) from ILCs (Figure 1.3 A) (Mukherjee & Hooper, 2015). ILCs secrete IL-22 in response to several signals such as microbial metabolites of the amino acid Tryptophan (Trp). Trp is provided through the diet and can be metabolized by gut microbes into ligands of the Aryl hydrocarbon receptor (AhR; Figure 1.3 B). In immune cells, the binding of AhR-ligands to AhR can induce secretion of IL-22, further contributing to an enhanced intestinal barrier, e.g., through upregulation of Reg3γ-expression (Agus et al., 2018).

As mentioned in section 1.2.2, important microbial metabolites include SCFAs. Butyrate generated by microbes such as Clostridia is taken up by colonocytes and subsequently processed through β-oxidation (Figure 1.3 C). In response, colonocytes restrict luminal oxygen, creating an environment supporting anaerobic microbes (Allaire et al., 2018).

Lastly, an important goblet cell response mentioned in section 1.3.2, is the massive flush of mucin in response to invading microbes. TLR binding of PAMP signals via MyD88 leads to activation of the pro-inflammatory inflammasome NLR Family Pyrin Domain Containing 6 (Nlrp6). Nlrp6 activation allows for activation of caspase-1, an enzyme that cleaves the pro-forms of inflammatory cytokines Il-18 and Il-1b, as well as pyroptosis-inducing Gasdermin D (Gsdmd). Pyroptosis is cell death induced by inflammation, important for the shedding of cells infected with intracellular pathogens. Additionally, Nlrp6 promotes signaling to neighboring goblet cells via Ca^{2+} that diffuses through gap junctions to secrete mucins (Allaire et al., 2018). Hence, a mass-activation of mucin secretion is conveyed throughout the epithelial layer.

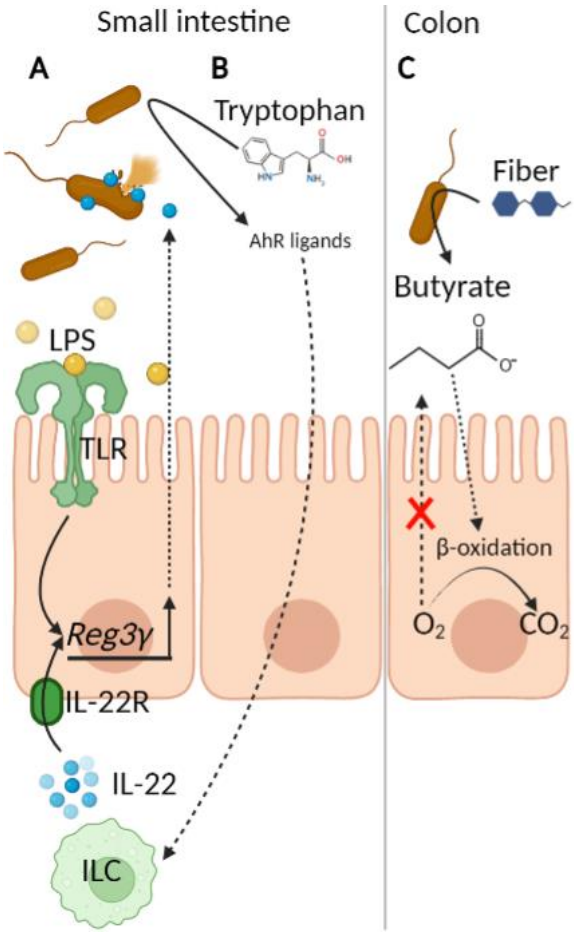

Figure 1.3 - IEC and microbiota interactions. **A**) induction of AMP expression through TLR signaling in SI, **B**) same as A, but through microbial metabolites of tryptophan, **C**) luminal O_2 restriction in response to metabolism of microbial metabolite butyrate in colon. ILC: innate lymphoid cell, LPS: lipopolysaccharide, TLR: Toll-like receptor, AhR: Aryl hydrocarbon receptor, IL: interleukin. Inspired by (Agus et al., 2018; Allaire et al., 2018; Mukherjee & Hooper, 2015). Created with Biorender.com.

1.6 The "hygiene hypothesis"

Observations made by Strachan of a decreased risk of developing hay fever or eczema in children that grew up in larger families led to the development of the "hygiene hypothesis", introduced in the late 1980's (Strachan, 1989). This hypothesis was therefore originally interpreted as a general lack of microbial exposure leading to an increased risk of allergy development. Since then, it has been further claimed that better hygiene and more use of antibiotics which has decreased the rates of infections has left the immune system unchallenged, causing it to be less capable of distinguishing pathogenic from nonpathogenic antigens (Parham, 2015; Scudellari, 2017). However, alternative explanations have been proposed, such as the "old friend hypothesis" by Rook and Brunet, stating that the increase in NCDs such as IBD and allergies are more likely due to the lack of exposure to "old friends"; microbes with whom humans originally have

coevolved with that help sustain a symbiotic and homeostatic state in the intestine and immune system, and not necessarily the general increase in "cleanliness" itself (Rook, 2005; Rook et al., 2014; Scudellari, 2017). Interesting studies have emerged from these hypotheses, investigating the relationship between NCDs and different sources of microbial exposure. Jakobsson and coworkers showed a decrease in Th1-inducing cytokines in children born by C-section, compared with those born vaginally (Jakobsson et al., 2014). This favors a shift towards a Th2-response and supports the idea proposed by the "hygiene hypothesis", because children born by C-section are not exposed to the rich microbiota in vaginal and fecal secretes, and Th2-responses are what drive allergies. However, studies such as one by Yazdanbahsh, Kremsner and van Ree show that people from developing countries have *increased* Th2 responses caused by more helminth-infections, but an overall *lower* risk of allergies (Yazdanbakhsh et al., 2002). Moreover, studies on large cohorts of individuals living off farming and agriculture display a decreased risk of cancer development, including cancers of the lung and CRC (Kayo et al., 2021; Tual et al., 2017). Generally, the consensus is that a more diverse (or "friendly") microbiota seems to stimulate immune system development and training, and it is likely that a combination of many factors such as birth mode, geography, diet, and antibiotics use contribute to which direction the immune response is shaped (Scudellari, 2017).

1.7 The mouse as a model of human biology

The house mouse (*Mus musculus*) has been a good model of human biology for decades. The C57BL/6 (B6) mice have ancestors dating back 150 generations (early 1900's). The inbred mouse strains provide a stable genetic background, which eliminates the genetic factor when investigating the effect of an experimental treatment (Hugenholtz & de Vos, 2018). Other advantages are their short gestation period (approximately 20 days), small size, and easy husbandry (Peters et al., 2007). Also, the genome is >90% conserved between humans and mice, but it is important to keep in mind the difference in regulation of gene expression. Especially regarding the immune system this can become an obstacle for transferring results of mouse studies to humans (Hamilton et al., 2020). Another important note is that research on mice cannot be directly translated to humans, but it allows for speculations and formation of hypotheses about human biology.

Mouse studies are often performed on Specific Pathogen Free (SPF) mice, meaning they have been systematically tested, and found free of, specific pathogens defined by the Federation of European Laboratory Animal Science Associations (FELASA, (Mähler et al., 2014)). They differ from germ free (GF) mice, which are completely free of microbes. The advantage of using SPF or GF mice is the opportunity they provide for reductionist studies by minimizing possible influencing factors. This is especially true of research on immunology and the intestinal system, as well as related diseases, which are largely affected by the intestinal microbiota. However, lab mice are derived from a small selection of wild house mouse subspecies, mainly *M. m. musculus*, *M. m. castaneus* and *M. m. domesticus* (Phifer-Rixey & Nachman, 2015). These are adapted to living around humans, such as on farms and in houses. Hence, the genetic background of the lab mice of today is

adapted to the natural habitat of the house mouse while they are housed in ultra clean facilities. It is therefore a highly debated topic today, whether experimental results derived from highly hygienic lab mice are realistic to what actually happens in nature (Arnesen et al., 2021a; Arnesen et al., 2021b; Beura et al., 2016; Fiege et al., 2021; Graham, 2021; Hamilton et al., 2020; Hild et al., 2021; Rosshart et al., 2017; Rosshart et al., 2019).

1.8 Modes of naturalization

The immune system of clean laboratory mice has been shown to be underdeveloped compared to an adult human and resembles more that of an infant's (Beura et al., 2016). Therefore, and as Fiege and coworkers revealed, conclusions gained from mouse studies might be challenging to generalize to adult humans (Fiege et al., 2021). They assessed the response to influenza vaccines in SPF and "dirty" mice (B6 mice cohoused with common pet store mice) and compared them to the response in humans. Responses in dirty mice resembled more that of humans than the responses in SPF mice did. This exemplifies the importance of researching "dirty" mice, especially in the immunology field. A "naturalization" model where lab mice were cohoused with (dirty) pet store mice was also demonstrated by Beura et al., where cohoused B6 lab mice showed levels of antigen-experienced memory T cells similar to those of adult humans, while SPF lab mice were more similar to newborn humans in that regard. Pet store and cohoused mice additionally cleared infection with *Listeria monocytogenes* at the same rate as *L. monocytogenes*-vaccinated SPF B6 mice, illustrating an important increase in resistance to infection. They argued that the cohousing model could become an important tool for modelling humans, with emphasis on immunological responses (Beura et al., 2016).

Other studies exploring effects of naturalizing mouse models are two by Rosshart and coworkers, one where SPF lab mouse embryos were transferred to surrogate wild house mice, giving birth to so called "wildling" mice (Rosshart et al., 2019), another where pregnant GF mice were given fecal transplants from wild mice for engraftment of a wild microbiome (Rosshart et al., 2017). The wildling microbiome resembled that of wild mice and was stable over time. In addition, they challenged the wildlings with treatments targeting innate and adaptive immune responses were lab mouse and human trials had previously failed to give similar outcomes. Wildlings responded similarly to the human trials, and they therefore argued that the wildlings could be better suited for research aiming at translating results to humans. The engrafted mice and their offspring were challenged with an Influenza virus infection, where 92% of the naturalized mice survived in contrast to the 17% survival of lab mice. Moreover, naturalized mice were protected against colitis-induced CRC in that they displayed a much lower invasiveness than the lab mice.

Further, "rewilding" models such as those by (Leung et al., 2018; Lin et al., 2020) involved housing lab mice in large, outdoor enclosures, which affected the gut microbiota and shifted immune responses towards Th1. Lastly, Arnesen et al. presented a model called "feralization" (Arnesen et al., 2021b), a middle ground between outdoor and indoor housing of laboratory mice where they are exposed to a farmyard-like environment in

large indoor “pens” together with wild mice. In this case, factors such as light, temperature, and humidity could be controlled for. The microbiota of the cohoused mice shifted towards that of the wild mice, and indications of antigen experienced immune cells were found. Moreover, a study using a mode of feralization that only included farmyard-material (without wild mice) protected lab mice against CRC (Arnesen et al., 2021a). This last definition of feralization is used further in this thesis.

2 AIMS

Studies on naturalized mice have shown that exposure to a "dirty" environment contributes to development of immune phenotypes characterized by greater antigen experience, improved immune responses to stimuli, and protection against CRC development. Different feralization experiments have been conducted either in the presence or absence of wild mice, and other experiments have exposed the lab mice to wild mice only (cohousing). We wanted to investigate whether microbial enrichment from farmyard material and wild mice contribute differentially to the altered immune phenotypes observed in these studies, with emphasis on examining gene expression in IECs isolated from the SI and colon of mice.

To optimally answer this question, the results of several housing scenarios should be compared by arranging them within a single, controlled, and randomized experiment. This is the main goal of the Modes of Feralization (MoF) project, which is a collaboration between NMBU, UiO (University of Oslo) and UMN (University of Minnesota). The overall aim of this project is to assess whether, and how, immune phenotypes and functions in laboratory mice are affected by different modes of naturalization, by creating several distinct, comparable environments that provide the mice with various loads and sources of microbes.

This thesis encompasses a sub-project of MoF with the purpose to investigate how various naturalization scenarios influence the murine intestinal barrier. We herein hypothesized that the different environments would have distinguishable effects on the murine intestinal barrier, reflected in differential expression of barrier- and immune related genes in IECs. We also expected differences between the colon and the small intestine due to their different physiological functions, anatomy, and microbial load. For the gene expression analysis to reliably represent the true condition in the IECs, it was necessary for the cell isolate to be as pure as possible. Hence, we also wanted to evaluate how well an already established cell isolation method succeeded in retrieving a pure IEC suspension. Additionally, it was important to monitor animal welfare and health, as disease states and stress can greatly affect the animals' general inflammatory state and possibly the gene expression in the IECs.

To summarize the specific objectives:

I. Evaluate any effect of different mouse naturalization modes on animal welfare and health, particularly regarding cohousing with wild house mice.
II. Evaluate an established method for isolating IECs and live LP immune cells from mouse intestines.
III. Determine if, and how, the murine intestinal barrier in the colon and SI is affected by different modes of naturalization, reflected in gene expression analysis of a panel of barrier- and immune-related genes in IECs.

3 MATERIALS AND METHODS

3.1 Experimental setup

96 female C57BL/6JRj (B6) mice were purchased from Janvier (Janvier Labs, Le Genest-Saint-Isle, France), three weeks old at arrival. Four experimental groups of 24 mice each were included in this experiment. One group (Lab) was housed in clean laboratory cages as controls, while the remaining three groups were housed in "mouse pens" (see section 3.2). One pen contained farm material for housing the feralized mouse group (Fer), the second pen contained clean bedding, i.e. no farm material, but included three female wild mice for the cohousing mouse group (Co), while the last pen contained both farm material and three female wild mice for the feralized+cohoused mouse group (Fer-Co) (Figure 3.1). Mice were euthanized and tissues sampled after 5 and 10 weeks of differential housing. This thesis includes analyses of samples from the second termination (week 10).

For a parallel experiment, additional mice were purchased and housed together with the mice in this experiment, giving a total of 36 B6 mice in Fer- and Fer-Co pens. To identify individual mice during the study, all mice were microchipped at trial start (week 0).

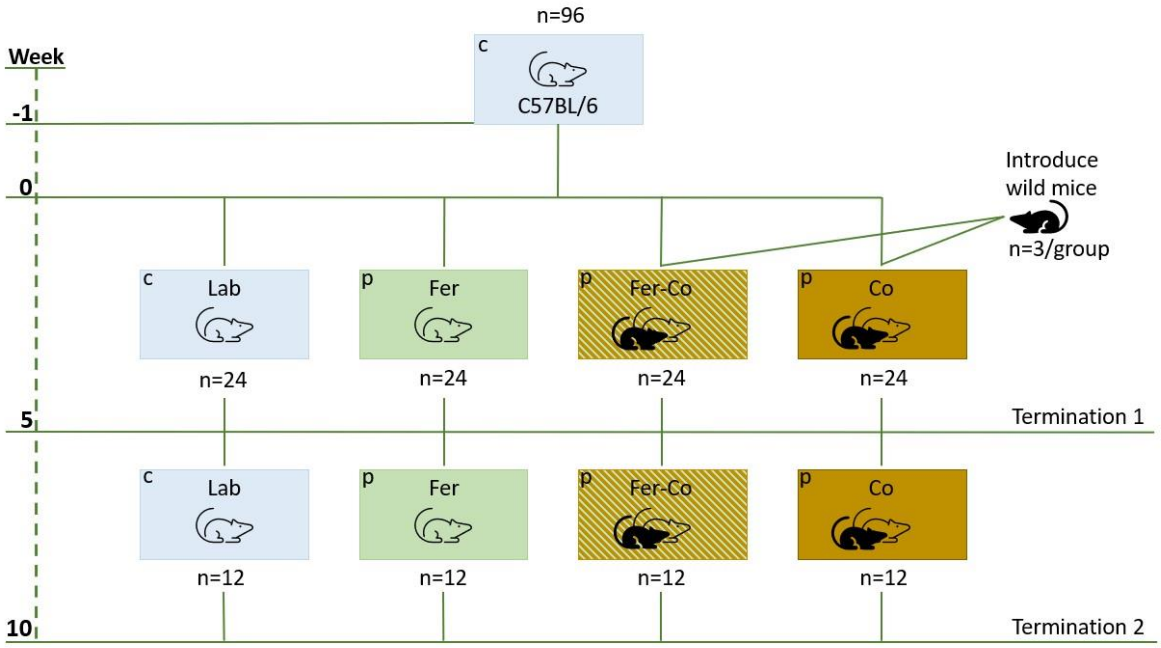

Figure 3.1 - Experimental setup. The figure shows the timeline of the experiment, illustrating division into the four experimental groups, introduction of wild mice to groups Fer-Co and Co, and the two terminations. Mice were housed in either c=cage, or p=pen. There were 24 mice in each group, and an additional three wild mice in each cohousing pen. Lab=control, Fer=feralized, Fer-Co=feralized + cohoused, Co=cohoused.

Ethical aspect

Use of all mice was approved by the Norwegian Food Safety Authority (FOTS application ID: 27618), and the capture of wild mice was approved by the Norwegian Environment Agency (Ref. 2021/7274). Guidelines, terms and conditions for handling and care of mice determined by the EU-commission was followed during all handling of mice throughout the experiment. All animals were checked and evaluated daily, and provided with food, water, and new cages, when necessary.

3.2 Animals and housing

Upon arrival, mice were randomly assigned to individually ventilated cages (IVCs; Innovive Inc., San Diego, CA) and acclimatized for one week with a maximum of five mice per cage. All animal housing included the following conditions: 25 to 27°C ambient temperature, 40 to 60% relative humidity, and 12-hour light/dark cycle. Standard rodent chow diet (RM1 (E), SDS; Special Diet Services, Witham, UK) and tap water were both given *ad libitum*. During acclimatization, all mice were kept in the clean animal laboratory facility at KBM, NMBU. Mice purchased from Janvier were SPF upon arrival. Housing at the KBM animal facility is not strictly SPF but considered *conventional* pathogen free due to strict rules of access to animal rooms, high hygienic standards, and low risk of contamination. The control mice were housed in IVCs in the clean animal lab throughout the experiment.

The experimental mouse pens used for conducting the experiment are illustrated in Figure 3.2, and were constructed as previously described (Arnesen et al., 2021a). Briefly, they consisted of steel plates with the dimensions 2.40 m x 1.10 m x 1.20 m (LxWxH), built in their own "pen room" with restricted access. In the current experiment, all pens were provided with a 10 cm layer of aspen woodchips (Scanbur, Nittedal, Norway) covering the steel floor of, running wheels, red mouse igloos, black plastic tubes and boxes for hiding/nesting, and a pallet for personnel to step on to protect the mice when entering the pens. Two out of three pens intended for feralization were additionally supplemented with organic plant soil (Plantasjen, Norway), straw and farm animal droppings (pig, poultry, cow, and sheep) collected at an organic farm in Eastern Norway (Ramme gård, Vestby, Norway). Fresh farm material from the same farm was added to the two pens every second week throughout the experiment to simulate the natural situation and sustain the environmental microbial load of a farmyard environment.

All equipment and material used for housing of mice is listed in *Appendix A – Equipment and instruments*.

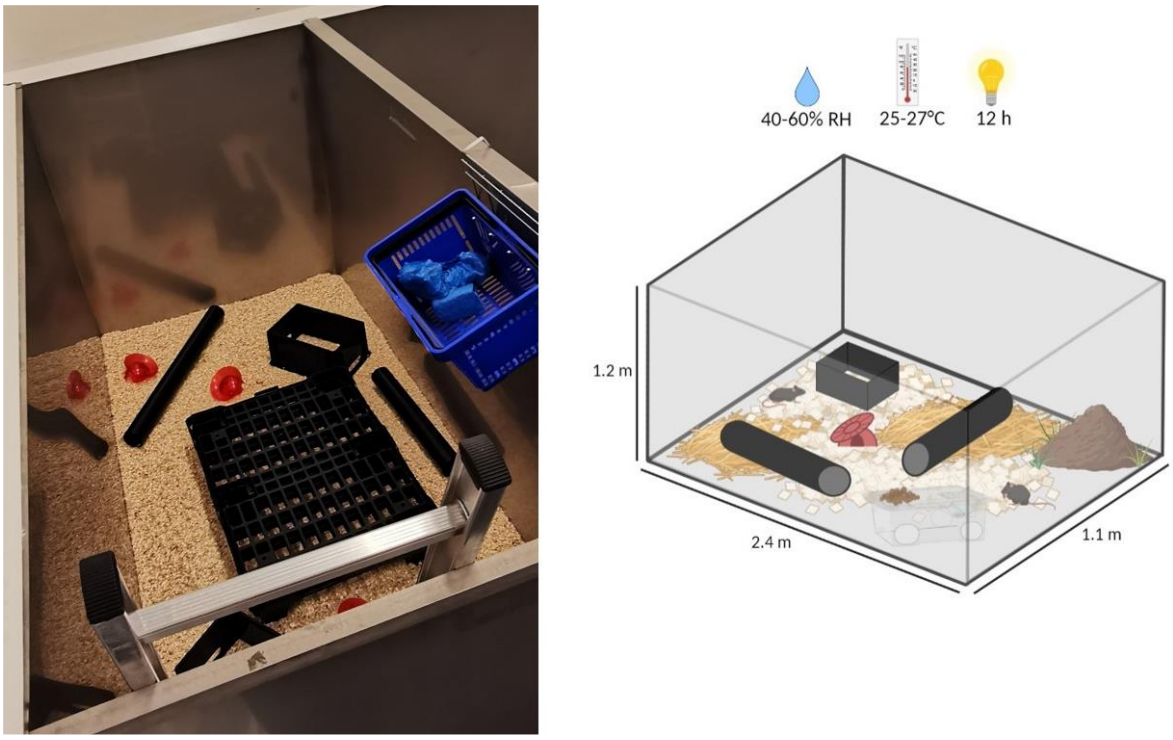

Figure 3.2 - Housing conditions for pen-mice. Picture **A** shows a "clean" pen including a stepping-pallet. Running wheels and igloos in red. Figure **B** illustrates the dimensions and conditions in the pens, including an illustration of the feeding/drinking station not shown in A (three per pen). RH=relative humidity. Created with Biorender.com.

3.3 Catching wild house mice (*Mus musculus*)

To catch wild house mice, local mills and farmers with barns or farm animals were visited after confirming recent mouse-sightings, coinciding with the time of the year when wild mice begin to seek indoor due to colder weather. Over a four-week period prior to the start of the experiment humane live traps (Ugglan Special No 1 live traps; Grahnab, Gnosjö, Sweden) were distributed at nine separate locations around Eastern Norway. The traps were placed strategically in places with food sources (grain or animal feed), fresh mouse feces, or cracks and holes that are typical mouse passages. Mice prefer to move along walls, so the traps were placed accordingly. The traps work by placing bait in one end that is only accessible through a trap door. It opens when the animal steps on it, closes behind them, and cannot open from the inside (Figure 3.3). The bait included peanut butter, liver pâté, RM1 pellets, and grapes (to provide fluids), and woodchips (for isolation). Traps were checked within 24 hours after placement.

Figure 3.3 - Live trap. Granhab AB Ugglan special live trap. Top: without lid, bottom: with lid. Picture borrowed from (De Pelsmaeker et al., 2020).

The wild house mouse looks almost identical to a B6 mouse aside from its light brown-grayish fur color and white belly (Frafjord, 2021a). The wood mouse (*Apodemus sylvaticus*) resembles the house mouse but with larger eyes and ears and a two-colored tail (Frafjord, 2021b), making these mouse species distinguishable from each other. The type of mouse species caught in the live traps were determined based on these characteristics. As the wood mouse was not the correct species intended for this experiment, any wood mice caught in the traps were humanely euthanized by neck dislocation shortly after being caught.

To avoid mating with the female B6 mice, only female wild mice were co-housed with the female B6 mice. Male wild mice were kept in separate laboratory cages in the pen room to use their cage contents (woodchips + feces) for enrichment of the cohousing pens with additional wild mouse material. The contents were homogenized and distributed equally between the two pens every two weeks throughout the experiment. All wild mice were euthanized by neck dislocation in conjunction with termination of the experiment (section 3.5), except from the three female wild mice in the Fer-Co mouse pen, as they were part of the forementioned parallel experiment.

3.4 Weight registration, sampling of feces, parasitology, and animal welfare

Every two weeks throughout the experiment all mice were weighed, and feces samples collected. This regular interaction with all mice allowed for a continuous informal assessment of animal welfare and health, as animals that were obviously discontented or showed pathological symptoms could be noticed. Additionally, all pens were assessed daily in conjunction with the regular daily checkup of all animals at KBM. A common health-indicator in mice is their fur quality, which should be glossy and groomed (FELASA,

2015; Fentener Van Vlissingen et al., 2015). Some feces samples were sent to the Parasitology Group at the Faculty of Veterinary Medicine at NMBU for examination of endoparasites by sucrose floatation test, and immunofluorescence antibody test (IFAT) to examine for *Giardia* cysts and *Cryptosporidium* oocysts. Analyses were conducted on either individual samples or pooled samples from 2-3 individual mice, including samples from all four experimental groups and some of the wild house mice.

3.5 Termination of the experiment

At each termination, 12 mice from every experimental group were euthanized and their tissues and blood sampled, distributed over four days. To avoid sampling bias, two to three mice from each experimental group were euthanized per day. Tissues that were collected included small and large intestine, caecum, spleen, mesenteric lymph nodes, lung, tail tip, blood, and liver. For this thesis, only SI and LI is described further. SI included duodenum, jejunum and ileum, and LI included colon and rectum (hereafter only referred to as "colon"). All reagents, kits, and solutions used throughout the experiment are listed in *Appendix B – Chemicals and reagents*, and all instruments and software in *Appendix A – Equipment and instruments* and *Appendix C – Software and websites*.

3.5.1 Sampling of intestinal tissues

Mice were weighed and feces samples collected prior to anesthesia with a cocktail containing zolazepam, rompun, and fentanyl (ZRF, injected intraperitoneal 10 µL/g mouse) followed by heart puncture for blood sampling and preparation of EDTA-plasma. Mice were euthanized by neck dislocation before further tissue sampling. Next, they were fixated on a clean surface where skin and underlying muscle on the ventral side was removed using scissors and forceps, before intestines were dissected out aseptically. The intestines were placed on a clean, disinfected and RNase-zap-treated cold plate with PBS where 2 cm of ileum and 2 cm of mid colon was collected for other purposes. PBS was quickly replaced by cold cRPMI, and intestines flushed with cold PBS to clear out luminal contents. Visible Peyer's Patches (on SI) and fat was removed before the intestines were cut open longitudinally. Finally, the processed intestines were added to a tube with cold cRPMI and kept on ice until further processing, as keeping everything cold was imperative to avoid cell death and RNA degradation (Peirson & Butler, 2007). cRPMI contained broad spectrum antibiotics to avoid microbial contamination, cell stimuli, and inhibit bacterial LPS, as well as fetal bovine serum (FBS, 2%) nourishing the cells.

3.5.2 IEC isolation

Small intestine and colon were handled as separate samples. The purpose of the isolation procedure was to retrieve a pure epithelial cell pellet and was based on a protocol by Goodyear et al. (Goodyear et al., 2014). This protocol was optimized for isolation of immune cells from the lamina propria, discarding the epithelial cells. Therefore, the protocol used in the current experiment was adjusted to keep the epithelial cell fraction (Figure 3.4).

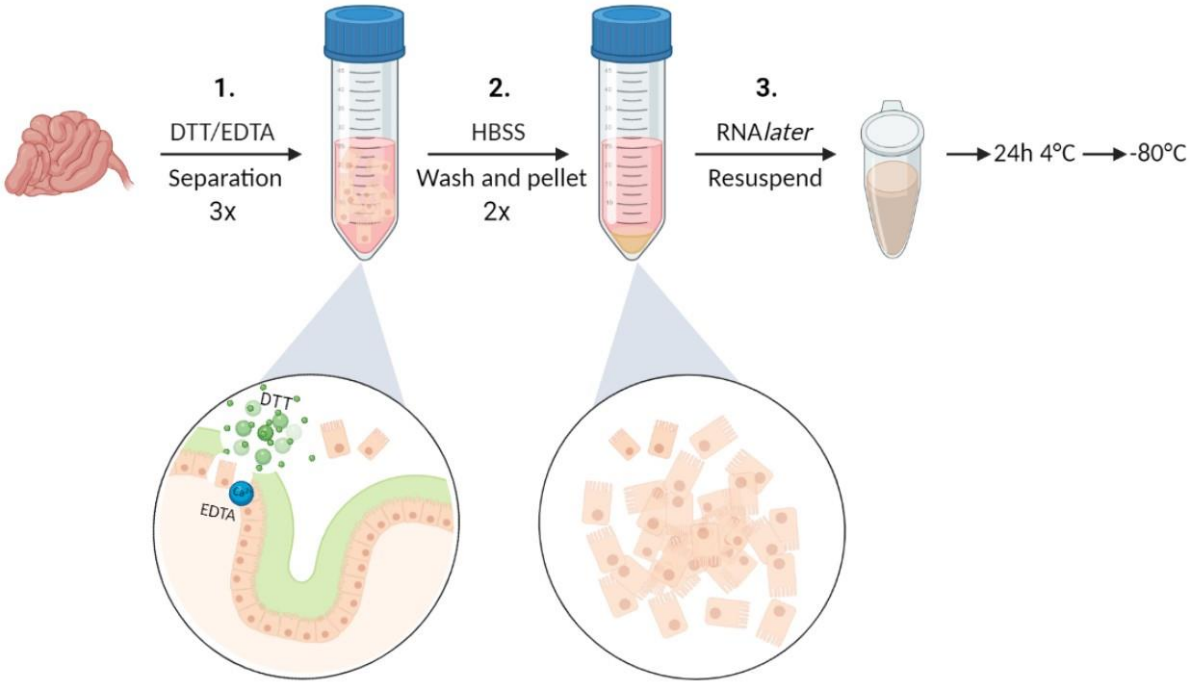

Figure 3.4 - Overview of IEC isolation protocol. Steps 1-3 show the solutions used for the different steps of epithelial cell isolation and their purpose. Final cell suspension stored at -80°C. Functions of DTT and EDTA are highlighted. Created with Biorender.com.

The intestinal tissue was moved from cRPMI to 10 mL freshly prepared, pre-heated, DTT/EDTA-solution and incubated at 175 rpm for 15 minutes at 37°C. DTT, dithiothreitol, is a mucolytic agent, breaking down the mucus layer. The mucins are denatured by reduction of disulfide bonds between cysteine residues (Cleland, 1964; Goodyear et al., 2014; Li et al., 2019). Ethylenediaminetetraacetic acid, EDTA, is a chelating agent reacting with Ca^{2+}. Calcium is an essential part of adherence junctions and desmosomes, and indirectly important for tight junctions and integrins. Hence, EDTA is a widely used reagent for separating epithelial cells from each other and from the basement membrane (Evstatiev et al., 2011; Goodyear et al., 2014).

Solution with intestinal tissue was then poured into a 70 µm cell strainer to remove crude particles and the remaining undigested LP-cell containing tissue. The resulting filtrate contained epithelial cells and was collected in a new tube on ice. This process was repeated twice with pre-heated EDTA-solution and the three filtrates were pooled and centrifuged at 300 x g for 5 minutes at 8°C. The resulting cell pellet was washed twice by resuspending in a cold HBSS + 2% FBS solution and centrifuged as before. Lastly, the final cell pellet was resuspended in 1 mL (C) or 2 mL (SI) RNA*later* (Invitrogen, Thermo Fischer Scientific, Vilnius, Lithuania) and incubated at 4°C overnight, according to the manufacturer's recommendation. Lastly, the cell suspension was stored at -80°C until further use.

3.5.3 Estimation of total cell number

Estimation of total cell number in the epithelial cell suspensions was necessary to assure similar cell numbers be used for RNA isolation and flow cytometry of all samples. Two different epithelial cell suspensions from each intestinal segment (i.e., SI and colon) were counted each day of termination using Countess™ 3 Automated Cell Counter (Invitrogen, Thermo Fischer Scientific, WA, USA) to estimate the total number of cells isolated from each intestine (*Appendix D – Cell numbers*). 10 uL cell suspension was combined with 10 uL 0.4% trypan blue stain (Life Technologies, OR, USA), of which 10 uL was added to a disposable counting slide and placed in the cell counter. Trypan blue enters dead cells and make them distinguishable from live cells. Total cell number for colon and SI was estimated by taking the overall average for each intestinal segment.

3.5.4 Flow cytometry of epithelial cell suspension to verify IEC isolation

For cell phenotyping and counting by flow cytometry, cells in the epithelial cell suspension were first stained with live/dead stain and Fc block. The volume giving one million cells was added to a 96-well plate for each sample and centrifuged at 8°C for 1 minute at 800 x g. Supernatant was removed by flipping the plate upside down, and cells resuspended in 25 µL Zombie L/D Near Infra Red (BioLegend, San Diego CA, USA). This stain binds residues expressed by dead cells, making them distinguishable from live cells. Further, 25 µL FC block (anti-mouse CD16/32 antibody; BioLegend, San Diego CA, USA) was added to all wells to block Fc-receptors that could lead to false positives. After a 10-minute incubation at room temperature (RT) and in the dark, all wells were topped with 150 µL Flow Cytometry Staining (FACS) buffer and plate centrifuged at 8°C for 1 minute at 800 x g.

For surface staining of cells to discriminate between cell types, the cell pellets were resuspended in 50 µL surface antibody cocktail. This included antibodies for EpCam (epithelial cell adhesion molecule, CD326, an epithelial cell marker (Haber et al., 2017; Wang et al., 2013)) and the immune cell marker CD45 (for comprehensive list of markers and fluorochromes, see *Appendix B – Chemicals and reagents*). Suspension was then incubated in the dark at 4°C for 20 minutes, then topped with 150 µL FACS buffer and plate centrifuged at 8°C for 1 minute at 800 x g. The supernatant was removed by plate-flipping, cells resuspended in 200 µL FACS, and centrifuged as before.

For assessment of proliferative status of the cells, they were additionally stained intracellular (IC) for Ki-67, a marker of cell proliferation (Sun & Kaufman, 2018), using the eBioscience™ IC staining kit (Invitrogen™ Thermo Fischer Scientific, Waltham MA, USA). Cells were resuspended in 100 µL fixation buffer and pulse vortexed before a 20-minute incubation in the dark at RT, then topped with 150 µL Perm/Wash buffer (P/Wb). The plate was centrifuged at 8°C for 1 minute at 800 x g. This was repeated with 200 µL P/Wb. Next, cells were resuspended in 50 µL intra antibody cocktail and incubated for 20 minutes in the dark at 4°C, then topped with 150 µL P/Wb and centrifuged as before. Finally, they were topped with 200 µL P/Wb, centrifuged as before, and resuspended in 150 µL FACS buffer.

All suspensions were then filtered through 70 μm nylon before placing the plate into the flow cytometry instrument (CytoFLEX LX, Beckman Coulter Ink., IN USA) using Kaluza 2.1 software (Beckman Coulter) for analysis.

3.6 Gene expression analysis

Gene expression analysis involves measuring the expression level of a specific gene by quantifying amounts of corresponding mRNA molecules in the cell. mRNA is a molecule complementary to the gene encoded by the DNA, synthesized by an RNA polymerase when a gene is actively expressed in a cell (the process of transcription). Normally, increasing the expression of a gene leads to an increased amount of mRNA produced by, and present in, the cell. To assess the intestinal barrier, the mRNA of genes encoding related proteins were assessed. The process of mRNA analysis included the following steps:

- RNA isolation from epithelial cells:
    - Analysis of RNA concentration and purity
    - Purification of RNA-samples to remove contaminants
    - Analysis of RNA integrity
- cDNA synthesis from RNA samples by reverse transcription
- Establishing a panel of relevant genes and primer assay
- Real-time qPCR
    - Primer assay validation by real-time qPCR
    - Analyzing primer efficiency and specificity
- High-throughput microfluidic real-time qPCR with Biomark™ HD (Fluidigm) that includes:
    - Preamplification of cDNA
    - Cleanup of preamp products
    - Relative quantification of preamplified products with Biomark™ HD (real-time qPCR)
- Processing real-time qPCR data

3.6.1 RNA isolation from epithelial cells

Total RNA was extracted from the isolated epithelial cells using the NucleoSpin RNA Mini kit following the manufacturer's protocol (Macherey-Nagel, 2019) with a few alterations. Briefly, this kit utilizes columns with silica membranes that bind RNA and DNA and allows for their separation from the solution by centrifugation through the membrane. The membrane is then treated with a reconstituted DNase (rDNase) to remove bound DNA and washed to get rid of any impurities before RNA is eluted with water. Figure 3.5 summarizes the workflow.

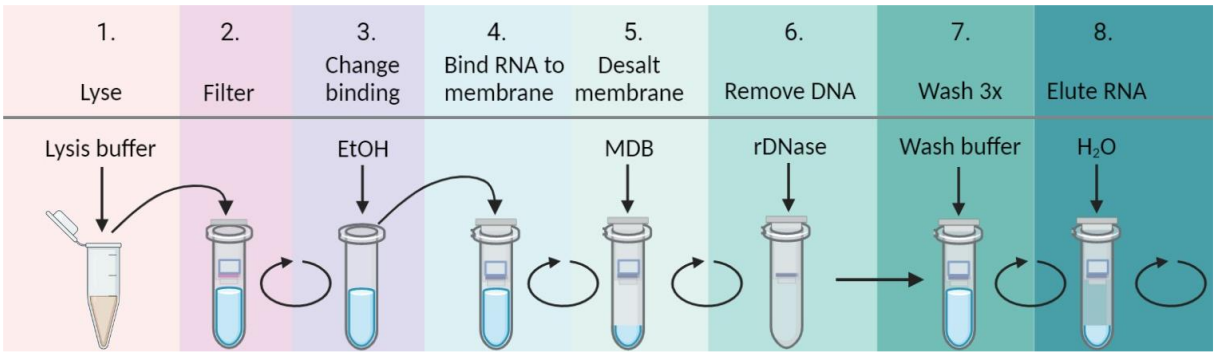

Figure 3.5 - RNA extraction protocol. Steps 1-8 summarize RNA extraction with NucleoSpin RNA Mini kit. Created with Biorender.com.

NucleoSpin allows for RNA purification from < 5 x 10^6 cultured cells. The volume of IEC-RNA*later*-suspension corresponding to five million cells was pipetted out of each cell suspension stock after thawing and vortexing. The volume was calculated using the average number of total cells from all counted SI and colon samples. The volume used for all samples was 91 µL and 403 µL for SI and colon, respectively.

Homogenization of cell suspension was done by vortexing after thawing samples on ice, and the forementioned volumes were transferred to 1.5 mL Eppendorf tubes. To remove RNA*later*, the samples were diluted 2:1 with sterile PBS and spun down at 6000 rpm (15 minutes (min), room temperature (RT)). The supernatant was pipetted off, and the cell pellet resuspended in 350 µL lysis buffer RA1 with 3.5 µL β-mercaptoethanol (β-ME, Sigma-Aldrich, Bayern, Germany). During the RNA isolation procedure and all downstream handling of the sample, the RNA is at risk of being degraded by the enzyme RNase. RNases are almost everywhere, such as on the skin, fingerprints, and in dust (Peirson & Butler, 2007). β-ME is a reducing agent of protein disulfide bonds, denaturing RNases and other proteins (Mommaerts et al., 2015). The chaotropic salt guanidinium thiocyanate (GTC) in RA1 also contributes to eliminating RNases, but its most important function is to lyse the cells (Mommaerts et al., 2015).

Since the number of cells exceeded one million, the suspension also had to be homogenized by passing it through a 20-gauge needle. To reduce the viscosity of the lysate, the homogenized sample was transferred to a NucleoSpin filter in a 2 mL collection tube and centrifuged (11 000 x g, 2 min, RT). Filter was discarded and 350 µL 70% ethanol (EtOH) added to the collection tube and mixed by pipetting up and down ten times to form a clear solution. EtOH was added to optimize the binding-properties of RNA by altering the pH of the solution, which was then transferred to the NucleoSpin RNA Column in a 2 mL collection tube and centrifuged (13 000 x g, 3 min, RT). During this process, the RNA binds to the column membrane. The column was transferred to a new collection tube and the filtrate was discarded.

Presence of DNA in RNA samples affects the final gene expression analysis and must be removed by treating the membrane with a DNase, a DNA degrading enzyme (see next paragraph). To increase effectiveness of the DNase digestion, 350 µL Membrane Desalting

Buffer (MDB) was added to the column for salt removal and centrifuged (13 000 x g, 3 min, RT). The column was then transferred to a new collection tube and filtrate discarded. A fresh mixture of 10 µL rDNase and 90 µL Reaction Buffer per sample was combined in a sterile 1.5 mL tube and mixed by flicking, of which 95 µL was added to the center of the membrane and incubated for DNA degradation (15 min, RT).

For removal of degraded DNA, rDNase, salts, and other impurities, the column membrane was washed three times. Once with 200 µL RAW1 buffer (11 000 x g, 2 min, RT), inactivating the rDNase, and twice with buffer RA3; once with 600 µL (11 000 x g, 2 min, RT) and once with 250 µL (11 000 x g, 3 min, RT). New collection tubes were provided between all washes. Lastly, RNA was eluted from the column by transferring it to a new, RNase-free, 1.5 mL tube and adding 40-60 µL RNase-free H_2O to the center of the column and centrifuging (11 000 x g, 2 min, RT). To get as high a concentration of RNA as possible, the elute was added back to the column a second time and centrifuged again. The eluates were placed on ice while the following analyses were performed, then stored at -80°C until further use.

Analysis of RNA concentration and purity

Downstream reactions such as cDNA synthesis and PCR can be inhibited by impurities in the RNA sample such as protein, GTC and other salts, and DNA. Therefore, concentration and purity of RNA eluates was measured using NanoDrop™ 2000 (Thermo Scientific™, USA). The instrument measures absorption of wavelengths 230 to 280 nm with 340 nm as background correction. Purity is analyzed as the ratio of absorption at 260 nm and 280 nm ($A_{260/280}$), and at 260 nm and 230 nm ($A_{260/230}$). The maximum absorption of nucleic acids lies at 260 nm while that of proteins and other impurities such as GTC lie at 230 nm. The $A_{260/280}$ gives information about the ratio of RNA to DNA, and a pure RNA sample has a higher ratio than a pure DNA sample. Moreover, a pure RNA sample gives a higher $A_{260/230}$, since the A_{230} will be small. Acceptable threshold values are commonly $A_{260/280}$ and $A_{260/230}$ >1.8 (Koetsier & Cantor, 2019); however, samples >1.7 were tolerated (*Appendix E – RNA purity and integrity*).

Repetitive freeze/thaw-cycles of RNA can result in degradation of RNA. Therefore, approximately half of the RNA eluate (stock) was used to prepare working solutions with concentrations of 100 ng/µL and 50 ng/µL for SI and colon, respectively, using RNase-free H_2O. The remaining stock solution of RNA was kept at -80°C as a backup. Working solutions were stored at -80°C until further use.

Purification of RNA samples to remove contaminants

Samples with absorption values ≪1.8 were considered impure and rinsed for removal of contaminants. Rinsing protocol was based on those by Maniatis and Riccio (Maniatis et al., 1989; Riccio, 2019). This briefly involved re-precipitating the RNA by adding 0.1xVol 3 M sodium acetate (NaAc) and 2.5xVol 70% EtOH (e.g., 100 µL RNA + 10 µL NaAc + 250 µL EtOH). The solution was mixed well and incubated on ice for 30 minutes. RNA was then pelleted by centrifugation at maximum speed (~21 000 x g) for 15 minutes and 4°C. The side of the tube facing outward of the centrifuge was marked, since RNA pellets are mostly

invisible. The supernatant was pipetted off on the opposite side of the marking followed by a wash of 150-200 µL EtOH and a new centrifugation as before. The supernatant was again pipetted off and the tube put in a fume hood for approximately 10 minutes at RT with the lids open to evaporate the last traces of EtOH. To loosen the pellet, the tube was tapped for about one minute, and lastly the RNA was resuspended in 40 µL RNase-free H_2O. The samples were measured anew with NanoDrop™, and working solutions prepared, before storing at -80°C.

Analysis of RNA integrity

Since RNA is a relatively unstable molecule, and RNases are everywhere, checking the integrity of the isolated RNA is critical for getting reliable data from mRNA quantification analyses. Ideally, all RNA molecules should be intact to correctly reflect the situation in the cell from which it is extracted (*Agilent Technologies*, 2020). RNA integrity was assessed using the RNA 6000 Nano kit with Agilent 2100 Bioanalyzer (Agilent Technologies, CA, USA). The samples were heat-denatured for 2 minutes at 70°C to remove RNA secondary structures, before they were added to a small chip containing a gel and RNA binding dyes and subjected to capillary electrophoresis for separation and detection of RNA by fluorescence.

The associated software calculates an RNA Integrity Number (RIN-value) for each sample by assessing the entire electrical trace from the electrophoresis. The main measurement involves calculating the ratio of the areas under the 18S and 28S peaks (ribosomal subunits) (Mueller et al., 2016). The software relies on an RNA marker added to the samples to be able to detect the correct peaks, but since the reagents that were used were a bit old the software had trouble detecting all peaks. The samples were therefore evaluated manually by comparing their electrographs to reference electrographs with established RIN-values (Figure 3.6). For further analyses to be useful, it is recommended that the RIN value is above 7 (NorwegianSequencingCentre, 2020); hence, all samples with estimated RIN>7 were cleared for further analysis (*Appendix E – RNA purity and integrity*).

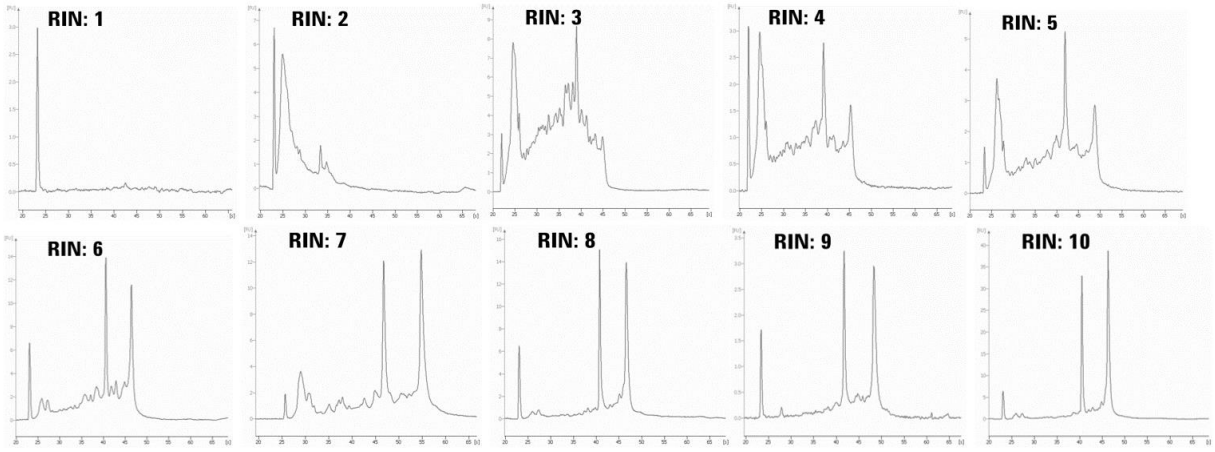

Figure 3.6 - RIN-value reference electrographs. The figure illustrates the electrographs of differently degraded RNA samples reflecting each RIN-value. From (*Agilent Technologies*, 2020).

3.6.2 cDNA synthesis of RNA samples by reverse transcription

Analyzing RNA with qPCR (see section 3.6.4) requires its conversion to a complimentary DNA (cDNA) strand. This is done by the enzyme reverse transcriptase through a process termed reverse transcription (Arya et al., 2005; Mo et al., 2012). Reverse transcriptases are DNA polymerases that can use RNA as a template (Gerard et al., 2002; NEB, NA). To begin synthesis, the enzyme needs to bind a template-primer hybrid. Primers are short nucleotide sequences (~20 nucleotides) complementary to the start site of the target sequence (NEB, NA). The reverse transcriptase used in this experiment was RNase H+ M-MLV reverse transcriptase. RNase H+ reverse transcriptase synthesizes a single cDNA strand using the RNA as a template, followed by degradation of the RNA-template. Hence, a single cDNA strand replaces each RNA strand, resulting in an unchanged concentration of nucleic acids (Gerard et al., 2002).

cDNA was prepared using a Fluidigm Reverse Transcription Master Mix (Fluidigm, CA, USA) following the manufacturer's protocol (Fluidigm corporation, 2019). The Master Mix contained dNTPs, random primers, oligo dTs, RNase inhibitor, and an RNaseH+ MMLV reverse transcriptase. The RNase inhibitor protects the RNA during setup of reactions. Primers in general are mostly target-specific, but for the purpose of making cDNA of all RNA present they are random/universal. Oligo dT primers bind poly-A tails common in mRNA.

In a nuclease-free area on ice, two pre-mixes were prepared by combining Master Mix and nuclease-free water (Table 3.1) and mixed by pipetting and a short vortex. 7.5 and 5 µL of the pre-mix was added to each well on a PCR plate for SI and colon samples, respectively. RNA was added to a well with pre-mix to give a total of 10 µL per well. The difference in volumes of RNA from SI and colon give equal amounts of total ng RNA per reaction. All reactions were mixed well by pipetting up and down. The PCR plate was sealed with film, spun down, and placed in a thermal cycler (Veriti 96 Well Thermal Cycler, appliedbiosystems USA). Incubation program is illustrated in Figure 3.7. Resulting cDNA was stored at 4°C until further use.

Table 3.1 - cDNA synthesis reaction mix. Volumes given in µL/reaction. Final concentration of RNA template was 25 ng/µL for all reactions. Volumes of H_2O and RNA differ from manufacturers protocol to adjust RNA concentration. SI=small intestine.

Component		**Volume colon (µL)**	**Volume SI (µL)**	**Final concentration**
Pre-mix	Reverse Transcription Master Mix	2	2	-
	RNase-free water	3	5.5	-
RNA template (Colon=50 ng/µL, SI=100 ng/µL)		5	2.5	25 ng/µL
Total		**10**	**10**	-

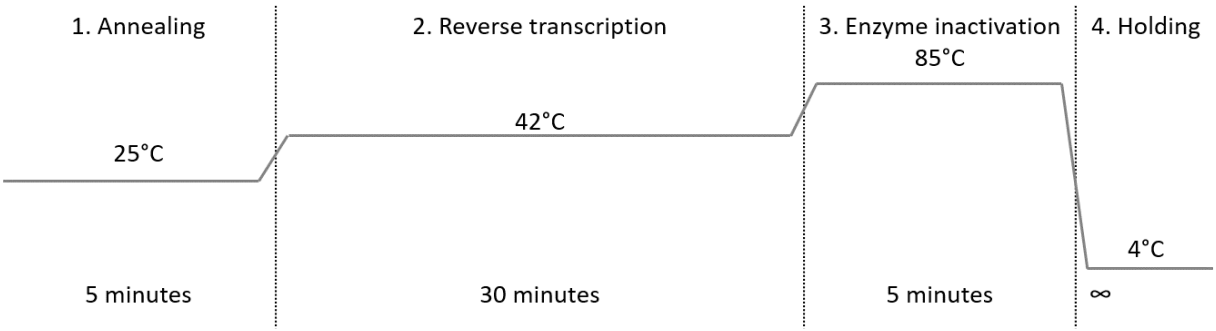

Figure 3.7 - Reverse transcription thermal cycler program. Steps 1-4 illustrate the conditions for each reaction stage of the cDNA synthesis.

3.6.3 Establishing a panel of relevant genes and primer assay

A list of 48 genes to be targeted in the gene expression analysis was compiled by searching for the following three criteria: (1) the gene has been shown to be expressed in murine IECs, either in colonocytes, small intestinal enterocytes, or both, (2) the gene expression level is affected by luminal microbial exposure or inflammation, and (3) the function of the gene must be related to at least one of the following categories: barrier (tight junctions, AMPs, mucus layer proteins), immunosurveillance, (anti)-inflammation, ROS/RNS production, and cell turnover. The full list of genes and the proteins they encode, including their function, is listed in *Appendix F – Full list of target genes*.

The final list of target genes was added to the D3 service provided by Fluidigm to request primer assay design and ordering the primers (*Appendix F – Full list of target genes*). In contrast to the primers used for cDNA synthesis, these primers need to be highly specific to bind only the targets of interest. Lack of specificity would make them unreliable. The service offers to design your primers to optimally fit their Biomark™ HD instrument regarding specificity and sensitivity in the real-time qPCR reactions (Fluidigm, 2020). It was requested that primers span exon-exon junctions to avoid amplification of possible genomic DNA (gDNA) contamination in the RNA isolates, since gDNA and pre-mRNA contain introns (Sandhu & Acharya, 2005).

3.6.4 Real-time qPCR

Real time quantitative polymerase chain reaction (real-time qPCR) is a method of DNA amplification that is monitored continuously (in "real-time"), as opposed to standard PCR where fluorescence is measured at the end of the run (Arya et al., 2005). Briefly, PCR involves combining a thermostable DNA polymerase with your template cDNA or DNA, dNTPs, primers, and a fluorescent dye such as SYBR Green. SYBR Green is nonspecific and binds any double stranded DNA, and its intensity is proportional to the amount of DNA present in the reaction. Hence, the fluorescence increases with increasing amounts of DNA. A thermal cycler controls the reaction by quickly changing between temperatures optimal for each reaction step: denaturation, annealing and elongation. Denaturation separates all double stranded DNA (dsDNA) to single stranded (ssDNA), allowing for annealing of the primers in the next step. During elongation, DNA polymerase binds the ssDNA-primer hybrid and synthesizes a new copy. These steps are normally repeated for 30 to 45 cycles. For each cycle, the DNA is amplified exponentially as the number of strands doubles (Arya et al., 2005).

The fluorescent dye emits a baseline fluorescence which is increased a thousand-fold when it binds dsDNA. The number of cycles required until the fluorescence can be detected above this baseline threshold value is termed quantitation cycle (Cq, phase 1 in Figure 3.8). The higher the amount of original template molecules the lower the Cq, as it takes fewer cycles until the amount of DNA copies, and hence the fluorescence, reaches this threshold. This value can be used to quantify the amount of template in the original sample (Arya et al., 2005). Fluorescence can be detected above the baseline when the reaction reaches the exponential phase (phase 2 in Figure 3.8). The reaction will eventually reach a plateau because it runs out of reagents (e.g., dNTPs, phase 3 in Figure 3.8).

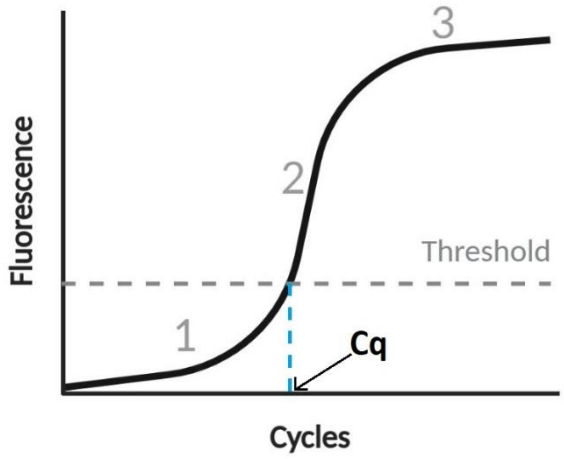

Figure 3.8 - qPCR amplification plot. The figure illustrates the amplification plot of a positive qPCR reaction. **1**: initiation phase, **2**: exponential phase, **3**: plateau phase. The point at which the curve meets the threshold gives the Cq-value of the sample. Created with Biorender.com.

Gene expression analysis commonly evaluates changes in gene expression under different experimental conditions. It is the difference between the samples that are of interest and

knowing the absolute number of RNA molecules in the original sample is therefore not necessary. Relative quantification assumes that the relative expression level of a gene is proportional to the difference in Cq between the gene of interest and a reference gene. Reference genes are commonly housekeeping genes because they are expressed equally in all cells under all (experimental) conditions. What is important for performing this comparison is that all primers have equal efficiencies (E-value), meaning how well they bind to the target (Klein, 2002). Exponential amplification of the target gene requires a doubling of amplicon per cycle, which gives E=2 (an efficiency of 100%). How well the primers bind depend on several factors such as the annealing temperature and the properties of the reaction mix, as well as the method used for nucleic acid extraction (Bustin & Huggett, 2017).

Primer assay validation by real-time qPCR

New primers that have not been tested experimentally need to be validated before use. This because of the forementioned variability in performance dependent on experimental conditions (Bustin & Huggett, 2017). Primer efficiencies deviating from 2 can be dealt with in several ways: adjusting reaction temperatures or primer concentrations, redesigning the primer, or adjusting the calculations of relative gene expression.

Validation involves testing all primer pairs (forward and reverse) with cDNA from the same tissue that is to be used in the final analysis. To achieve good precision, at least two technical replicates should be included (Bustin et al., 2009). A No Reverse Transcriptase Control (NRT) should also be included to control for potential gDNA contaminations. When there is no enzyme present no cDNA will be synthesized; hence, fluorescent signals in NRT indicate gDNA contaminations. Since the Fluidigm Reverse Transcriptase Master Mix came pre-mixed, it was not possible to make NRTs, but almost all primers span exon-exon junctions which should counteract amplification of gDNA if present (*Appendix F – Full list of target genes*). A pool of cDNA from colon and SI was prepared by combining 4 µL of each cDNA sample.

For primer validation, all primer stocks were first thawed on ice and aliquoted on a PCR plate for further use, to avoid repeated freeze-thaw cycles which can cause primer degradation. The primer stock concentration was 100 µM and working solutions of 10 µM were prepared. A 5-fold dilution series was prepared of the pooled cDNA by combining one part of the previous dilution with four parts nuclease-free H_2O. The cDNA concentration in the dilution series ranged from 25 to 0.008 ng/µL. The purpose of a dilution series is primarily that the titration curve that can be calculated from the fluorescence data can be used to calculate primer efficiency, but also to evaluate the dynamic range of the primers (Bustin et al., 2009).

The real-time qPCR was performed using SSoFast™ EvaGreen® Supermix (Bio-Rad Laboratories, Inc., Hercules, CA), as the same supermix is used in the final qPCR-reaction in the Fluidigm Biomark™ HD. A master mix was prepared in a sterile tube on ice in a nuclease-free area. The components were combined as described in Table 3.2 and mixed by short vortexing. Master mix and cDNA was added to a PCR plate, mixed well, sealed

with film, and spun down for 20 seconds at 500 x g. 16 primers were tested per plate, including five cDNA dilutions and one No Template Control (NTC), hence a total of three plates were prepared to test all 48 primer pairs. NTCs were included to check for contaminations in the master mix by substituting cDNA with nuclease-free H_2O. Due to restrictions in reagents and time, no technical replicates were included.

Table 3.2 - qPCR reaction mix. Volumes per qPCR raction.

Component	Volume (µL)
2X SsoFast EvaGreen Supermix	5
Nuclease-free H_2O	2.5
Primer (forward + reverse mix)	0.5
Pooled cDNA	2
Total	**10**

Primer assay validation real-time qPCR was performed using the CFX96 Touch Real-Time PCR instrument (Bio-Rad Laboratories, Ink. CA, USA) with the program illustrated in Figure 3.9. Fluorescence is measured at the end of step 3 ("plate read"). A melting curve was included at the end to evaluate primer specificity (Ririe et al., 1997). By constantly measuring fluorescence while slowly increasing the temperature from 60 to 95°C, product melting temperature (Tm) can be observed by an abrupt decrease in fluorescence due to denaturation of the double stranded molecule. Amplification products can vary in length and GC-content (percentage of the molecule consisting of the bases guanine and cytosine) that greatly affects the Tm. Inverting the plot turns the drop into a peak for easier interpretation, and several peaks can be observed if the reaction contains primer-dimers, amplified gDNA, or off-target products due to non-specificity of the primer.

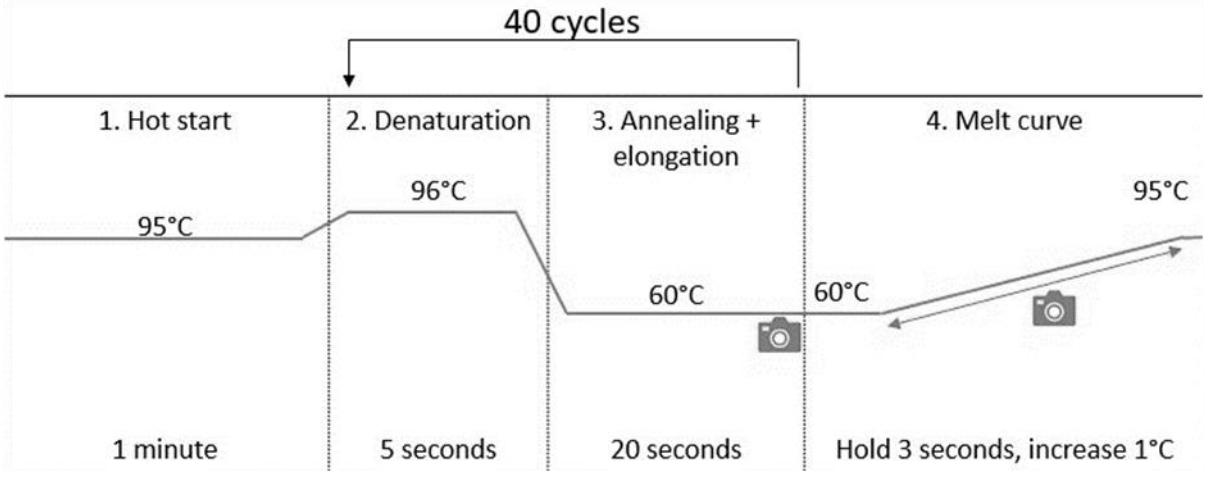

Figure 3.9 - Real-time qPCR program. Steps 1-3 illustrate the conditions for each reaction stage of the PCR. Step 4 illustrates the melt curve analysis. Camera icon=plate read. The same temperature program is used by the Biomark™ HD.

Analyzing primer efficiency and specificity

The Bio-Rad software associated with the CFX96 Touch instrument automatically calculates the E-value based off the titration curve (plotting cDNA dilution against Cq). However, these titration curves were unfit to estimate an E for all primers, who were therefore assessed using the LinRegPCR analysis software (Ruijter et al.). LinRegPCR calculates an E-value for each individual reaction which can be used to estimate the E-value for each primer pair by taking the overall average of the E-values. The program uses the raw fluorescent amplification data and corrects the baseline for each individual reaction. After identifying four points in the exponential phase, a linear regression is run. The slope of this line is then used to estimate the E-value (Ruijter et al.). An average E-value was only calculated for primers that showed amplification in at least three consecutive reactions. The coefficient of determination, R^2, is also calculated, indicating how well the data points fit to the regression line. Primer pairs that had an $\hat{E}$ and R^2 within the acceptable range ($\hat{E}=2\pm0.1$ and $R^2>0.98$) were included in further analyses. Additionally, reactions with more than one melt peak were excluded for lack of specificity (*Appendix F – Full list of target genes*).

3.6.5 High-throughput microfluidic real-time qPCR with Biomark™ HD

Biomark™ HD (Fluidigm, CA, USA) is a real-time qPCR instrument in which thousands of qPCR reactions are measured simultaneously in Integrated Fluidic Circuits (IFC, Figure 3.10). IFC's are chips utilizing microfluidics to run thousands of instrument-controlled nanoscale PCR reactions in the reaction controller. The primers are added to the primer inlets, samples to the sample inlets, and control line fluid into the accumulators. Control line fluid controls movement and avoids contamination between samples and is used by the IFC Controller MX instrument (Fluidigm, CA, USA) to load the primers and samples into the reaction chamber. 48.48 Dynamic array IFC's allow all samples to mix with all primers in 48x48 individual reactions (Fluidigm, 2021). Workflow of Fluidigm gene expression analysis is summarized in Figure 3.11. For this thesis, two separate 48.48 IFCs (1 and 2) were run on two separate occasions to include all samples from the second termination.

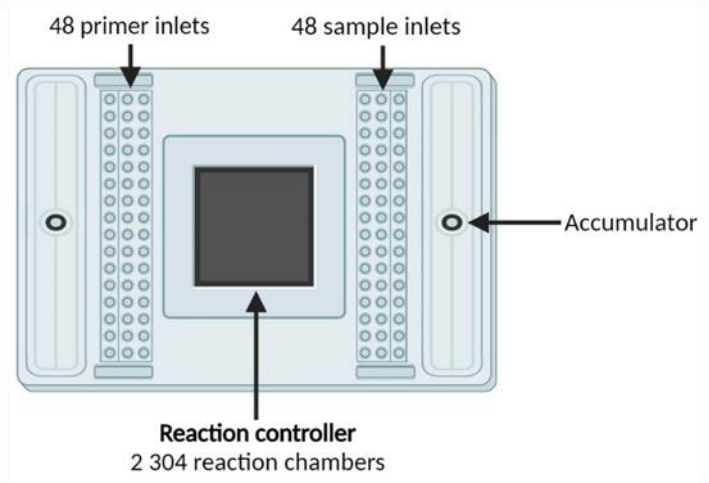

Figure 3.10 - Dynamic array 48.48 IFC. Created with Biorender.com.

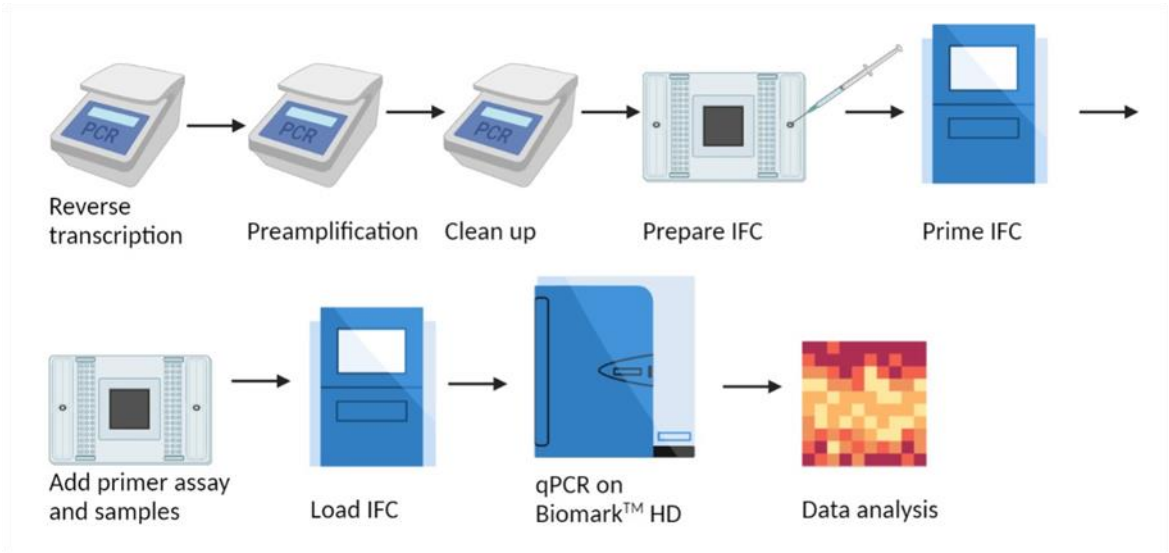

Figure 3.11 - Fluidigm gene expression analysis workflow. Figure illustrates the steps described in this section. Preparing IFC involves adding control line fluid. Created with Biorender.com.

Preamplification of cDNA

Since the IFC combines nanoliters of sample and primer, high concentration of target cDNA is required in all samples. Preamplification (preamp) involves running a PCR of all samples with a pool of all primers to be tested, giving a high concentration of the targets. This further requires treatment with an Exonuclease, to remove excess primers and ssDNA (Fluidigm, 2021). All following steps were performed following manufacturers protocol (Delta Gene Assays, Fluidigm), using Fluidigm reagents unless stated otherwise. cDNA was prepared as described in section 3.6.2, once for primer validation and the first run, and a second time for the second run.

Briefly, preamp of cDNA involved preparing a "primer pool" by combining 1 µL of 100 µM stock of each of the primer pairs in a nuclease-free microcentrifuge tube with TE-buffer (Macherey-Nagel, Düren, Germany), giving a final volume of 200 µL and a concentration of 500 nM of each primer. A pre-mix was prepared in a nuclease-free microcentrifuge tube by combining Preamp Master Mix, pooled primer mix and nuclease-free water (Mediatech, Inc. Manassas, VA, USA) according to Table 3.3. To a new 96-well plate, preamp pre-mix and cDNA was added to the wells for a total of 5 µL (Table 3.3). The plate was vortexed briefly and centrifuged (1000 x g, 1 min, 4°C), before placing it in a thermal cycler (Veriti 96 Well Thermal Cycler, appliedbiosystems USA). Figure 3.12 illustrates the thermal cycler program used for preamp.

Table 3.3 - Preamplification reaction mix for Fluidigm cDNA preamp. Volumes given in µL per reaction.

Component		Volume (µL)
Preamp pre-mix	Preamp Master Mix	1
	Pooled primer mix	0.5
	DNase-free water	2.25
cDNA		1.25
Total		**5**

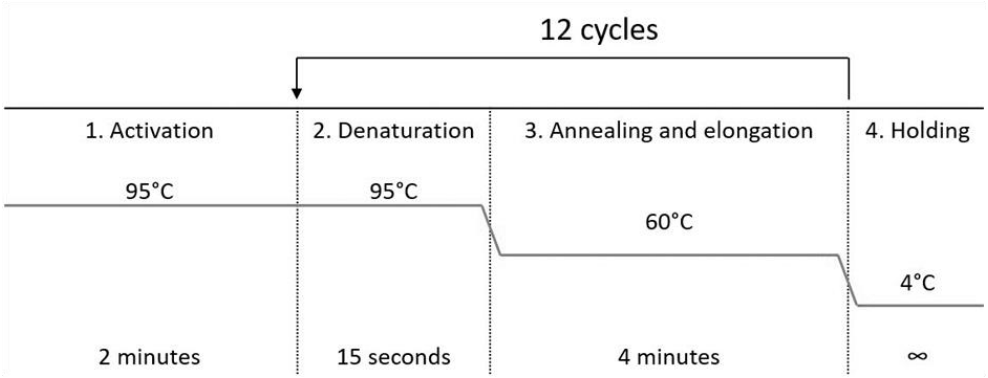

Figure 3.12 - Preamplification thermal cycler program. Steps 1-4 illustrate the conditions for each reaction stage. Protocol recommends starting with ten cycles, but twelve cycles were used as recommended by colleagues.

Clean up of preamp products

All preamp products were treated with Exonuclease I (Exo I) to clean up the preamplified cDNA before gene expression analysis. Exo I removes excess primers and ssDNA by degradation in the 3'- to 5'-direction (Thermo Fischer Scientific, CA, USA). Exo I reaction mix was prepared by diluting 20 U/µL Exonuclease I (Thermo Fischer Scientific, CA, USA) with nuclease-free H_2O (Mediatech, Inc. Manassas, VA, USA) and Exonuclease I Reaction Buffer (Thermo Fischer Scientific, CA, USA) according to Table 3.4. 2 µL Exo I reaction mix was added to each reaction well. Following a short vortex and centrifugation (1000 x g, 10 seconds), the plate was placed in a thermal cycler (Veriti 96 Well Thermal Cycler, appliedbiosystems USA) and incubated as illustrated (Figure 3.13). After treatment, the samples were diluted 5-fold using TE-buffer (Macherey-Nagel, Düren, Germany).

Table 3.4 - Exo I reaction mix. Volumes given in µL per reaction.

Component	Volume (µL)
DNase-free water	1.4
Exonuclease I Reaction Buffer	0.1
Exonuclease I, 20 U/µL	0.4
Total	**2**

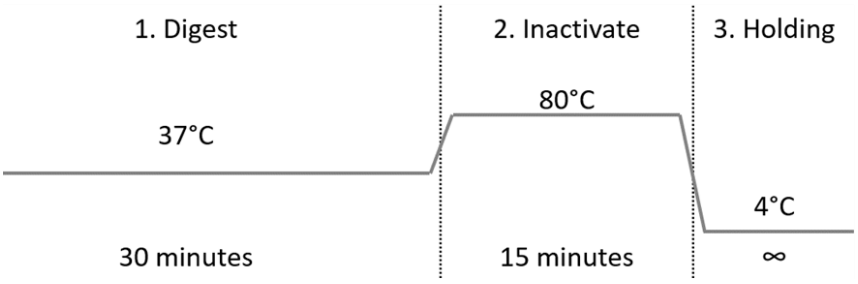

Figure 3.13 - Exonuclease I thermal cycler program. Steps 1-3 illustrate the conditions for each stage of the Exo I treatment.

Relative quantification of preamplified products with Biomark™ HD (real-time qPCR)

A 48.48 IFC was injected with control line fluid into each accumulator before placing it into the IFC Controller MX instrument (Fluidigm, CA, USA) to run the prime script. In a 1.5 mL tube, a pre-mix was prepared by combining SsoFast EvaGreen® Supermix (Bio-Rad Laboratories, Inc., CA, USA) and 20X DNA Binding Dye Sample Loading Reagent, followed by vortexing and centrifugation for 10 seconds at 1000 x g. 3.3 µL of the pre-mix and subsequently 2.7 µL of the diluted Exo I treated preamplified samples were added to a new PCR-plate, vortexed and centrifuged for 10 seconds at 1000 x g before 5 µL of each sample was added to the IFC (right inlets). Two water samples were included (NTC) by replacing the Exo I treated, preamplified samples with PCR-grade H_2O (Mediatech, Inc. Manassas, VA, USA).

25 µL stocks of diluted primers were prepared in microcentrifuge tubes by combining 1.25 µL of 100 µM combined forward and reverse primers with 11.25 µL TE-buffer (Macherey-Nagel, Düren, Germany) and 12.5 µL 2X Assay Loading Reagent. The primer mixes were then vortexed briefly and centrifuged for 10 seconds at 1000 x g before adding them to the IFC (left inlets). After adding 5 µL of primers and samples to the IFC inlets, the IFC was placed back into the controller instrument to run the load-transcript. Finally, the IFC was moved to the Biomark™ HD instrument for real-time qPCR with the same program as previously described (Figure 3.9), but with 30 cycles instead of 40.

3.6.6 Processing of real-time qPCR data

Gene expression analysis data was transformed to relative expression levels (REL) using an alternative to the Livak method (Livak & Schmittgen, 2001). RELs were calculated using the Fluidigm Real-time PCR Analysis software (version 4.8.1) and Microsoft Excel (version 2204). All values are normalized to the two reference genes *Gapdh* and *Tbp* by the Fluidigm software. It uses the arithmetic mean of the reference gene Cq-values, individually for each sample. Fluidigm Real-time PCR Analysis software calculated ΔCq for each sample and each gene of interest (GOI) as follows:

$$\Delta Cq_{sample,GOI} = Cq_{sample}\,(GOI) - \left(\frac{Cq_{sample}(Gadph) + Cq_{sample}(Tbp)}{2}\right)$$

Next, all ΔCq values were transported to Excel, and transformed by multiplying by (-1) to give more intuitive data. Negative values indicate lower expression relative to reference genes, positive values indicate higher expression relative to reference genes.

Further, data from the two separate runs of gene expression analysis were combined, and each individual sample was normalized to the control group by calculating ΔΔCq in Excel as follows:

$$\Delta\Delta Cq_{sample,GOI} = \Delta Cq_{sample,GOI} - mean\ of\ \Delta Cq_{control\ group}$$

Important to note here is the use of the (arithmetic) mean of the control group, which includes the ΔCq values of control (Lab) from **both** runs. This was done to merge the data

of both runs. Finally, RELs were calculated as Fold Change (FC) using the following formula:

$$Fold\ change = 2^{\Delta\Delta C_q}$$

It follows that ΔΔCq is the log base 2 of the fold change, termed "log fold change". The formula assumes a doubling of amplicons in each cycle, hence the number "2". The resulting fold change describes how many times more the gene is expressed in the test sample relative to the control group. In the case where FC<1, the gene is lower expressed relative to Lab. In the text in the results section (4), these numbers are transformed to fold-values by calculating *1/FC*. For example, if *FC=0.25*, then *1/0.25=4*. This is read as "this gene is four-fold lower expressed". In the following statistical analyses, the data within each group from the two runs were treated as one merged group.

3.7 Statistical analyses

Statistical analyses were performed using GraphPad Prism 9.3.1. For each target gene, the most suitable statistical test was determined after checking the assumptions of the test. Which tests that were used is specified in each figure legend and Table 4.4 in the results (section 4). Throughout all analyses, the threshold α-value used was 5% (significant p-value <0.05), and a p-value<0.1 was considered a trend. The p-value is the probability of observing the differences that are observed in your data given that the assumptions of the statistical test are met (Motulsky). The assumptions included the null-hypothesis H_0, which stated that there is no real difference (no effect of treatment), and that the observed differences are due to random sampling. When this probability becomes very small, it is more likely that the observed differences are caused by an effect of treatment (Dean et al., 2017).

Statistical tests were done on the log fold change data ($\log_2 (2^{\Delta\Delta Cq}) = \Delta\Delta Cq$), as the fold change data are logarithmic and difficult to analyze with the following statistical tests and often require a log-transformation anyway. Although statistics were done on the ΔΔCq, figures in the results (section 4) show the plot of fold change ($2^{\Delta\Delta Cq}$) as the fold change is easier to interpret visually, and is also how the results are presented in Table 4.4. Hence, no data-transformations were done during testing of statistical significance.

Outliers (extreme values) were detected using ROUT method (Q=1%) (Motulsky). Outliers can affect descriptive statistics such as the mean, which is used in several statistical tests. However, the criteria for removing outliers are very strict because all observations are real biological values that say something about the population, unless the extreme values are caused by an error in the lab.

Comparing the mean of more than two groups is commonly done using a one-way analysis of variance (one-way ANOVA) (Motulsky). The assumptions include that the data are independent, have equal variances, and that the residuals are normally distributed. Testing for equal variances (homogeneity of variance) checks if the variance of each group differs significantly. This was tested using Brown-Forsythe test because this test is not as

sensitive to deviations from normality as other tests, which is not uncommon when handling groups with small n (n=number of observations) (Motulsky). Further, normality of the residuals was tested using Shapiro-Wilks W test because all groups had n<12, and the W test is the most suitable normality test for small groups (Royston, 1995).

Data meeting the assumptions of one-way ANOVA were tested for significant differences in the mean using this parametric test. The test answers the question if there is any significant difference between any groups. If a significant difference was found, a *post hoc* test was done by comparing all groups with each other to determine *which* groups were different. To keep the overall $\alpha < 5\%$, the p-values from these multiple comparisons were corrected by Tukey's multiple comparison correction (Motulsky).

Data that had significantly different variances were tested using the Welch test, an alternative to one-way ANOVA that does not assume equal variances, only normal distribution (Motulsky). Multiple comparisons were corrected by Dunnett's T3 correction (Motulsky). Data that were not normally distributed, independent of equal variances, were tested using the nonparametric Kruskal Wallis test with Dunn's correction for multiple comparisons (Motulsky; Motulsky).

Finally, Principal Component Analyses (PCAs) were carried out using RStudio on all fold change data from colonic epithelium (version 2022.02.1+461, script in *Appendix G – R-script*). A PCA assesses the entire data set and attempts to find "principal components" that can describe the variations observed in the data (Ringnér, 2008). Moreover, it cannot deal with missing values, hence all mice that had no calculated FC-value for at least one gene were excluded from the analysis. Due to time restrictions, analysis of colonic data was prioritized, and no PCA on SI data are presented.

3.8 Own contribution

The past ten months I have learned a lot about planning an experiment and the handling of both laboratory mice and wild house mice. My supervisors were responsible for the experimental setup; however, veterinary student Harriet Stendahl and I were included in several meetings about the execution of the experiment. Harriet and I randomized the lab mice both at arrival and trial start and took a big part in the catching of wild mice. We also microchipped all lab mice; however, supervisor Professor Preben Boysen microchipped the wild mice. PhD student (at the time, now Dr.) Henriette Arnesen was responsible for the daily tasks related to the experiment, but Harriet and I helped with all preparations including filling the pens and starting the experiment by moving the lab mice into the pens.

Together with Henriette and Harriet, I spent many hours in the animal lab sampling feces and weighing all the mice every two weeks and helped with refilling the pens with farmyard material. For the termination of the experiment, Henriette, Harriet, and supervisor Professor Harald Carlsen executed the euthanization and dissection of all mice, while I was ultimately responsible for isolating the IECs, in addition to the isolation of LP immune cells from the same tissue on behalf of the project (not described in this thesis). Harriet counted total cell numbers using Countess. Preben, Henriette and Harriet were responsible for executing the flow cytometry, however I occasionally helped with the surface staining of cells.

I isolated all RNA from the epithelial cells by myself, in addition to all NanoDrop and Bioanalyzer measurements (Henriette helped me with the first BA chip and prepared the gel). Further, I performed all qPCR analyses of the primers and the associated processes, as well as processing samples for the Biomark™ HD analyses and final gene expression analyses. Harriet analyzed the flow cytometry data. Lastly, I independently performed all statistical analyses of gene expression data using GraphPad and RStudio.

4 RESULTS

4.1 Animal welfare and health in naturalized housing conditions

4.1.1 Wild house mice and lab mice adapted well to their new habitat

A total of nine female and nine male wild house mice, and one wood mouse, were caught from the same location (a private barn in Vestby, Norway). After release into the pens, the mice were observed for a brief period to assure their well-being. The B6 mice seemed curious about the wild mice, who at first appeared skeptical of the B6 mice. After a few days, it looked like all mice had found their place in the pens and got along well, but the wild mice seemed more skittish throughout the experiment (especially when we went into the pens). After a couple of weeks, they were found nestled together with the B6 mice. Wild mice added at later time points were unfortunately found dead after 1 to 2 days, but without any signs of struggle or other indications of cause of death. The final number of wild mice in each cohousing pen was therefore three. Throughout the experiment, no mice showed any signs of discontent or pathological symptoms that would give cause of concern and generally appeared healthy. In conclusion, housing female lab mice together with female wild mice, when added to the new habitat simultaneously, allows for friendly interactions with no obvious negative effects on animal welfare.

4.1.2 Feralized mice gained less body weight than the other groups

A weight development curve was plotted for each experimental group from the body weight registered every two weeks (Figure 4.1 A). There was no significant difference in mean group weight the first two weeks (W0 and W2), but mice in the Fer group had consistently lower mean weight compared to one or more of the other experimental groups from W4-W10. The mean weight increase (Δweight) from the beginning of the experiment to the second termination in week ten showed that mice in the Fer group gained significantly less body weight compared to the other three groups (Figure 4.1 B).

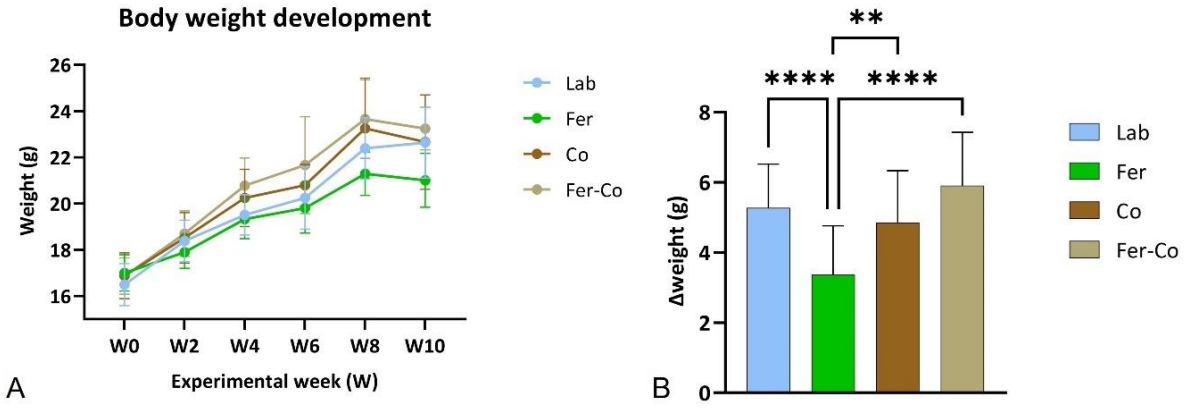

Figure 4.1 - Body weight development. A) Weight is given in grams and as the average of all weighed mice in each experimental group over the 10-week period of the experiment. Error bars represent the standard deviation of each group. **B**) Average delta weight in grams calculated as $weight_{W10}$ – $weight_{W0}$. Error bars

represent the standard deviation of each group. Tested using Kruskal Wallis with Dunn's correction for multiple comparisons and α=0.05. P-values: **≤0.01, ****≤0.0001.

4.1.3 Parasites were detected in feces from naturalized and wild mice

Parasitic eggs, cysts or oocysts were discovered in fecal samples from all naturalized and cohoused mouse groups, in addition to the wild house mice (Table 4.1). All parasitic eggs, cysts and oocysts included in the test were detected in samples from Co-pen wild house mice, while none were detected in the Lab-mice. The coccidia *Cryptosporidium* (Bouzid et al., 2013) was the most abundant parasite, its oocysts detected in several samples from both wild mice and B6 mice in the cohousing pens, while *Giardia* cysts (Heyworth, 2014; Xu et al., 2020) were detected only in samples from one Co-pen wild mouse and one Fer-pen B6 mouse. The nematode *Heligmosomoides polygyrus* (Niimi & Morimoto, 2021) and the coccidia *Eimeria* (Jarquín-Díaz et al., 2019) were only detected in one sample from a Co-pen wild mouse.

Table 4.1 - Presence and grade of parasites in samples from all experimental groups. * Individual samples; ** each sample was a pool of feces from 2-3 mice, *** a combination of * and **; + 1-9, ++10-49, and +++ >50 visible parasite eggs at 4X or cysts/oocysts at 20X. ND=not detected, IFAT: immunofluorescence antibody test.

	Wild mice in Fer-Co pen*		**Wild mice in Co pen***		**Fer-Co****		**Co*****		**Fer*****		**Lab*****	
Number of samples analyzed	5		7		6		6		5		4	
	Sucrose floatation											
	Presence	Grade	Presence	Grade	Presence	Grade	Presence	Grade	Presence	Grade	Presence	Grade
Heligmosomoides polygyrus	ND		1	+	ND		ND		ND		ND	
Eimeria	ND		1	+	ND		ND		ND		ND	
	IFAT											
	Presence	Grade	Presence	Grade	Presence	Grade	Presence	Grade	Presence	Grade	Presence	Grade
Cryptosporidium oocysts	2	+	1	+	3	+	2	+	ND		ND	
Giardia cysts	ND		1	+	ND		ND		1	+	ND	

In conclusion, different parasites seem to accompany the naturalizing environment, with the wild mice seemingly being the primary source.

4.2 Isolation of intestinal epithelial cells from mouse intestines

4.2.1 Flow cytometry analyses revealed immune cells in the epithelial cell suspensions

To evaluate the level of cell-purity in the suspension of isolated IECs, as this could have implications on gene expression analysis, cells were analyzed by flow cytometry. CD45 is a surface marker of immune cells (leukocytes), meaning that the CD45 negative (CD45-) cell fraction contains all other types of cells, and is where the IECs are found. Further characterization of IECs was done by gating those that were EpCam+ (epithelial cell

marker CD326) and CD45- within the fraction of live cells. This revealed an average of 74.17 and 64.43% of IECs of all live cells in the colon and SI, respectively (Table 4.2). The results also indicate that a substantial number of immune cells (leukocytes, CD45+) in both colon and SI (Figure 4.2, Table 4.2). The percent of IECs and CD45+ cells was higher in the colon than the SI in all groups. Moreover, the percent of leukocytes was higher in cohoused mice than Fer and Lab.

Table 4.2 - Purity of IEC isolates. Presented as the average percent of all live cells in the epithelial cell suspension that are IECs, defined as CD45-EpCam+, in colon and SI of each group. Also shown is the average percent of all live cells in the epithelial cell suspension that are immune cells (leukocytes), defined as CD45+ (both EpCam- and +), in colon and SI of each group. SI=small intestine.

Segment - % cell	Group				Overall average (%)
	Co	Fer	Fer-Co	Lab	
SI - % IECs	68.13	67.61	60.54	61.46	64.43
Colon - % IECs	70.32	78.59	72.56	75.20	7417
SI - % Leukocytes	13.86	5.33	16.56	4.99	10.18
Colon - % Leukocytes	11.32	3.16	7.48	2.09	6.01

The cell numbers were gathered from the gating illustrated in the plot of EpCam versus CD45 within the live-cell fraction (Figure 4.2). The highest cell density lies within the EpCam+CD45- fraction ("true" IECs).

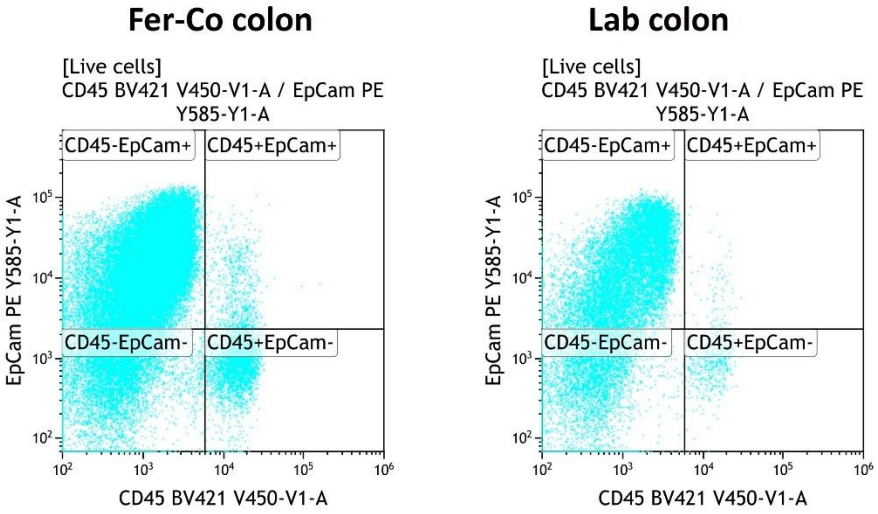

Figure 4.2 - Flow cytometry of colonic epithelial cell suspension. Shown are two representative examples of plots of EpCam (intestinal epithelial cell) versus CD45 (immune cell) within the live cell fraction from Fer-Co and Lab mouse colonic epithelium. Each blue dot is one single cell.

These results indicate contamination of cell types other than intestinal epithelial cells in the epithelial cell suspensions, including immune cells, of which the percent was higher in cohoused mice than Fer and Lab.

4.2.2 Rate of epithelial cell turnover was higher in the colon of naturalized mice

The epithelial cell fraction of isolated cells was stained with intracellular cell proliferation marker Ki-67 to check the level of active cell proliferation in the intestinal epithelium, reflecting the rate of epithelial cell turnover. Flow cytometry analysis of Ki-67 positive (Ki-67+) cells showed a higher average level of cell division in SI IECs (48.66%) compared to colonic IECs (35.68%), as well as higher level of division in all groups compared to Lab, particularly in the colon (Table 4.3).

Table 4.3 - Active cell division in the IECs. Presented as average percent of live EpCam+CD45- cells that were also Ki67+ in each intestinal segment of each group. SI=small intestine.

Segment	Group				Overall average (%)
	Co	Fer	Fer-Co	Lab	
SI (%)	51.67	47.71	49.86	45.40	48.66
Colon (%)	42.67	38.97	37.51	23.58	35.68

The higher percent of cells positive for the active cell proliferation marker Ki-67 seen in the colon of all naturalized mice compared to lab mice suggest an effect of housing conditions on cell turnover in the colon of naturalized mice.

4.3 Mode of naturalization differentially affects expression of barrier-function related genes in intestinal epithelial cells

To investigate the effect of different naturalization modes on the intestinal barrier in mice, high-throughput microfluidic real-time qPCR on mRNA from the cells of an epithelial cell suspension was performed, using primers targeting genes related to the barrier, immunosurveillance, inflammation, antimicrobials, and ROS/RNS production. The relative expression level of these genes were calculated based on the qPCR data and tested for significant differences between the experimental groups (Figure 4.3 to Figure 4.8 and Table 4.4). Presented are combined data from the first and second run, as explained in section 3.6.6.

4.3.1 Expression of genes related to mucus structure and rearrangement was found higher in the colon of cohoused mice

Several genes encoding proteins related to barrier function and mucus structure including mucus proteins, junction proteins and proteins important for mucus organization were investigated. The two genes related to mucus structure and rearrangement, *Clca1* and *Fcgbp*, were most affected by housing conditions (Figure 4.3, Table 4.4). *Clca1*, which is important for mucus structure, was 7.17- and 9.84-fold higher expressed in colonocytes from Co and Fer-Co mice, respectively, relative to Lab mice. The same effect was also found in small intestinal enterocytes although the magnitude of difference was smaller and only significant for Co (2.45-fold higher). *Fcgbp*, important for mucus rearrangement, was found 3.07- and 5.43-fold higher expressed in colonocytes of Co and Fer-co, respectively, relative to Lab mice. However, the same was not observed in the SI. For other

barrier related genes, a 1.54- and 1.47-fold higher expression of *Cdh1* (encoding adherence junction protein) was observed in the SI of Co and Fer-Co mice, respectively, albeit only significant in Co mice. *Muc3* (mucus protein) was found 1.70-fold higher expressed in SI of Fer mice (Table 4.4).

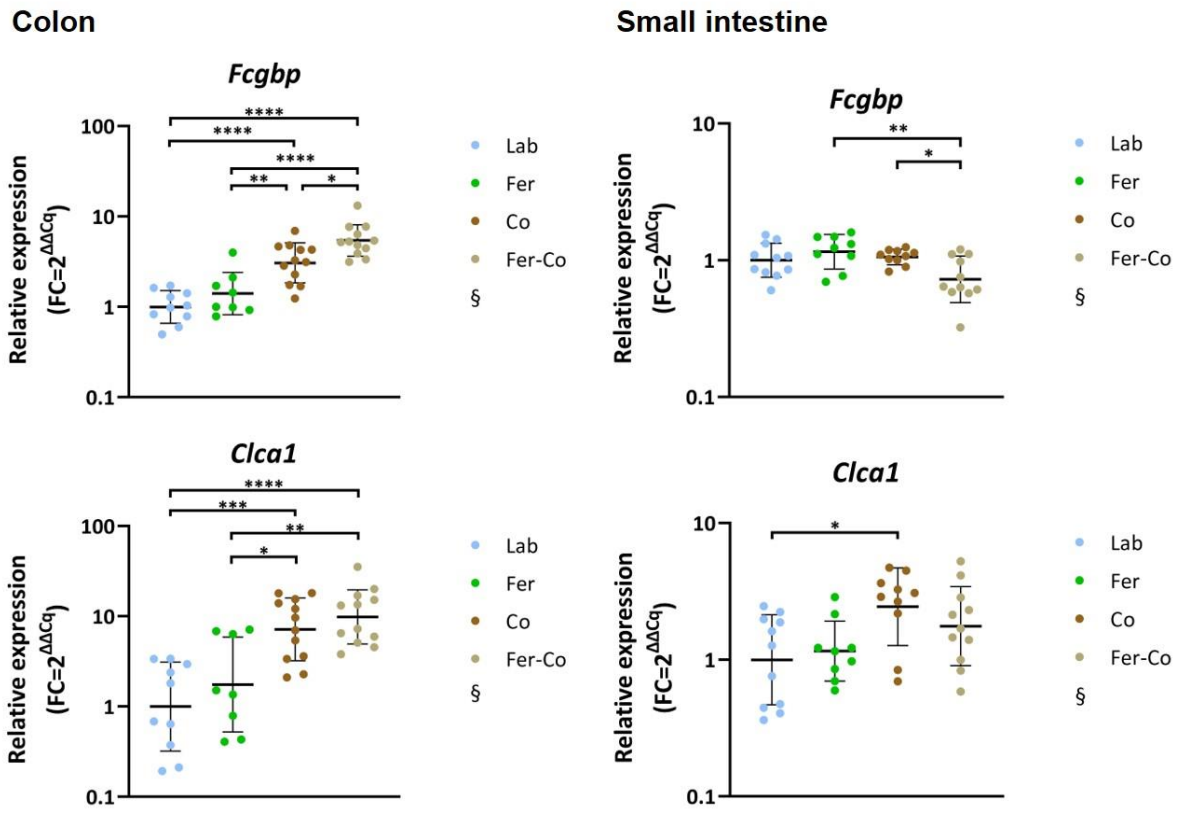

Figure 4.3 - Relative expression of barrier-function related genes in cells from colonic and small intestinal epithelium. Plotted is the relative expression of two of the barrier-function related genes in cells from colonic and small intestinal epithelium. Each symbol represents one animal, the horizontal bars represent the geomean of the group, and the error bars represent the standard deviation in each group. Relative expression ratios expressed as fold change $FC=2^{\Delta\Delta Cq}$ relative to the mean of control group on a log10 scaled axis. Symbol indicating statistical test: §=ordinary one-way ANOVA with Tukey's correction. Significant p-values: *≤0.05, **≤0.01, ***≤0.001, ****≤0.0001.

In conclusion, these results suggest that naturalization has a particular impact on colonic expression of two genes related to mucus structure and rearrangement, but not the genes encoding the mucus proteins themselves or other barrier-related genes.

4.3.2 Genes related to antimicrobial functions were found differentially expressed in the colon of cohoused mice

The gene encoding the antimicrobial peptide Relm-β, *Retnlb*, was higher expressed in both the colon and SI of cohoused mice (52.51- and 10.99-fold in Co and 59.79- and 16.84-fold in Fer-Co, respectively) (Figure 4.4, Table 4.4). Moreover, relative expression of the AMP-encoding gene *Ang4* was highly increased in the colon of *all* groups relative to Lab (7.61-fold, 59.71-fold, and 75.76-fold in Fer, Co, and Fer-Co, respectively), while only minor changes were observed in the SI (1.81-fold higher in Fer-Co). Only observed in the colon of cohoused mice was an extreme increase in expression of *Itln1*, another AMP (112.02- and 147.56-fold in Co and Fer-Co, respectively): however, a trend was detected in Fer as well ($p<0.1$ for a 9.90-fold increase). Also higher expressed in the colon, but not the SI, of the cohoused groups was the alpha-defensin (AMP) gene *Defa24* (38.94- and 30.30-fold in Co and Fer-Co, respectively). However, the Cq-value of *Defa24* in the colon was high, indicating low mRNA expression (not shown). Both *Reg3* genes (AMPs) were found significantly lower expressed in the colon of cohoused mice: *Reg3γ* in both (4- and 5.88-fold in Co and Fer-Co, respectively) and *Reg3β* only in Fer-Co (10-fold). In the SI, *Reg3γ* was found lower expressed in cohoused mice, albeit only significantly in Fer-Co mice (1.96-fold).

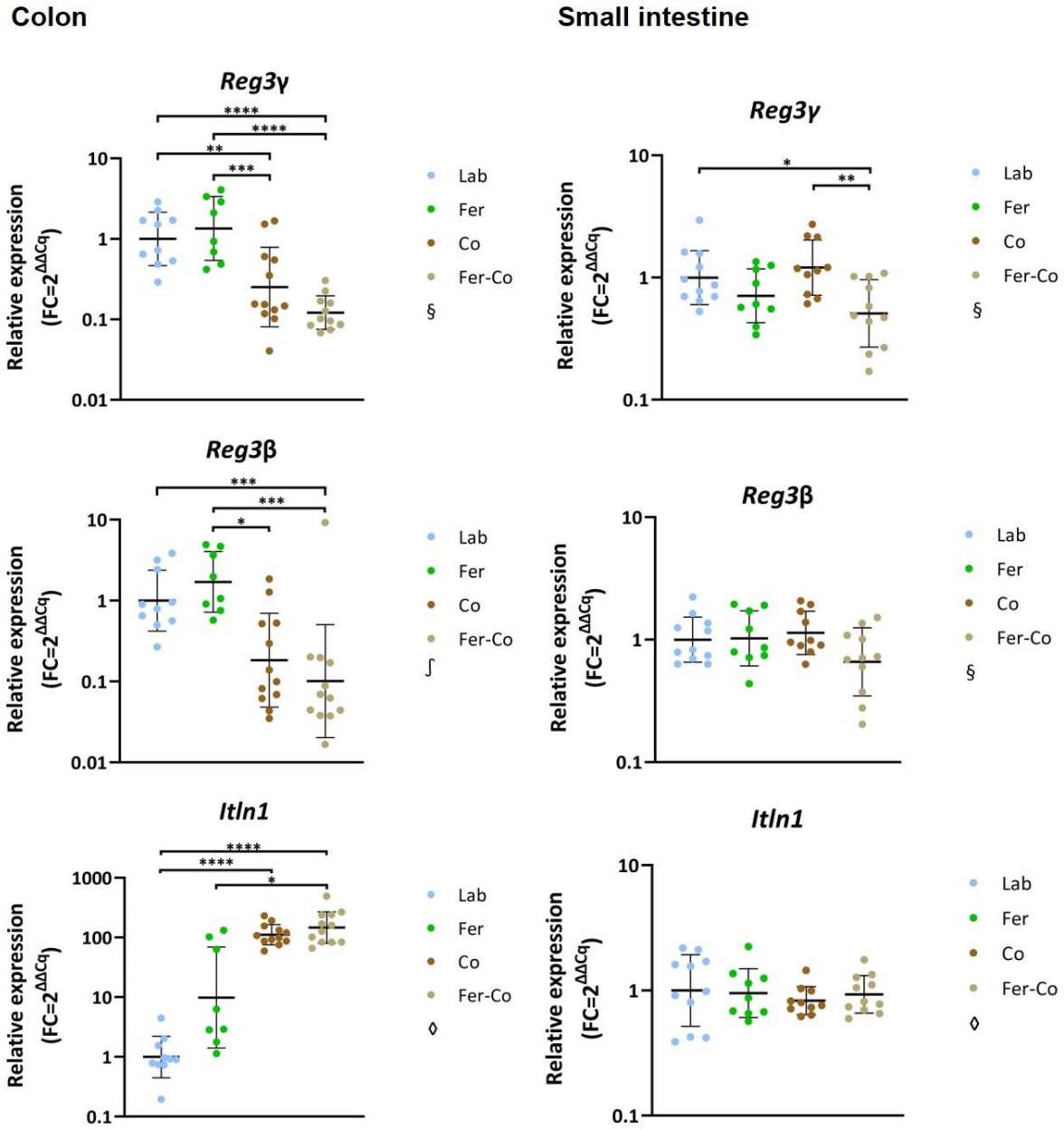

Figure 4.4 - Relative expression of antimicrobial-function related genes in cells from colonic and small intestinal epithelium. Plotted is the relative expression of some of the antimicrobial-function related genes in cells from colonic and small intestinal epithelium. Each symbol represents one animal, the horizontal bars represent the geomean of the group, and the error bars represent the standard deviation in each group. Relative expression ratios expressed as fold change $FC=2^{\Delta\Delta Cq}$ relative to the mean of control group on a log10 scaled axis. Symbols indicating statistical test: §=ordinary one-way ANOVA with Tukey's correction, ∫=Kruskal Wallis with Dunn's correction, ◊=Welch's test with Dunnett's T3 correction. Significant p-values: *≤0.05, **≤0.01, ***≤0.001, ****≤0.0001. (Continues on next page).

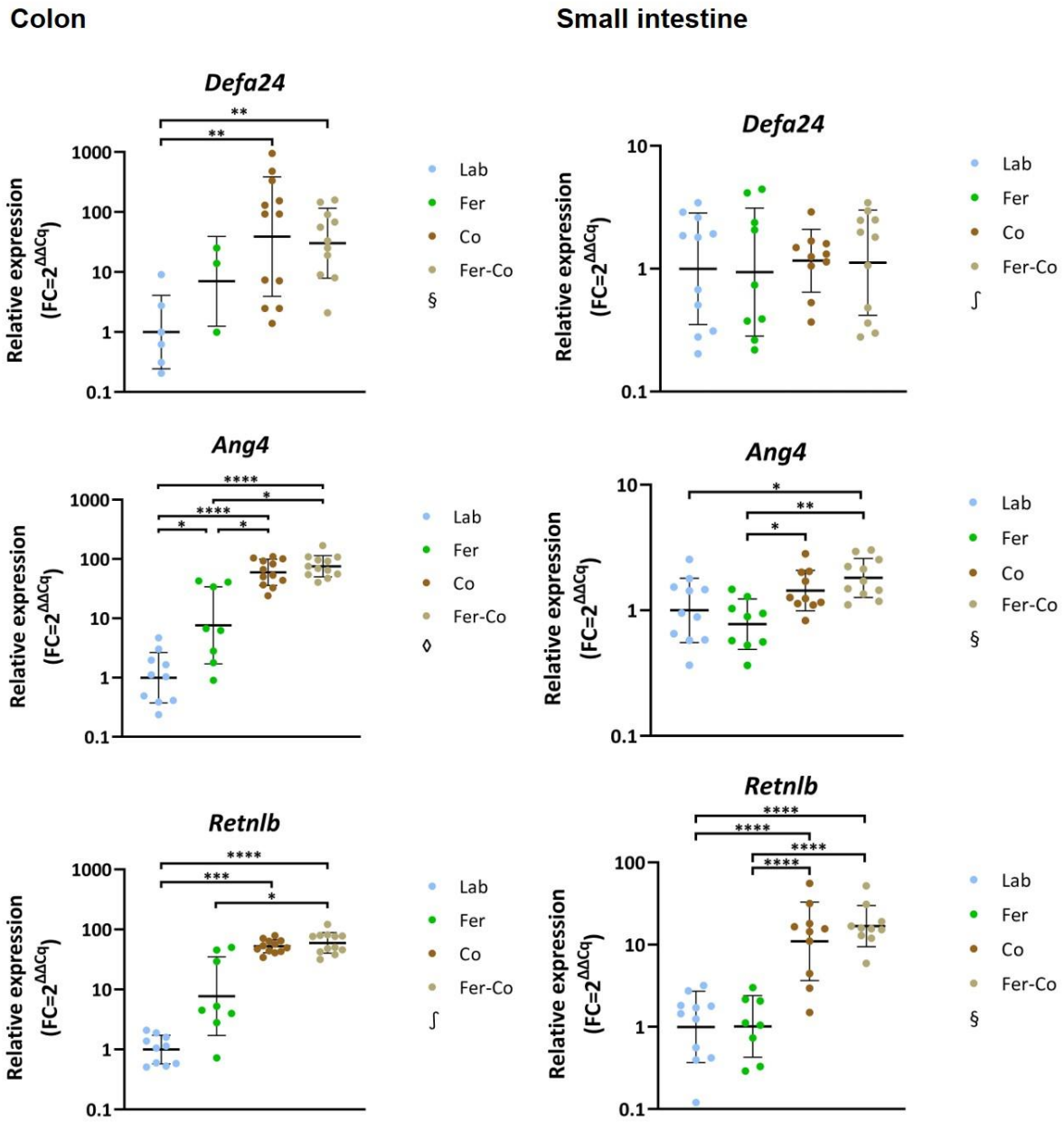

Figure 4.4 - Relative expression of antimicrobial-function related genes in cells from colonic and small intestinal epithelium. (Continued).

All things considered, cohousing with wild mice seems to affect expression of all the antimicrobial peptides analyzed in the colon of B6 mice, as well as on the expression on some of the AMPs in the SI, suggesting an activation of microbial responses in the intestine.

4.3.3 Most genes related to immunosurveillance were found differentially expressed in the small intestine of cohoused mice

Relative expression of *Zbp1* mRNA, encoding a pathogenesis-recognizing protein related to virus infections, was found higher expressed in both colon and SI of cohoused mice (16.08- and 3.79-fold in Co and 8.10- and 3.39-fold in Fer-Co, respectively) (Figure 4.5). Moreover, the PRR *Tlr5* (receptor of microbial molecular patterns) was found lower expressed in both colon and SI of cohoused mice (2.33- and 2.04-fold in Co and 1.88- and 2.08-fold in Fer-Co, respectively), while *Tlr2* was only found higher expressed in the SI of cohoused mice (2.46- and 2.20-fold in Co and Fer-Co, respectively). *Tlr4* was only found significantly higher expressed in the colon of Fer-Co (1.72-fold) (Table 4.4). Relative mRNA levels of the NLRs *Nod1* and *Nod2* (also receptors of microbial molecular patterns) were found higher in the SI of cohoused groups (2.66- and 2.27-fold in Co and 1.88- and 2.75-fold in Fer-Co, respectively), while in the colon only Co mice were significantly different from Fer mice.

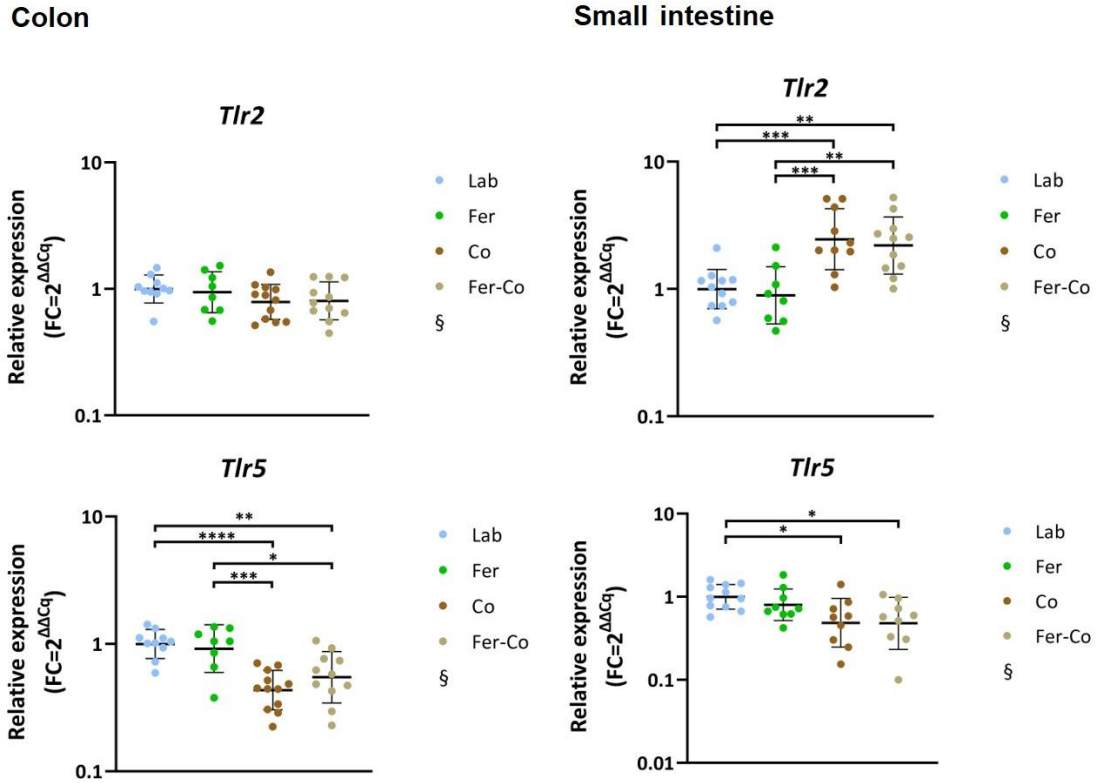

Figure 4.5 - Relative expression of immunosurveillance related genes in cells from colonic and small intestinal epithelium. Plotted is the relative expression of some of the immunosurveillance related genes cells from colonic and small intestinal epithelium. Each symbol represents one animal, the horizontal bars represent the geomean of the group, and the error bars represent the standard deviation in each group. Relative expression ratios expressed as fold change $FC=2^{\Delta\Delta Cq}$ relative to the mean of control group on a log10 scaled axis. Symbols indicating statistical test: §=ordinary one-way ANOVA with Tukey's correction, ∫=Kruskal Wallis with Dunn's correction. Significant p-values: *≤0.05, **≤0.01, ***≤0.001, ****≤0.0001. (Continues on next page).

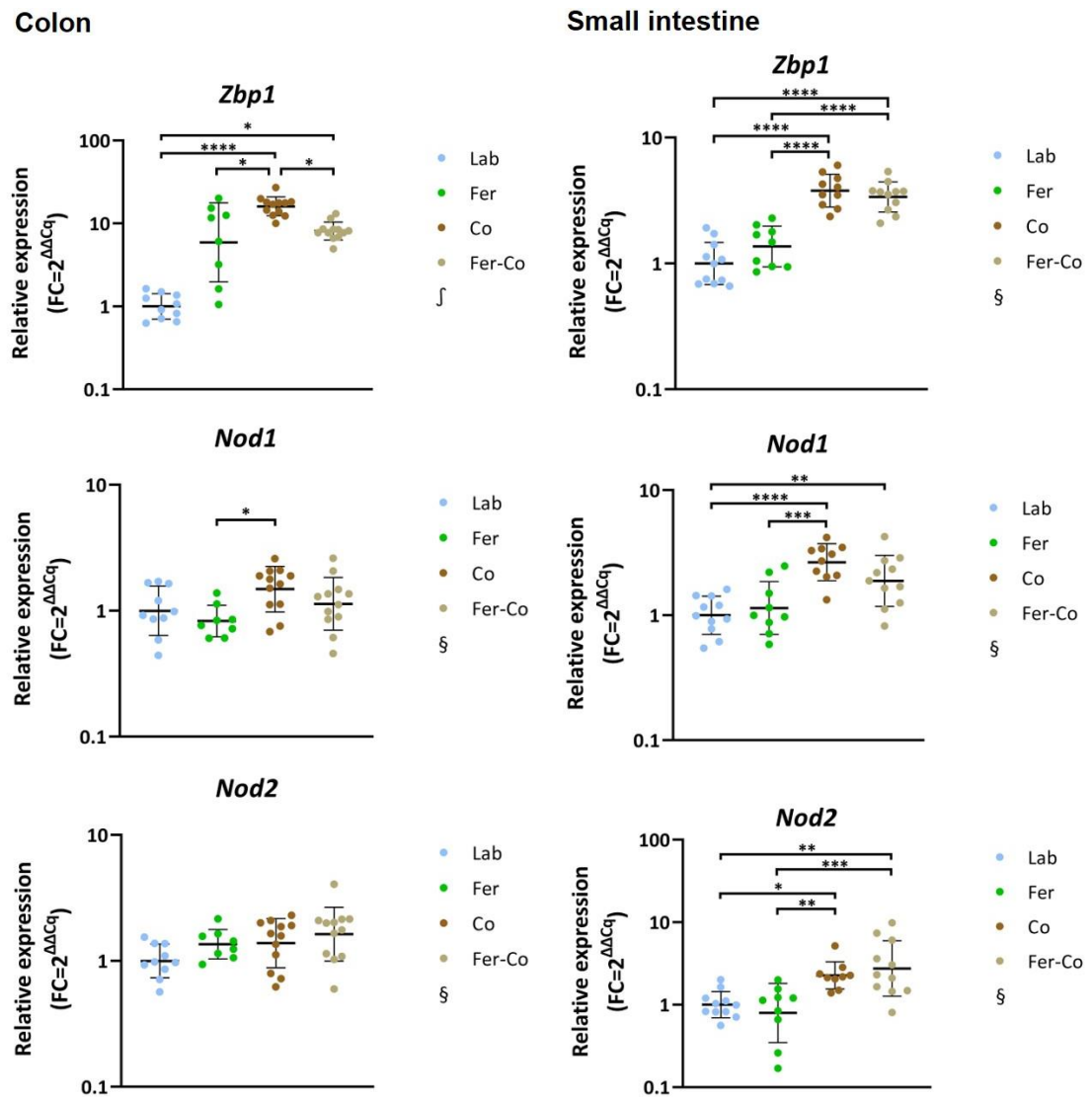

Figure 4.5 - Relative expression of immunosurveillance related genes in cells from colonic and small intestinal epithelium. (Continued).

In summary, these observations imply an effect of cohousing on the expression of immunosurveillance-related genes, including microbial recognizing receptors, especially in the SI.

4.3.4 Genes related to inflammation were found differentially expressed in both the colon and small intestine of cohoused mice

Expression of several genes encoding inflammatory cytokines and inflammation-related proteins was analyzed. *Il-18*, encoding an inflammatory cytokine, was observed considerably lower expressed in both the colon and SI of cohoused mice (3.45- and 2.38-fold in Co mice and 1.92- and 2.94-fold in Fer-Co mice, respectively) and in the colon of Fer mice (2.13-fold lower, Figure 4.6). Moreover, expression of *Il-10*, encoding an anti-inflammatory cytokine, was higher expressed in both the colon and SI of Co-mice (23.40- and 8.33-fold, respectively). Encoding another inflammatory cytokine, *Il-1b* was only higher expressed in the colon of Co mice (2.42-fold higher), and *Tgfb1*, encoding a

cytokine important in the development of CD4+ T cells into Tregs or Th17 cells, as well as IgA production by B cells, was higher expressed in the SI of cohoused mice (2.26- and 2.53-fold higher in Co and Fer-Co, respectively), but no change was observed in the colon.

Expression of *Nlrp6*, encoding a pro-inflammatory inflammasome, was higher expressed only in the colon of Fer-mice (1.59-fold higher), and no difference in colonic expression *Saa1* (inducer of Th17 and other inflammatory responses) was observed. However, in the SI, no changes were found for *Nlrp6,* but *Saa1* expression was increased in Co-mice (7-fold higher). Moreover, *Gsdmc* (encoding a protein related to pyroptosis) was considerably higher expressed in the colon of cohoused mice relative to Lab mice (6.66- and 4.61-fold higher in Co and Fer-Co, respectively), while no differences were found for *Gdsmd* with similar functions in either intestinal segment. Lastly, no changes were found in the expression of *Alpi* (a target gene of Tlr4), *Il-25* (encoding an inflammatory cytokine), *Lcn2* (a common marker of gut inflammation), nor for *Mir31* that promotes cell proliferation in response to inflammatory cell damage (Table 4.4).

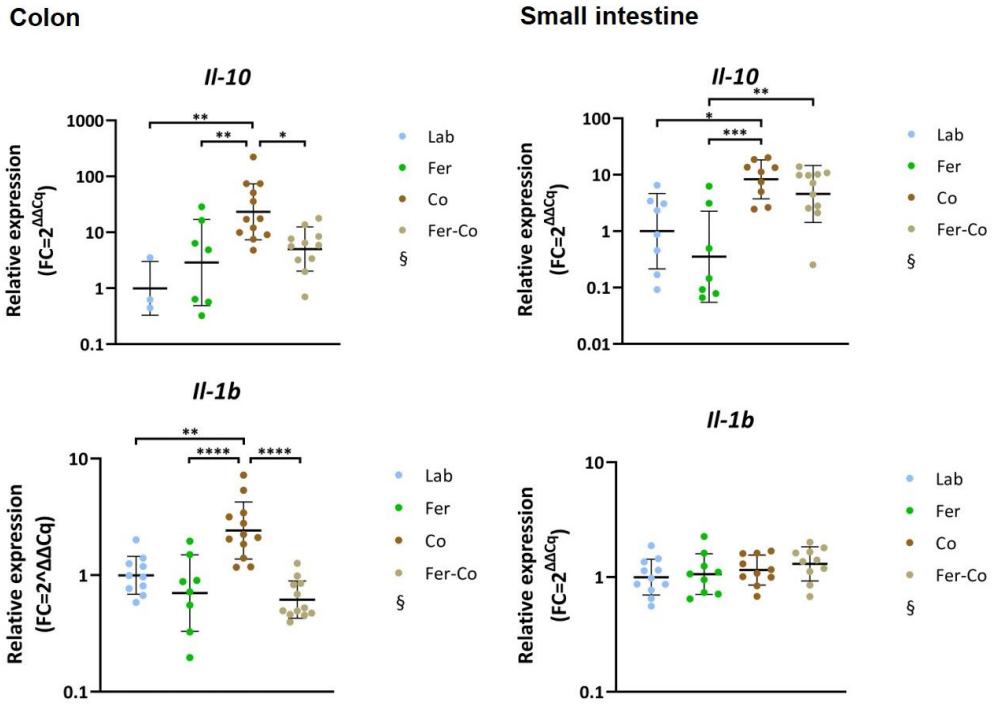

Figure 4.6 - Relative expression of inflammation related genes in cells from colonic and small intestinal epithelium. Plotted is the relative expression of some of the inflammation related genes in cells from colonic and small intestinal epithelium. Each symbol represents one animal, the horizontal bars represent the geomean of the group, and the error bars represent the standard deviation in each group. Relative expression ratios expressed as fold change $FC=2^{\Delta\Delta Cq}$ relative to the mean of control group on a log10 scaled axis. Symbols indicating statistical test: §=ordinary one-way ANOVA with Tukey's correction, ◊=Welch's test with Dunnett's T3 correction. Significant p-values: *≤0.05, **≤0.01, ***≤0.001, ****≤0.0001. (Continues on next page).

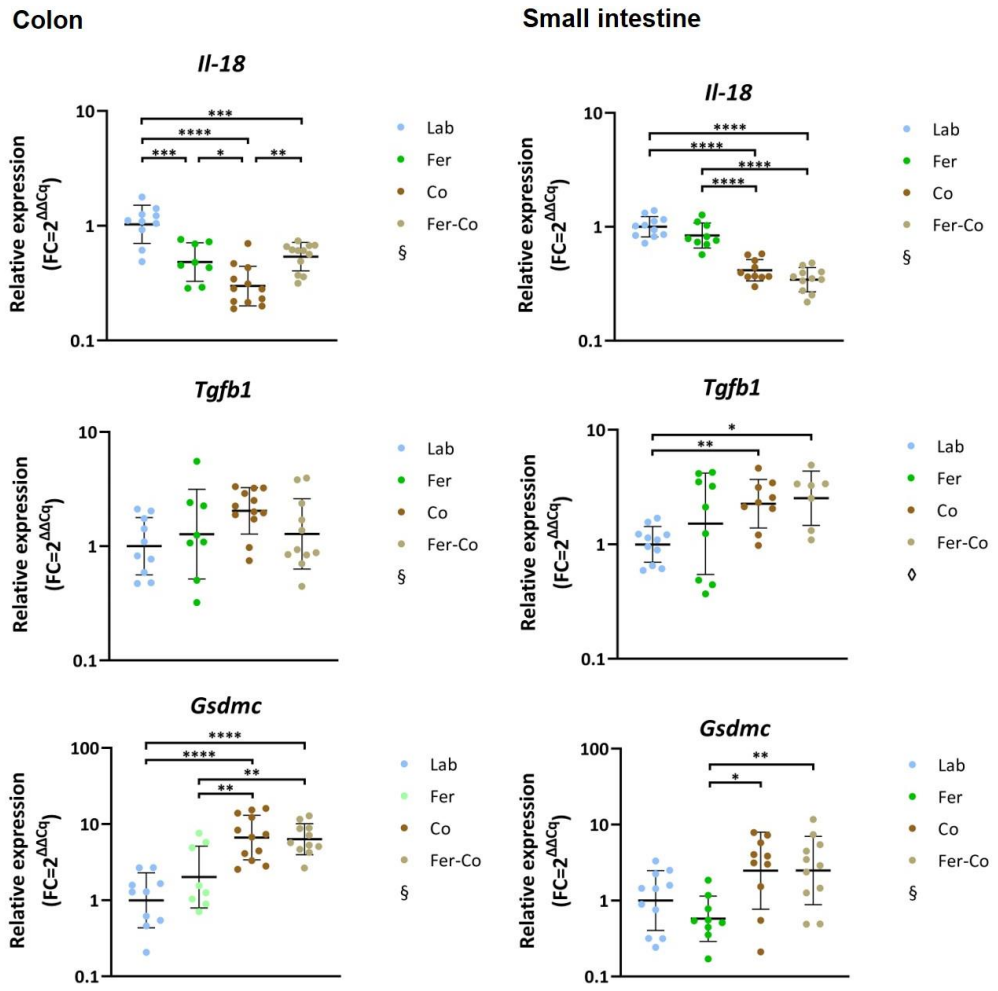

Figure 4.6 - Relative expression of inflammation related genes in cells from colonic and small intestinal epithelium. (Continued).

In conclusion, the expression of these inflammation-related genes show similar expression patterns in both colon and SI and seem highly affected by cohousing with wild mice.

4.3.5 Expression of genes related to ROS/RNS production were increased in both colon and small intestine of cohoused mice

Expression of several of the genes important for ROS/RNS production in the gut were found higher in the colon as well as the SI of cohoused mice relative to Lab mice and Fer mice (Figure 4.7). *Duox2* and *Nox1*, encoding ROS-producing enzymes, were higher expressed in the colon of Co mice (4.89- and 3.66-fold, respectively) and Fer-Co mice (4.50 and 4.81-fold, respectively), as well as *Nos2*, encoding an RNS-producing enzyme (37.40- and 20.65-fold higher in Co and Fer-Co, respectively). Moreover, only *Duox2* and *Nos2* were differentially expressed in the SI (3.14- and 2.57-fold higher in Co mice and 3.26- and 1.7-fold higher in Fer-Co mice, respectively). No changes were found for the Nrf2-pathway target genes *Nqo1* and *Hmox1* that are involved in protection against oxidative stress on cells due to increased ROS/RNS production (Table 4.4). These results indicate a

higher expression of ROS/RNS-producing enzymes mRNA in cohoused mice both in colon and SI in response to a microbially enriched environment.

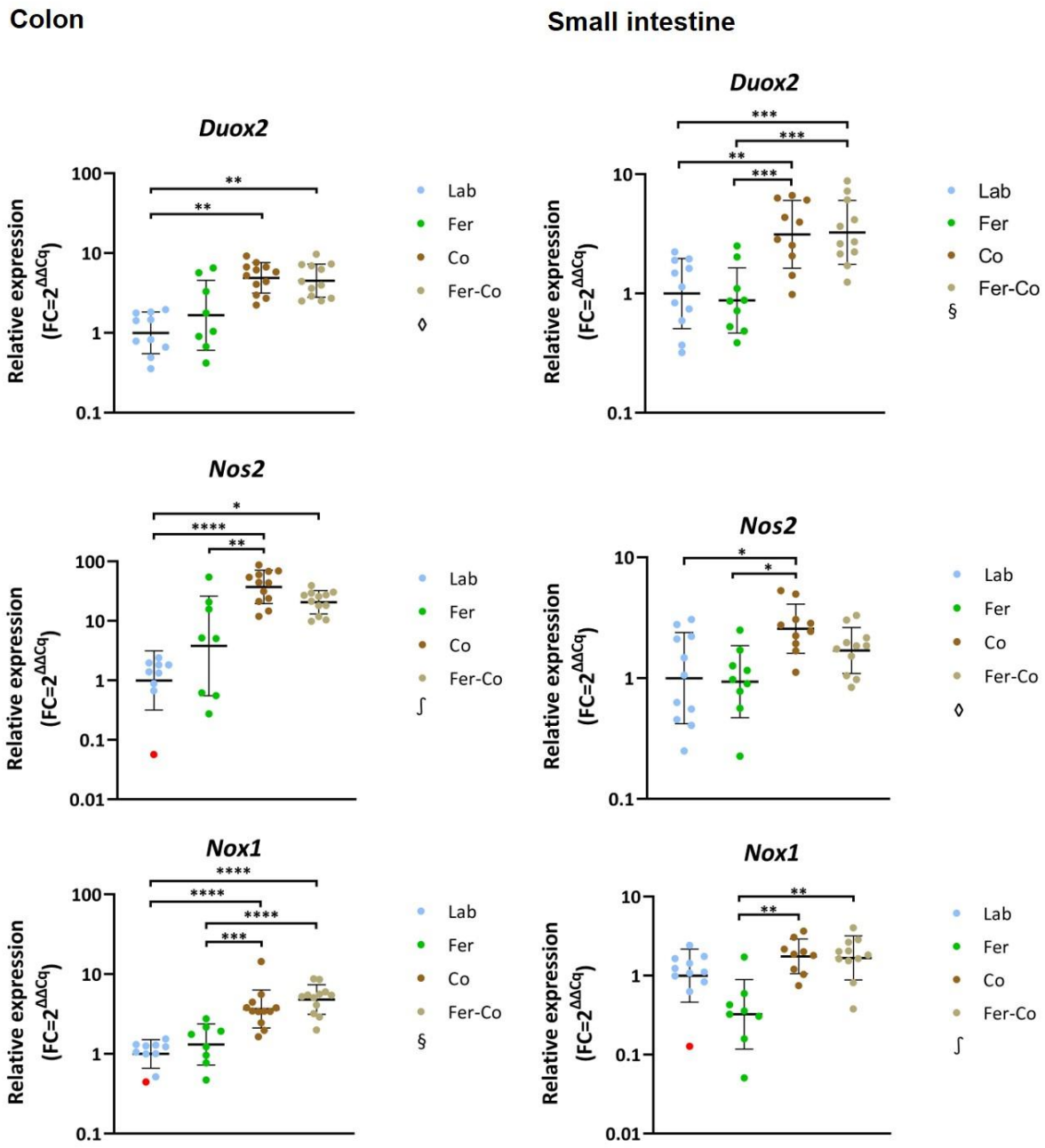

Figure 4.7 - Relative expression of ROS/RNS related genes in cells from colonic and small intestinal epithelium. Plotted is the relative expression of some of the ROS/RNS related genes in cells from colonic and small intestinal epithelium. Each symbol represents one animal, the horizontal bars represent the geomean of the group, and the error bars represent the standard deviation in each group. Relative expression ratios expressed as fold change $FC=2^{\Delta\Delta Cq}$ relative to the mean of control group on a log10 scaled axis. Symbols indicating statistical test: §=ordinary one-way ANOVA with Tukey's correction, ∫=Kruskal Wallis with Dunn's correction, ◊=Welch's test with Dunnett's T3 correction. Significant p-values: *≤0.05, **≤0.01, ***≤0.001, ****≤0.0001. *Red dots*: identified as outlier and not included in statistical analysis. Included in figure for the purpose of making geomean (Lab)=1. Outcomes of statistical analyses were the same with or without.

Although most prominently in the colon, there appears to be a considerable effect of cohousing on the general expression level of genes related to the oxidative environment in the intestinal epithelium.

Table 4.4 – (Next page) Fold change of gene expression in cells from colonic and small intestinal epithelium relative to Lab. Presented are the fold change value of each gene in colon and SI for all experimental groups as the geomean of the group. C=colon, SI=small intestine, Test=type of statistical test of differences between group means with α=0.05. Group comparisons: 1: Lab vs. Fer, 2: Lab vs. Co, 3: Lab vs. Fer-Co, 4: Fer vs. Co, 5: Fer vs. Fer-Co, 6: Co vs. Fer-Co. Statistical test: a: ordinary one-way ANOVA with Tukey's correction for multiple comparisons, b: Kruskal Wallis with Dunn's correction for multiple comparisons, c: Welch's test with Dunnett's T3 correction for multiple comparisons. Significant p-values: *≤0.05, **≤0.01, ***≤0.001, ****≤0.0001. †: outlier(s) removed from group. FC-values with **bold font**: significantly different from Lab. Seg. = (intestinal) segment.

Function			Fold change ($2^{\Delta\Delta Cq}$)						P-value		Test	
	Seg.	Both	C			SI						
	Gene	Lab	Fer	Co	Fer-Co	Fer	Co	Fer-Co	C	SI	C	SI
Barrier	*Cdh1*	1	0.93	1.15	1.14	1.04	**1.54†**	1.47	0.40	*2, 4	b	a
	Clca1	1	1.75	**7.17**	**9.84**	1.16	**2.45**	1.76	***2 ****3 *4 **5	*2	a	a
	F11r	1	0.95	1.06	1.01	1.10	1.16†	1.07	0.93	0.40	b	a
	Fcgbp	1	1.41	**3.07**	**5.43**	1.15	1.06	0.73	*6 **4 ****2, 3, 5	*6 **5	a	a
	Muc2	1	0.83	0.96	1.26	0.98	1.32	0.93	0.18	0.06	a	a
	Muc3	1	1.09	1.34	1.18	**1.70**	0.79	0.89	0.47	*1 **4, 5	b	a
	Mylk	1	1.23	0.94	0.85	0.97	0.99	0.89	*4, 5	0.55	c	c
	Ocln	1	0.85	0.66	0.83	0.90	0.56	0.69	0.16	0.06	b	b
	Tjp1	1	0.92	1.00	0.96	1.11	1.01	0.89	0.98	0.74	a	a
Antimicrobial	*Ang4*	1	**7.61**	**59.71**	**75.76**	0.78	1.44	**1.81**	*1, 4, 5 ****2, 3	*3, 4 **5	c	a
	Defa24	1	7.05	**38.94**	**30.30**	0.94	1.16	1.12	**2, 3	0.99	a	b
	Itln1	1	9.90	**112.02**	**147.56**	0.96	0.83	0.93	*5 ****2, 3	0.71	c	c
	Reg3b	1	1.70	0.18	**0.10**	1.02	1.14	0.66	*4 **3 ***5	0.08	b	a
	Reg3g	1	1.35	**0.25**	**0.17†**	0.71	1.21	**0.51**	**2 ***4 ****3, 5	*3 **6	a	a
	Retnlb	1	7.74	**52.51**	**59.76**	1.01	**10.99**	**16.84**	*5 ***2 ****3	****2, 3, 4, 5	b	a
Immuno-surveillance	*Nod1*	1	0.83	1.49	1.13	1.14	**2.66**	**1.88**	*4	**3 ***4 ****2	a	a
	Nod2	1	1.36	1.38	1.63	0.80	**2.27**	**2.75**	0.06	*2 **3, 4 ***5	a	a
	Tlr2	1	0.94	0.79	0.81	0.89	**2.46**	**2.20**	0.28	**3, 5 ***2, 4	a	a
	Tlr4	1	1.46	1.43	**1.72**	2.82	1.29	2.05	*3	0.09	a	a
	Tlr5	1	0.92	**0.43**	**0.55**	0.80	**0.49**	**0.48**	*5 **3 ***4 ****2	*2, 3	a	a
	Zbp1	1	**5.92**	**16.08**	**8.10**	1.37	**3.79**	**3.39**	*1, 3, 6 ****2	****2, 3, 4, 5	b	a
Inflammation	*Alpi*	1	1.42	1.85	1.40	1.34	0.99	1.15	0.36	0.69	b	b
	Il-10	1	2.90	**23.40**	5.04	0.35	**8.33**	4.58	*6 **2, 4	*2 **5 ***4	a	a
	Tgfb1	1	0.96	0.81	0.91	1.52	**2.26**	**2.53**	0.09	*3 **2	a	c
	Il-18	1	**0.47**	**0.29**	**0.52**	0.84	**0.42**	**0.34**	*4 **6 ***1, 3 ****2	****2, 3, 4, 5	a	a
	Il-1b	1	0.70	**2.42**	0.62	1.06	1.15	1.09†	**2 ****4, 6	0.36	a	a
	Il-25	1	1.25	1.09	1.25	0.81	0.41	0.73	0.98	0.36	b	a
	Nlrp6	1	**1.59**	1.24	1.17	1.12	1.18	1.07	*5 ***1	0.82	a	a
	Saa1	1	1.02	0.82	0.81	1.57	**7.00**	4.32	0.66	*4 **2	a	b
	Lcn2	1	0.63	1.01	0.62	1.73	**6.28**	2.61	0.58	**2	c	a
	Gsdmc	1	2.02	**6.66**	**4.61†**	0.58	2.47	2.49	**4, 5 ****2, 3	*4 **5	a	a
	Gsdmd	1	1.54	2.10	1.38	1.52	1.66	1.57	0.16	0.29	b	a
	Mir31	1†	0.31	0.65	1.20	0.27	1.27	0.83	0.28	0.06	a	a
ROS/RNS-production	*Duox2*	1	1.66	4.89	4.50	0.88	3.14	3.26	****2, 3	**2 ***3, 4, 5	c	a
	Hmox1	1	0.65	**1.12**	**1.05**	0.83	**4.44**	**1.67**	0.90	0.10	b	b
	Nos2	1†	3.81	37.40	20.65	0.93	2.57	1.70	*3 **4 ****2	*2, 4	b	c
	Nox1	1††	1.31	**3.66**	**4.81**	0.33	**1.75**	1.68	***4 ****2, 3, 5	**4, 5	a	b
	Nqo1	1	0.96	**0.83**	**0.83**	0.74	0.93	0.90	0.75	0.41	a	a

As a general and final remark, these results indicate a significant effect of cohousing with wild house mice, as cohoused mouse groups show significantly altered expression of genes within all categories. The most dramatic changes are seen in the colon, with genes

such as *Itln1* being expressed almost 150-fold higher in Fer-Co. In the SI, the biggest change is an increase of 17-fold of *Retnlb* mRNA in Fer-Co. Moreover, expression is significantly altered in a higher number of genes in the colon than in the SI.

4.3.6 Possible effect of conducting the gene expression analysis in two separate runs

For some genes it was observed large variation in the expression rates within groups, and it appeared that values were separated in two discrete clusters around the means. This gave concern that other factors beside the treatment could cause or affect the observed differences in relative gene expression between groups. An illustrative example is seen in *Hmox1* (Figure 4.8). Highlighting the Fluidigm plate (IFC) from which the data came (which of the two runs) supported this concern and brought the name "run effect". This "run effect" was especially noticeable in genes with low expression (high Cq-values, not shown), which was the case for *Hmox1* in the example below.

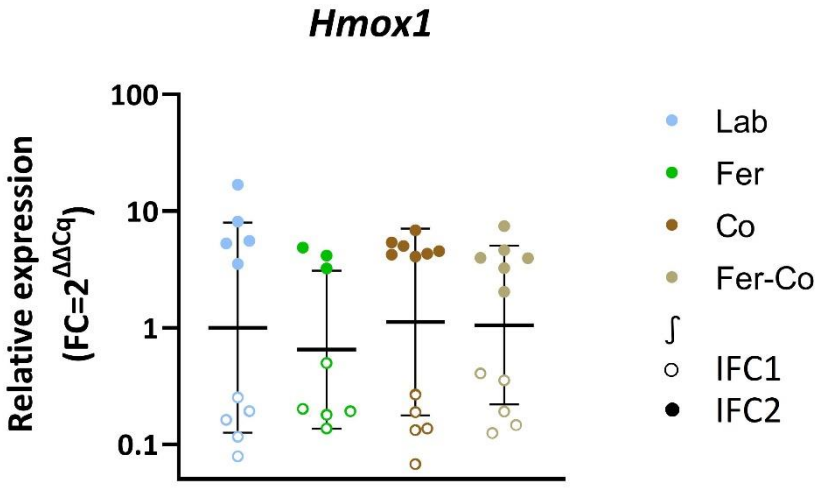

Figure 4.8 - Relative expression of *Hmox1* in colonic epithelium with IFC source. Open points are from IFC1 (run 1), filled points are from IFC2 (run 2).

To test whether the "run effect" was a global issue affecting all genes in the panel, a principal component analysis (PCA) was conducted on the colonic fold-change values of all genes to further assess the observed variation in the gene expression data. Principal components (PCs) are uncorrelated, linear variables drawn from the original data, along which the data are observed to spread (Ringnér, 2008). Hence, they contain a proportion of the variance within the data set, the largest proportion found in the first component. Highlighting the run number/IFC plate (1 or 2) in the plot of PC1 (contains 37.4% of variance) against PC2 (contains 18.0% of variance) revealed a separation of data according to which run/plate the data came from along PC1 (Figure 4.9). Along PC2, the data seemed to spread more according to group (Figure 4.9), more clearly observed in the plot of PC2 against PC3 (contains 9.4% of variance) (Figure 4.10).

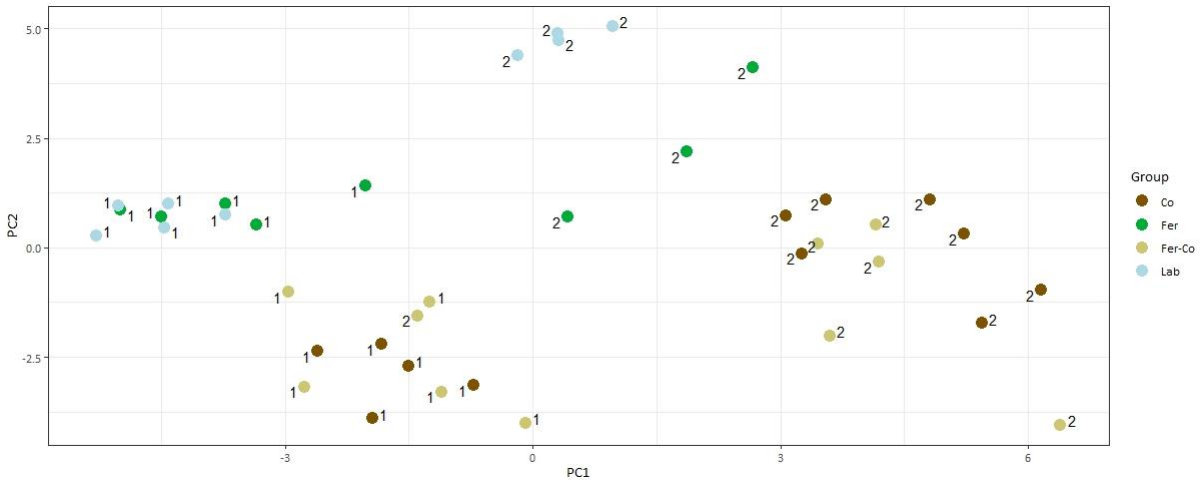

Figure 4.9 – "Run effect" on colonic gene expression data. Plotted are PC1 and PC2 explaining 37.4% and 18% of the variance, respectively. 1=from first run (IFC1), 2=from second run (IFC2).

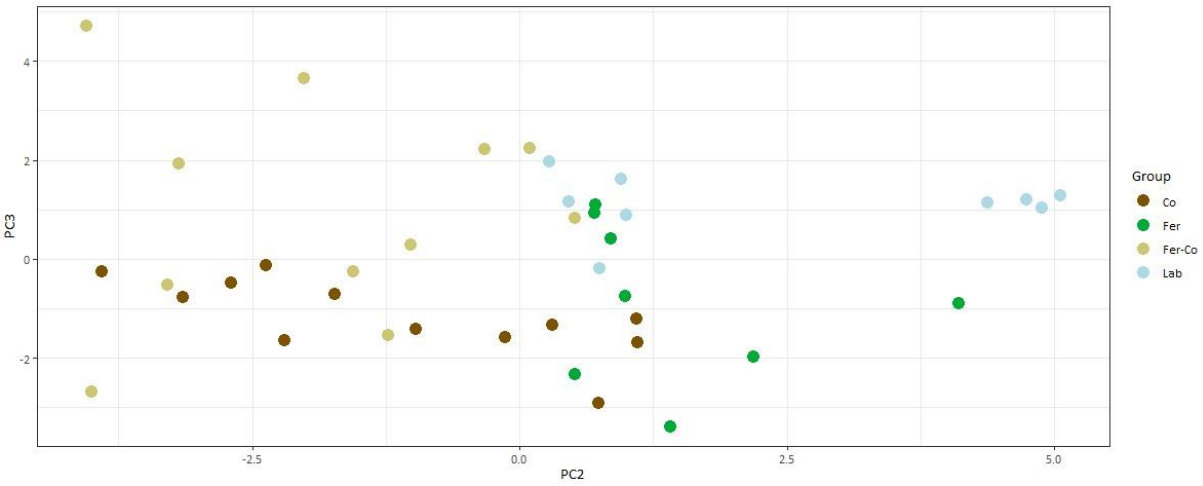

Figure 4.10 - PCA plot of colonic relative gene expression ratios. Plotted are PC2 and PC3 explaining 18% and 9.4% of the variance, respectively. Cohoused mice (brown and khaki) cluster more to the left than Fer and Lab (green and light blue).

In conclusion, these plots indicate a possible variation in the data relating to which of the two runs they originated from; however, the second-to-largest proportion of variation appears to be caused by treatment.

5 DISCUSSION

Previous studies have suggested significant effects of naturalization on murine immune responses, development, and training. The intestinal epithelial layer is an important part of the innate immune system but has not been studied as extensively as the cellular and humoral immune responses. The aim of the current study was to assess the effect of different modes of naturalization on the intestinal barrier in mice, reflected in the relative expression levels (REL) of genes related to this function. B6 mice were exposed to three different modes of naturalization, and the REL of intestinal-barrier-function-related genes mRNA in IECs was determined using high-throughput microfluidic real-time qPCR.

This current project showed that differential housing of B6 mice significantly altered the REL of barrier-function-related genes in cells from colonic and small intestinal epithelium. All three modes of naturalization differ significantly from the control group; however, the results suggest a greater effect on RELs by cohousing with wild house mice than feralization alone. Genes relating to the antimicrobial function stood out in the results, a response supporting previous findings of an enriched and altered gut microbiota, in addition to greater activation of immune-related functions, in naturalized mice.

The following will be the main points of discussion:

1. Animal welfare and health in new housing conditions
2. Effect of naturalization mode on relative gene expression in cells from colonic and small intestinal epithelium
3. Methodological considerations

5.1 Animal welfare and health in new housing conditions

5.1.1 Detection of parasitic eggs and (oo-)cysts in naturalized mice

Giardia cysts were detected in fecal samples from wild mice (from the Co-pen) and Fer mice in this study; however, this was not detected in fecal samples of feralized mice in the study of Arnesen et al. from 2021 when testing for *Giardia* and *Cryptosporidium* (Arnesen et al., 2021a). One possible explanation for this difference is that the previous study failed to detect them, and another being that the mouse pens in the current study were contaminated with wild mouse feces or parasitic eggs/(oo-)cysts via equipment used to collect fecal samples. Cysts and oocysts can easily survive outside of its host and are resistant to several decontaminating chemicals, making the risk of contamination more likely (Pineda et al., 2020). Interestingly, although *Giardia* was detected in samples from wild mice from the Co pen, it was not detected in any of the cohoused B6 mice. Mice in which *Giardia* was detected were from different housing groups, suggesting that the Fer-pen was either contaminated, or *Giardia* cysts must have come from the feralizing material. In fact, *Giardia* has previously been detected in livestock, so it cannot be ruled out that the feralizing material was also a carrier of parasites (Cao et al., 2020; Koudela et al., 1991; McAllister et al., 2005; Paruch & Paruch, 2022; Petersen et al., 2015; Robertson, 2009).

5.1.2 Lower weight development in feralized mice

All mice showed an increase in body weight from start to end of the experiment, but weight increase in the feralized mice was significantly smaller compared to the other groups. As this was not further investigated, only speculations can be made about this observation. Influence of microbiota on efficiency of nutrient metabolism and uptake, as well as correlations between obesity and altered gut microbiota, has been demonstrated by others (Aoun et al., 2020; Hild et al., 2021). Hild and coworkers demonstrated that B6 mice with a wild-mouse-derived microbiota ("wildlings") were protected against extreme weight gain when fed a high fat diet over a 10-week period, reflected in the finding of a significantly higher body fat percent in standard SPF B6 mice compared to wildlings. The same was observed for SPF B6 mice and wildings that were fed a regular chow diet. They further determined that the difference in fat percentage between SPF B6 mice and wildlings was *not* due to differences in food intake, loss of nutrients in feces, or different absorption. Instead, they found marked changes in metabolic markers including higher secretion of digestive hormones, and energy expenditure in brown fat tissue, in wildlings. Hence, changes in metabolism due to an altered gut microbiota may propose a possible explanation for the difference observed in this study. It was therefore surprising that this was only observed in feralized mice, who were not in contact with wild mice, and not the cohoused mice. Interestingly, feralized B6 mice in the study by Arnesen et al. showed significantly *higher* weight increase than "clean" B6 mice (Arnesen et al., 2021a). Thus, there could possibly be something else explaining the observation in the current study. Despite contradictive results compared to previous studies, there are compelling evidence that differences in the gut microbiota affects weight development, and it would be interesting to further investigate effects of naturalization on metabolism.

Moreover, the most common sign of infection with *Giardia* in mice is reduced weight gain (Barthold, 1997). Interestingly, the lowered weight development observed in the Fer mice in this current study could agree with a *Giardia* infection. *Giardia* was not detected in samples from B6 mice from Co and Fer-Co pens, which may explain why the same lowered weigh development was not observed in these two groups. However, other parasitic (oo-)cysts were detected there. Further evaluation of the possibility that parasitic infections had implications in weight development would require assessment of more fecal samples from all experimental weeks.

5.1.3 Immune cell fraction in the epithelial cell suspension

The results from flow cytometry showed that a portion of the IEC suspension was CD45+ indicating an immune cell (leukocyte) contamination. Although IECs made up the major fraction of the epithelial cell suspension, it cannot be ruled out that other cells have been a source of some of the isolated mRNA, affecting gene expression results to a varying and unknown degree. This is important to keep in mind as they may perhaps have been the source of gene expression patterns that were difficult to explain based on the knowledge of IECs.

5.1.4 Elevated cell turnover in the colon of naturalized mice

Ki-67 is an intracellular marker of active cell division, and its expression in the colon of all three naturalized mouse groups was higher than in lab mice. Elevated cell turnover rates comply with an increased presence of microbes, and matches findings by Reikvam and coworkers where cell turnover rates reflected in Ki-67+ cells were lower in microbiota depleted mice compared to conventionally raised mice (Reikvam et al., 2011). Increased cell turnover is also important in restitution of the epithelial cell layer after death of cells as a consequence of infection and inflammation. The difference in the SI was not as prominent as in the colon, which complies with the much lower abundance of microbes in the SI. Moreover, the overall turnover rate is commonly higher in the SI than the colon due to thinner mucus (Williams et al., 2015). In conclusion, the colonic increase in epithelial cell turnover facilitates a healthy colonic barrier by renewing IECs exposed to luminal microbes, as they are more prone to damage and stress caused by an increased complexity of the gut microbiota.

5.2 Effect of naturalization mode on relative gene expression in cells from colonic and small intestinal epithelium

5.2.1 Barrier related genes

Relative expression of Clca1 and Fcgbp mRNA was higher in the colon of the cohoused groups, while the expression of Muc2 an Muc3 mRNA remained unchanged. Findings presented in paper IV (not published) in the dissertation of Arnesen included upregulation of Fcgbp in colonic mucosa of feralized mice, and similar mucus thickness in both colon and ileum when comparing feralized and lab mice (Arnesen, 2021). These findings support the observed higher levels of Fcgbp mRNA and unchanged mucin expression in this current study. A different study by Nyström et al. speculated that the cleavage of Muc2 N-terminal domain by Clca1 is important in mucus structural rearrangements (Nyström et al., 2019). Moreover, although the function of Fcgbp is still not fully understood, Ehrencrona and coworkers mentioned in their study that Fcgbp is possibly involved in mucus formation and rearrangement (Ehrencrona et al., 2021). Therefore, it could be argued that even though the thickness may not have changed, the composition and structure could still have been altered. A study supporting this argument is one by Jakobsson et al. showing that SPF B6 mice from the same strain that were housed in two different rooms in the animal lab had different colonic mucus properties (Jakobsson et al., 2015). However, they did not find significant differences in protein abundance (including proteins such as Fcgbp, Clca1, and Muc2). They additionally found that the colonic mucus in wild house mice was thicker and less penetrable (i.e., stronger) than that of B6 mice. Interestingly, the difference in mucus phenotype seen in mice from the two separate rooms was reproduced in GF mice following transfer of cecal material from the two mouse groups into GF mice. Bacterial composition was almost identical in mice from the two rooms, suggesting that only a few specific bacteria were sufficient for creating different mucus properties. Although no differences were found in protein abundance, the hypothesis that few and specific bacterial species can affect mucus

properties could complement the observations in this current study. It could also complement all other observations, since altered mucus properties affects the probability of contact between microbes and the epithelium.

Another interesting aspect of Clca1 is that in a mouse-study from 2016, its expression was correlated with the impaired immunity that resulted from lacking AMCase, a digestive enzyme induced by infection with the parasite *H. polygyrus* (Vannella et al., 2016). This parasite was detected in one of the wild mice in the Co-pen. Although not detected in the B6 mice, it could be interesting to investigate if this has been a possible driver of increased *Clca1*-expression in cohoused mice since this gene was *not* found to be different in Fer.

No changes were found in the expression of junction-encoding genes, except from a slight increase of *Cdh1* in the SI of the Co-group. Albeit not significant, there seemed to be a slightly higher expression level of this gene in the Fer-Co group as well. The adherence junction protein E-cadherin encoded by *Cdh1* is important in cell-cell contact and is reduced and degraded during inflammation (Schnoor, 2015). Moreover, it is also known to be an important epithelial surface marker that is lost when epithelial cells obtain epithelial-to-mesenchymal-transition phenotype where E-cadherin is downregulated, commonly found in tumor progression and metastasis (Serrano-Gomez et al., 2016). This because the cells are then more likely to leave the monolayer and escape to other tissue sites, a behavior associated with cancerous cells. Thus, E-Cadherin is an important tumor suppressor protein, and its upregulation could be important in protection against tumor development. However, an increase of *Cdh1* expression in this study was only seen in the SI, and SI-cancers are relatively uncommon (Chen et al., 2021). Nevertheless, the observed increase in *Cdh1* mRNA levels indicates strengthened cell-cell adherence which is beneficial for the barrier integrity (Schnoor, 2015).

5.2.2 Antimicrobial related genes

Reg3 proteins are antimicrobial peptides whose expression is commonly increased in response to detection of luminal microbes through TLR-MyD88 signaling ((Mukherjee & Hooper, 2015), section 1.5). The observed decrease in Reg3 mRNA levels in the colon of cohoused mice was therefore unexpected because the expression of genes encoding these proteins are higher when microbial exposure is higher, which is assumed to be the case in the naturalized mice in this current study based on previous studies ((Arnesen et al., 2021b; Leung et al., 2018; Lin et al., 2020; Rosshart et al., 2019), section 1.8). Moreover, mice depleted of their microbiota show decreased expression levels of AMPs including *Reg3γ* and *-β*, *Ang4*, and *Retnlb* in colonic IECs, supporting an expectation of increased expression (Reikvam et al., 2011). Other studies have shown that the specific type of microbe have different effects on *Reg3*-expression; some induce, others reduce (Sonnenburg et al., 2006). Burger-van Paassen and coworkers showed a connection between altered microbiota and altered *Reg3*-expression, while Cash et al. proposed that other defense mechanisms such as increased sIgA secretion limited contact between epithelium and microbes, and therefore there was less stimulation of *Reg3*-expression (Burger-van Paassen et al., 2012; Cash et al., 2006). Moreover, changes in mucus

properties (as suggested in section 5.2.1) could alter the contact between the microbiota and the epithelium, thus affecting expression. However, this is not reflected in conventionally raised mice lacking the poly-Ig-receptor (aka not secreting IgA), where the expression of *Reg3* mRNA was not different from wild type mice (Reikvam et al., 2012). Although it is difficult to provide detailed explanations of the observations made in this current study regarding *Reg3* expression, it is likely due to an altered microbiota composition or altered microbe-IEC interactions, nonetheless.

Little or no change in expression of Reg3 mRNA was observed in the small intestine. Burger-van Paassen et al. also showed in their study from 2012 that Reg3-proteins are weakly expressed in the small intestine of WT mice, but increased in Muc2-deficient mice, supporting the idea of mucus being important in limiting microbe-epithelium contact and thus induction of Reg3 mRNA expression. It is important, however, to remember that these plots are relative, and comparing colon and small intestine do not answer questions about abundance.

Expression of antimicrobial peptides *Ang4*, *Itln1* and *Retnlb* was significantly higher in the colon of the cohoused mice and complies with expected responses to increased microbial exposure (Hooper et al., 2003; Levy et al., 2015; Nonnecke et al., 2021; Propheter et al., 2017). Their increased expression has been shown to be induced by Il-18 via Nlrp6 (Levy et al., 2015). However, *Il-18* expression was found downregulated in this present study, and no significant changes were seen in relative expression of *Nlrp6* (see section 5.2.4). Therefore, a different mechanism may explain the increased expression of these AMPs, but Il-18 stimulation can also come from other cells than the IECs themselves. Thus, the observed decreased mRNA level of *Il-18* does not necessarily rule out this cytokine as a driver of the heightened AMP expression observed in this present study.

Itln1 was almost 150-fold higher expressed in colon of Fer-Co relative to Lab, which can seem quite extreme, however it is important to note that these are relative values, and *Itln1* is generally higher expressed in the SI than in the colon (Almalki et al., 2021). Nevertheless, there is a clear upregulating effect of cohousing in these three AMPs, suggesting a strengthened barrier in response to increased microbial exposure. An interesting remark is that the protein encoded by *Retnlb*, Relm-β, is also involved in host defense against parasites (Artis et al., 2004; Propheter et al., 2017).

The α-defensin gene *Defa24*, encoding an AMP highly secreted by Paneth cells, showed high expression in the colon of naturalized mice compared to Lab mice. However, α-defensins have been shown to be restricted to small intestinal epithelium (Castillo et al., 2019). The Cq values of colonic *Defa24* were much higher compared to those in the SI samples, indicating that it is much less expressed in the colon. This may also account for the large variation in the data. Castillo et al. argue that interpretation of lowly expressed *Defa*-genes should be executed with caution. Moreover, detecting distinct *Defa*s has been shown to be quite difficult due to their high sequence similarity. Therefore, the *Defa24*-colon plot may give limited information. No change in expression was seen for *Defa24* in the SI.

5.2.3 Immunosurveillance related genes

Zbp1 encodes the pathogenesis-recognizing protein Zbp1 and has been related to related to immune responses to virus infections (Kuriakose & Kanneganti, 2018). Zbp1 mRNA was higher expressed in both small intestine and colon of cohoused mice and, albeit not significant, there seems to be some elevation in the colon of Fer as well. *Zbp1* was also previously found to be higher expressed in mucosa of feralized mice (not published (Arnesen, 2021)). Zbp1 has been shown to induce proinflammatory cytokine production through activation of NF-κB in response to immunostimulatory DNA (e.g., viral) (Kuriakose & Kanneganti, 2018). Its elevated mRNA levels may possibly indicate presence of viruses in the intestinal epithelium, and it has been shown that both viruses and parasites are highly prevalent in wild *M. m. domesticus* (Viney et al., 2015). Transfer of a significant virus burden was highly likely in co-housed mice, and conceivable also in feralized mice; however, this would need further investigation.

Nod1 and Nod2 are important intracellular PRRs, and the Nod mRNA expression was found higher in the small intestine of cohoused mice. Nod2 is mostly expressed in Paneth cells, while Nod1 has been found to be expressed in all IECs. Nod expression is important in homeostasis, considering their downstream signals to induce production of AMPs and cytokines, and influencing TLR signaling, in response to microbially derived ligands (Chu & Mazmanian, 2013; Parham, 2015). The observed expression increase could be an adaptation to increased microbial abundance in naturalized mice, to sustain the homeostatic environment.

Tlr5, another PRR that specializes in bacterial flagellin recognition, was surprisingly found downregulated in both colon and SI of cohoused mice. TLRs are normally expected to show increased expression in response to an elevated microbial load, as demonstrated by comparing expression levels in GF and SPF mice (Lundin et al., 2008). Tlr5 induces proinflammatory responses to flagellin, so it could be tempting to speculate if it is downregulated to maintain the anti-inflammatory state in the intestine due to an increased flagellin exposure. Alternatively, less contact is made between Tlr5 and flagellin because there is a decrease in the proportion of flagellated bacteria or because of altered mucus properties (section 5.2.1) (Eshleman & Alenghat, 2021; Gewirtz et al., 2001). Tlr2 (binds microbial lipoprotein) mRNA was found higher expressed in the SI. In humans, Tlr2 has been shown to induce an anti-inflammatory state through stimulation of Tregs that secrete Il-10 in response to specific metabolites of *Bacteroides fragilis* (Chu & Mazmanian, 2013). Hence, increased expression may help improve the barrier by adapting to specific microbes in an altered gut microbiota, as the promotion of Treg development is mostly beneficial in the gut to avoid unnecessary inflammation and tissue damage.

5.2.4 Inflammation related genes

The increased expression of the cytokine Il-10 mRNA found in the colon of all naturalized mice, although only statistically significant in Co-mice, as well as in the Co-mouse small intestine, supports an improved barrier function; not only because Il-10 is anti-inflammatory, but also its seeming importance in regulation of intracellular junctions, and

the impaired barrier that results from Il-10 receptor deficiency (Andrews et al., 2018; Kominsky et al., 2014). Il-10 expression has also been shown to increase in response to Tlr2 and -4 activation, further supporting its role in barrier integrity (Latorre et al., 2018).

The role of the cytokine Il-18 is debated in research and argued to be context dependent, as it can both protect against and promote inflammatory states in the intestine (Nowarski et al., 2015; Williams et al., 2019). However, it is mostly considered a proinflammatory cytokine, as is Il-1β, important to maintain intestinal homeostasis through for example promotion of AMP secretion (Williams et al., 2019; Zheng et al., 2021). Surprisingly, in this current study, Il-18 was significantly lower expressed in both the colon and SI in all groups (only not significant in SI of Fer), while Il-1β was higher expressed in Co-mouse colon; no other differences were found for Il-1β. This is somewhat contradictive with the literature, as these two cytokines are normally co-regulated through Nlrp6 – whose expression was not different either, except from a slight elevation in Fer colon. Nlrp6 is in the NLR-family and activates IL-18 and Il-1β in response to MAMP-recognition (Zheng et al., 2021). No change was found in expression of Il-25 mRNA in either segment in any group. Il-25 is a pro-inflammatory cytokine constitutively secreted by tuft cells and expression is increased in response to helminth infection (Allaire et al., 2018). Interestingly, this could contradict the previous suggestions of parasite infection being an explanation of other observations; however, Il-25 may only be secreted during the active presence of a live parasite in the lumen and not when there are only eggs, or the parasite is in another stage of its life cycle. Investigating expression at earlier time points could perhaps answer this question. It is difficult to draw any conclusions about these observations, and a more thorough examination of these and many more cytokines should be conducted for more information about naturalization effects on cytokine expression.

Expression of Saa1, an acute phase protein that induces pro-inflammatory responses, has previously been shown to increase in response to SFB in ileum (Sano et al., 2015). The observed increase in Saa1 mRNA expression in the small intestine of Co-mice may indicate an increased number of SFB derived from wild mice, albeit the relative expression was not significant in the Fer-Co mice. No difference in Saa1 mRNA expression was observed in the colon, however this complies with the fact that SFB mainly colonize in the ileum (Oemcke et al., 2021). Moreover, Saa1 is involved in activation and recruitment of Th17 cells. Although these cells are considered as pro-inflammatory, they are important for barrier homeostasis in that they protect against invading microbes in the gut and can for example induce epithelial cells to increase secretion of AMPs (Atarashi et al., 2015; Oemcke et al., 2021; Sano et al., 2015).

Gsdmc is a pyroptotic protein related to inflammatory responses, and a target gene of type 2 cytokines which promotes a type 2 response in tuft cells to parasite infection (Xi et al., 2021). It induces pyroptosis by forming a pore in the cell membrane, which is in part to allow release of pro-inflammatory cytokines such as Il-1β to induce an immune response against the detected pathogen. Gsdmc mRNA expression was higher in the colon of cohoused mice, and its involvement in parasite defense could perhaps explain this

observation due to findings of parasitic eggs, cysts and oocysts, and elevation in other genes also related to a parasite response. However, it may also be a general response to increased microbial load, complying with its reduced expression observed in microbiota-depleted mice (Reikvam et al., 2011) and the fact that many parasites reside in the SI. Gsdmd has similar functions, although is not associated with a parasite response, and is also found to mediate Il-1β release without inducing pyroptosis and has been associated with pathogenesis of IBD (Bulek et al., 2020). However, no differences were observed in expression of Gsdmd mRNA.

5.2.5 ROS/RNS production related genes

Nox1, Nos2, and Duox2 are enzymes that produce ROS and RNS in response to elevated microbial exposure and inflammation (Aviello & Knaus, 2017; Aviello & Knaus, 2018; Matziouridou et al., 2018). Results show increase levels of Nox1 mRNA in colon of cohoused mice, and a significant difference in SI between Fer and the cohoused groups. Moreover, Nos2 is higher expressed in cohoused SI and colon. It could be expected to see equal elevation of the two, as the ROS/RNS they produce can react and form peroxynitrite which is toxic for bacteria (Matziouridou et al., 2018). Their expression is expected to increase in response to higher bacterial exposure, so this indicates an activation of expression to control colonization in the gut of naturalized mice – a crucial barrier function. *Duox2* expression is generally regulated by microbiota, such as induction by SFB (Aviello & Knaus, 2017; Aviello & Knaus, 2018). The heightened levels of *Duox2* mRNA in the SI of cohoused mice could comply with the observed increase in Saa1 mRNA in the SI of Co-mice, while in the colon other specific microbes or a general increased microbial load could account for the observed differences. In conclusion, the observed increase in ROS-enzyme gene expression follows the assumed increased microbial exposure in naturalized mice to maintain a healthy barrier by controlling the colonization and composition of the gut microbiota.

5.3 Methodological considerations

5.3.1 Experimental setup

Naturalized housing forms a complex environment, and to minimize variation and the possibility of observed effects being cause by something other than the treatment (naturalization), one should account for as many factors as possible. Controlled ambient temperature, relative humidity, and lighting, as well as standard feed and randomizing mice at every possibility, all contribute to increased experimental control. Considering the housing of mice in pens, it could have been an advantage to include a pen-control in which a group of B6 mice were housing in a "clean" pen with only woodchips and the standard essentials. This could perhaps help assessing possible cross contamination issues, and account for an effect of pen-housing itself.

Moreover, with naturalized mouse models comes a possible trade-off between experimental control and physiological relevance (Figure 5.1). With GF mice that live in sterile conditions, nearly all possible influencing factors can be controlled for. Simultaneously, this situation is the furthest away from nature, as illustrated with the wild house mice on the opposite side of the scale. They are as natural as can be, but with limited potential for control of environmental factors.

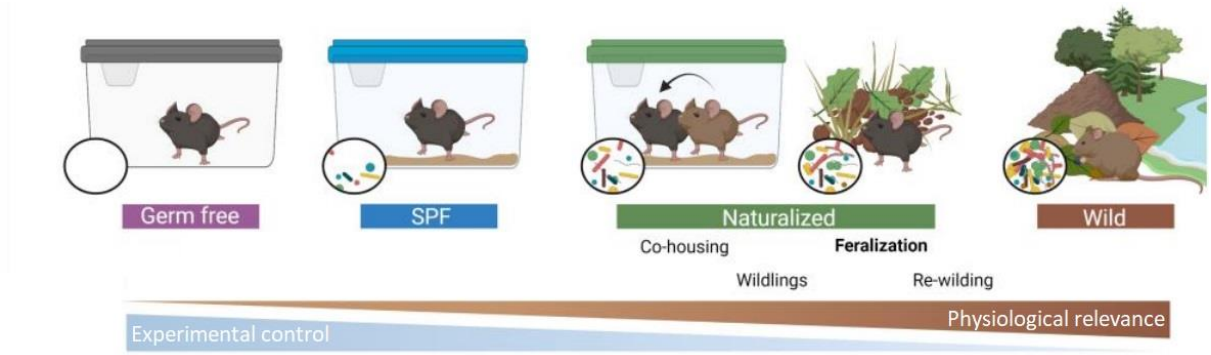

Figure 5.1 – Experimental control and physiological relevance of different modes of mouse naturalization. The figure illustrates how different mouse models can be placed on a scale of physiological relevance and experimental control, where increased physiological relevance of a housing model may come at the expense of experimental control. Illustrated is an increasing microbial complexity with increasing "dirtiness" and physiological relevance. Modified with permission from (Arnesen, 2021).

Hence, the downside of naturalization of laboratory mice may be that the physiological relevance comes at the expense of experimental control, as proposed by Arnesen in her PhD dissertation (Arnesen, 2021). Moreover, a different issue lies in reproducibility of naturalized mouse models. Different sources of naturalizing material has been used for all studies such as this current one, and for all to be comparable one would need a standardized naturalizing "formula". This could for example be a concoction of different bacteria, parasites, and viruses; however, this would again remove some of the naturalistic aspects. Nevertheless, a combination of studies done on mice in different housing conditions could be an advantage for drawing biologically relevant conclusions.

What should also be considered regarding housing conditions is the argument that mice from the same pen might not be considered as independent observations, which would have implications in statistics. This is in part because mice are known for coprophagy, which in this study is also something that is exploited because this is a way for the wild mice to share their microbiota with the B6 mice. However, this causes B6 mice to also share microbiota with each other. The same argument is used for mice housed in cages: their interaction with each other causes concern for the "cage effect", in that mice from the same cage should be considered as one experimental unit by using the average of the cohoused mice as the measured value (McCafferty et al., 2013; Åhlgren & Voikar, 2019). The same way, mice from the same pen could be affected by a "pen effect", perhaps accounting for the observed difference in body weight in mice in this current study.

5.3.2 Cohousing with wild house mice

Three wild mice were housed in each of the two cohousing pens, but optimally there should have been more to increase wild mouse microbial enrichment and avoid possible differences between the pens caused by random differences in the wild mice (e.g., which parasites they carry). Regarding the wild mice that were found dead speculations could be made if it was stress-induced, considering them lacking any of signs of struggle or injury. As mentioned in section 4.1.1, they were added later than the other wild and B6 mice, who were allowed to establish a colony before new wild mice were added. Territorializing by B6 mice could cause the newest members to struggle with adapting to the pen. Additionally, it could maybe have caused them to be unable to reach the feeding/drinking stations. Considering all other wild mice survived, it is not likely that they could not adapt to drinking from the water bottle. However, being restricted from both water and food sources for >24 h significantly alters physiology and wellbeing and could eventually lead to terminal dehydration (Bekkevold et al., 2013). Closer monitoring of mouse pens and their interactions would be necessary to further evaluate the cause of death. The reason they were added later than the other mice was simply that there was a limited catch, as it was not a "mouse year" in the season of autumn/winter 2021-2022. Moreover, the catch was conducted in the beginning of September, when it is still relatively warm outside, while most mice will move indoors closer to winter. This should be considered in future cohousing experiments.

5.3.3 Cell and RNA isolation

gDNA contaminations greatly affect gene expression analysis since it can function as a template for primers in a PCR reaction even though no mRNA is transcribed by the cell. Hence, it causes false positive samples. To further exclude the possibility of gDNA contamination, a NRT control should be included. It was not possible with the reagents used in this thesis but is highly recommended. However, the Bioanalyzer electrograms showed no signs of presence of gDNA, and nanodrop values would also uncover this contamination. Based on that, we proceeded with further analyses assuming the RNA was pure enough for qPCR. In future gene expression analyses with Fluidigm Biomark™ HD,

additional testing of new primers using reagents allowing the making of NRTs should be conducted for increased reliability of the results.

Combined treatment with DTT and EDTA was partly done to save time, both to make the protocol more efficient and to reduce total tissue incubation time to avoid cell death. However, a study aiming at isolating IELs showed that this combined treatment led to contamination with IECs and possibly LP cells (Qiu & Sheridan, 2018). This indicates that the protocol followed in this thesis may not be optimal to get pure epithelial cell isolates and may be the source of the previously mentioned cell contaminations (section 5.1.3). Another, although time consuming, alternative is to perform microbead separation of the isolated cell fraction, in which CD326-sepcific beads retain epithelial cells in a column while other cells are flushed through (*CD326 (EpCAM) MicroBeads Mouse*, 2021). This would not be realistic to do in this study due to the large number of samples but should be considered in smaller studies.

Further, also worth considering for future experiments is isolating cells from the entire intestinal segments, or specific segments. Genes such as those for oxidative stress are expressed the highest in the ileum because of the larger bacterial load than elsewhere in the small intestine. In this study, two pieces of the intestinal tracts were not included in isolation of IECs as they were dissected out for other purposes. This may influence detection of segment-specific genes. That said, all samples were treated equally, so the observed differences are not biased somehow due to tissue processing, and this would be more important in absolute quantification of mRNA. However, this should be accounted for if future experiments are to be comparable with this one (may affect reproducibility).

5.3.4 Primer assay validation and gene expression analysis

Not all primers were estimated to have an efficiency = 2. The use of "2" in calculations of FC assumes this, meaning the final FC-values may be inaccurate due to nonoptimal primers. Assuming E=2 when it actually is not, could potentially cause large variation in estimated number of mRNA in the original sample (highly over- or underestimating). Factors affecting primer efficiency that were not tested include dynamic range, optimal temperature, and optimal primer concentrations. Primers may vary in dynamic range, meaning they bind more optimally to the target under certain concentrations of template. Using a single concentration for all reactions, as done here, could cause some reactions to become saturated and others to bind nonoptimal and underestimate the number of template molecules. Due to differences in length and GC-content, primers have individual optimal annealing temperatures, and the concentration of forward and reverse primer could also affect binding efficiency (Bustin & Huggett, 2017). However, doing this had no purpose in this current study because the conditions in the Biomark™ HD instrument were pre-set, and the forward and reverse primers came pre-mixed. A preferrable alternative for further ensuring optimal primers would be to allow the Fluidigm company to test and optimize the primers in their own wet lab.

Moreover, for better estimation of primer efficiency, technical replicates should have been included, and the optimal testing could additionally need an accurate dilution series that could also assess the dynamic range mentioned above. The nonoptimal primer testing could be a limitation to this study and could be redone later since material is currently still available.

Further, the reference gene stability in the tissue to be analyzed should also be assessed, to avoid inappropriate normalization of Cq values. This is also a reason to use more than one reference gene. The choice of reference genes was based on previous studies on mouse intestines, albeit under different experimental conditions than ours. However, experimental conditions should not affect housekeeping-gene expression, but there are studies indicating that a particular reference gene could be more easily affected than others (e.g., *Gadph* vs. *Tbp* (Eissa et al., 2017)).

5.3.5 Implications of the "run effect"

Concern about a "run effect" rose from observations of data clustering in plots of relative gene expression according to which of the two runs of IFCs they originated from (first or second, example shown in section 4.3.6 (Figure 4.8)). The clustering observed along PC1 makes the "run effect" a possible explanation for the clustering observed in plots of relative gene expression. Ringnér noted that variation in data from high-throughput technology is much caused by experimental artifacts, of which the "run effect" is a good example (Ringnér, 2008). This was both surprising and not, as the execution of the first run (IFC1) was also the first time performing gene expression analysis with Biomark™ HD and inexperience can greatly affect performance; however, internal controls were included for this exact purpose (reference genes) and normalizing with reference genes should in theory remove variations due to, e.g., pipetting errors. The fact that the genes in question also had high Cq values could perhaps propose an explanation as very small differences in volume could greatly affect the initial number of mRNA molecules added to the PCR plate/IFC, a difference that becomes considerably large after preamplification and/or during the qPCR analysis due to the exponential nature of PCR (Korenková et al., 2015). Moreover, high Cq values could also simply be caused by noise. Issues rising from problems with variation caused by separating the samples on two different runs are mainly implicated in statistics as it increases variation within each group. This could make it difficult to observe significant differences between groups by using analysis of variance. It is likely that the variation would become smaller if the samples were run on the same day or simultaneously on one single IFC. Moreover, it is important to remember that a PCA does not identify directions of group separation, simply a direction in a multi-dimensional plot that accounts for the largest data variation. Characteristics used for identification of clusters are simply added to the plot for visualization of what may cause this identified variation. Hence, the effect of treatment is still an essential contributor to differences in relative gene expression levels and should still be considered the driver of differences between groups. In retrospect it would perhaps be an advantage to use an IFC that could fit all samples on one plate, allowing for all samples to be run simultaneously.

Different variants of IFCs are available, such as the 96.96 Dynamic Array IFC. In conclusion, the results argue that the effect of treatment is intact despite variation within groups caused by the “run effect”, which should be considered in future experiments using Fluidigm.

6 SUMMARY AND CONCLUSION

The main aim of this study was to determine if, and how, the murine intestinal barrier in the colon and the small intestine is affected by different modes of naturalization through gene expression analysis of a panel of barrier- and immune-related genes in IECs. Moreover, animal welfare and health, as well as the successfulness of IEC isolation, needed evaluation to expose factors possibly affecting gene expression.

Naturalization of lab mice does not seem to generally affect animal welfare negatively; however, awareness should perhaps be raised of the possibility of wild house mice to bring pathogenic microbes. Based on the aim and type of experiment, it should be considered that the laboratory mice might be infected with, e.g., parasites, which might bring symptoms such as weight loss/reduced weight gain and could possibly explain the observed impaired weight gain in feralized mice in this current study. However, exposure to microbes such as parasites was part of the point of cohousing with wild mice for lab mice to gain antigen experience that reflects a naturalistic setting and evaluate the effect on the immune phenotype. Hence, detection of parasites in both wild and lab mice brought confirmation that naturalization allows for laboratory mice to live in a setting resembling nature.

Intestinal epithelial cells were successfully isolated from mouse intestines. However, detection of cell portions positive for the immune cell marker CD45 raises questions about the efficiency of the cell isolation protocol to obtain pure IEC isolates. This could have implications in gene expression analysis, and further purification steps might improve cell suspension purity.

The genes that were found to be higher expressed in naturalized mice are linked to responses to an increased microbial load, clearly indicating an activation of responses to the naturalizing environment and an increased microbial exposure. This was also reflected in an increased level of epithelial cell turnover in the colon of naturalized mice. Moreover, it appears that cohousing has a significantly greater effect on the relative gene expression levels than feralization alone, as cohoused mice were significantly different in a greater number of genes and the differences seen in the cohoused groups compared to lab mice were much greater than in feralized mice. Increased expression of these genes is associated with positive effects on the intestinal barrier, supporting previous findings that naturalization improves intestinal barrier function and thus gut homeostasis.

7 FUTURE PERSPECTIVES

Samples analyzed in this thesis were from the end of the 10-week trial. However, samples were collected at the halfway point as well, and it would be interesting to evaluate any possible effect of exposure time or assess if there were signs of inflammatory states earlier on. Moreover, feces samples were collected from all mice approximately every two weeks. Preforming microbiota analyses of these could be useful in identifying possible drivers of the observed changes in gene expression. Additionally, mucus property examinations regarding thickness and permeability, as well as identifying SFB abundance and their grade of binding to IECs, may give additional information on the altered barrier function.

Some of the genes higher expressed in cohoused mice seem to have possible connections to parasite infection. Doing reductionistic studies on lab mice by inoculating with single parasites, followed by gene expression analysis, could help answer questions about this aspect.

Including tissue samples from the wild mice in the gene expression analysis would also give indications on how close to a wild mouse/the natural situation the cohoused mice became following cohousing. Further, using the naturalized mice in disease-experiments, such as in a DSS-induced colitis model, as well as models inducing CRC development, could provide further insight into possible protective effects of naturalization in disease states.

REFERENCES

Agace, W. W. & Persson, E. K. (2012). How vitamin A metabolizing dendritic cells are generated in the gut mucosa. *Trends in Immunology*, 33 (1): 42-48. doi: 10.1016/j.it.2011.10.001.

Agilent Technologies. (2020). Agilent 2100 Bioanalyzer System 2100 Expert Software User's Guide, SD-UF0000050 Rev. D.00: Agilent Technologies. Available at: https://www.agilent.com/cs/library/usermanuals/public/2100_Bioanalyzer_Expert_USR.pdf.

Agus, A., Planchais, J. & Sokol, H. (2018). Gut Microbiota Regulation of Tryptophan Metabolism in Health and Disease. *Cell Host Microbe*, 23 (6): 716-724. doi: 10.1016/j.chom.2018.05.003.

Alberts, B., Johnson, A., Lewis, J., Morgan, D., Raff, M., Roberts, K. & Walter, P. (2015). *Molecular Biology of the Cell*. Sixth ed. USA: Garland Science, Taylor & Francis Group.

Allaire, J. M., Crowley, S. M., Law, H. T., Chang, S. Y., Ko, H. J. & Vallance, B. A. (2018). The Intestinal Epithelium: Central Coordinator of Mucosal Immunity. *Trends Immunol*, 39 (9): 677-696. doi: 10.1016/j.it.2018.04.002.

Almalki, F., Nonnecke, E. B., Castillo, P. A., Bevin-Holder, A., Ullrich, K. K., Lönnerdal, B., Odenthal-Hesse, L., Bevins, C. L. & Hollox, E. J. (2021). Extensive variation in the intelectin gene family in laboratory and wild mouse strains. *Scientific Reports*, 11 (1). doi: 10.1038/s41598-021-94679-3.

Andrews, C., McLean, M. H. & Durum, S. K. (2018). Cytokine Tuning of Intestinal Epithelial Function. *Frontiers in Immunology*, 9. doi: 10.3389/fimmu.2018.01270.

Aoun, A., Darwish, F. & Hamod, N. (2020). The Influence of the Gut Microbiome on Obesity in Adults and the Role of Probiotics, Prebiotics, and Synbiotics for Weight Loss. *Prev Nutr Food Sci*, 25 (2): 113-123. doi: 10.3746/pnf.2020.25.2.113.

Arnesen, H. (2021). *Housing of laboratory mice in a natural habitat – influence on immune system, gut microbiota, and colorectal cancer development*: Norwegian University of Life Sciences, Faculty of Veterinary Medicine. ISSN 1894-6402, ISBN 978-82-575-1874-5.

Arnesen, H., Hitch, T. C. A., Steppeler, C., Muller, M. H. B., Knutsen, L. E., Gunnes, G., Angell, I. L., Ormaasen, I., Rudi, K., Paulsen, J. E., et al. (2021a). Naturalizing laboratory mice by housing in a farmyard-type habitat confers protection against colorectal carcinogenesis. *Gut Microbes*, 13 (1): 1993581. doi: 10.1080/19490976.2021.1993581.

Arnesen, H., Knutsen, L. E., Hognestad, B. W., Johansen, G. M., Bemark, M., Pabst, O., Storset, A. K. & Boysen, P. (2021b). A Model System for Feralizing Laboratory Mice in Large Farmyard-Like Pens. *Frontiers in Microbiology*, 11. doi: 10.3389/fmicb.2020.615661.

Artis, D., Wang, M. L., Keilbaugh, S. A., He, W., Brenes, M., Swain, G. P., Knight, P. A., Donaldson, D. D., Lazar, M. A., Miller, H. R. P., et al. (2004). RELMbeta/FIZZ2 is a goblet cell-specific immune-effector molecule in the gastrointestinal tract. *Proceedings of the National Academy of Sciences*, 101 (37): 13596-13600. doi: doi:10.1073/pnas.0404034101.

Arya, M., Shergill, I. S., Williamson, M., Gommersall, L., Arya, N. & Patel, H. R. H. (2005). Basic principles of real-time quantitative PCR. *Expert Rev. Mol. Diagn.*, 6 (2): 209-219. doi: 10.1586/14737159.5.2.209.

Atarashi, K., Tanoue, T., Ando, M., Kamada, N., Nagano, Y., Narushima, S., Suda, W., Imaoka, A., Setoyama, H., Nagamori, T., et al. (2015). Th17 Cell Induction by

Adhesion of Microbes to Intestinal Epithelial Cells. *Cell*, 163 (2): 367-380. doi: 10.1016/j.cell.2015.08.058.

Avershina, E., Lundgard, K., Sekelja, M., Dotterud, C., Storro, O., Oien, T., Johnsen, R. & Rudi, K. (2016). Transition from infant- to adult-like gut microbiota. *Environ Microbiol*, 18 (7): 2226-36. doi: 10.1111/1462-2920.13248.

Aviello, G. & Knaus, U. G. (2017). ROS in gastrointestinal inflammation: Rescue Or Sabotage? *Br J Pharmacol*, 174 (12): 1704-1718. doi: 10.1111/bph.13428.

Aviello, G. & Knaus, U. G. (2018). NADPH oxidases and ROS signaling in the gastrointestinal tract. *Mucosal Immunol*, 11 (4): 1011-1023. doi: 10.1038/s41385-018-0021-8.

Barrett, K. E. (2014). *Gastrointestinal Physiology*. 2 ed. Lange. USA: McGraw Hill Education.

Barthold, S. W. (1997). Giardia muris Infection, Intestine, Mouse, Rat, and Hamster. In Jones, T. C., Popp, J. A. & Mohr, U. (eds) *Digestive System. Monographs on Pathology of Laboratory Animals*, pp. 422-426. Berlin, Heidelberg: Springer Berlin Heidelberg.

Baulies, A., Angelis, N. & Li, V. S. W. (2020). Hallmarks of intestinal stem cells. *Development*, 147 (15). doi: 10.1242/dev.182675.

Bekkevold, C. M., Robertson, K. L., Reinhard, M. K., Battles, A. H. & Rowland, N. E. (2013). Dehydration parameters and standards for laboratory mice. *J Am Assoc Lab Anim Sci*, 52 (3): 233-9.

Belkaid, Y. & Harrison, O. J. (2017). Homeostatic Immunity and the Microbiota. *Immunity*, 46 (4): 562-576. doi: 10.1016/j.immuni.2017.04.008.

Bergstrom, K., Liu, X., Zhao, Y., Gao, N., Wu, Q., Song, K., Cui, Y., Li, Y., McDaniel, J. M., McGee, S., et al. (2016). Defective Intestinal Mucin-Type O-Glycosylation Causes Spontaneous Colitis-Associated Cancer in Mice. *Gastroenterology*, 151 (1): 152-164.e11. doi: 10.1053/j.gastro.2016.03.039.

Beura, L. K., Hamilton, S. E., Bi, K., Schenkel, J. M., Odumade, O. A., Casey, K. A., Thompson, E. A., Fraser, K. A., Rosato, P. C., Filali-Mouhim, A., et al. (2016). Normalizing the environment recapitulates adult human immune traits in laboratory mice. *Nature*, 532 (7600): 512-6. doi: 10.1038/nature17655.

Bouzid, M., Hunter, P. R., Chalmers, R. M. & Tyler, K. M. (2013). Cryptosporidium Pathogenicity and Virulence. *Clinical Microbiology Reviews*, 26 (1): 115-134. doi: 10.1128/cmr.00076-12.

Brandtzaeg, P. & Prydz, H. (1984). Direct evidence for an integrated function of J chain and secretory component in epithelial transport of immunoglobulins. *Nature*, 311 (5981): 71-73. doi: 10.1038/311071a0.

Bray, F., Ferlay, J., Soerjomataram, I., Siegel, R. L., Torre, L. A. & Jemal, A. (2018). Global cancer statistics 2018: GLOBOCAN estimates of incidence and mortality worldwide for 36 cancers in 185 countries. *CA: A Cancer Journal for Clinicians*, 68 (6): 394-424. doi: 10.3322/caac.21492.

Bulek, K., Zhao, J., Liao, Y., Rana, N., Corridoni, D., Antanaviciute, A., Chen, X., Wang, H., Qian, W., Miller-Little, W. A., et al. (2020). Epithelial-derived gasdermin D mediates nonlytic IL-1β release during experimental colitis. *Journal of Clinical Investigation*. doi: 10.1172/jci138103.

Burger-van Paassen, N., Loonen, L. M., Witte-Bouma, J., Korteland-van Male, A. M., de Bruijn, A. C., van der Sluis, M., Lu, P., Van Goudoever, J. B., Wells, J. M., Dekker, J., et al. (2012). Mucin Muc2 deficiency and weaning influences the expression of the innate defense genes Reg3β, Reg3γ and angiogenin-4. *PLoS One*, 7 (6): e38798. doi: 10.1371/journal.pone.0038798.

Bustin, S. & Huggett, J. (2017). qPCR primer design revisited. *Biomolecular Detection and Quantification*, 14: 19-28. doi: https://doi.org/10.1016/j.bdq.2017.11.001.

Bustin, S. A., Benes, V., Garson, J. A., Hellemans, J., Huggett, J., Kubista, M., Mueller, R., Nolan, T., Pfaffl, M. W., Shipley, G. L., et al. (2009). The MIQE Guidelines: Minimum Information for Publication of Quantitative Real-Time PCR Experiments. *Clinical Chemistry*, 55 (4): 611-622. doi: 10.1373/clinchem.2008.112797.

Cao, S., Xu, M., Jiang, Y., Liu, H., Yuan, Z., Sun, L., Cao, J. & Shen, Y. (2020). Prevalence and Genetic Characterization of Cryptosporidium, Giardia and Enterocytozoon in Chickens From Ezhou, Hubei, China. *Frontiers in Veterinary Science*, 7. doi: 10.3389/fvets.2020.00030.

Cash, H. L., Whitham, C. V., Behrendt, C. L. & Hooper, L. V. (2006). Symbiotic Bacteria Direct Expression of an Intestinal Bactericidal Lectin. *Science*, 313 (5790): 1126-1130. doi: 10.1126/science.1127119.

Castillo, P. A., Nonnecke, E. B., Ossorio, D. T., Tran, M. T. N., Goley, S. M., Lönnerdal, B., Underwood, M. A. & Bevins, C. L. (2019). An Experimental Approach to Rigorously Assess Paneth Cell α-Defensin (Defa) mRNA Expression in C57BL/6 Mice. *Scientific Reports*, 9 (1): 13115. doi: 10.1038/s41598-019-49471-9.

CD326 (EpCAM) MicroBeads Mouse. (2021). Product manual 130-105-958. Bergisch Gladbach, Germany: Miltenyi Biotec B.V. & Co. KG.

Chelakkot, C., Ghim, J. & Ryu, S. H. (2018). Mechanisms regulating intestinal barrier integrity and its pathological implications. *Exp Mol Med*, 50 (8): 1-9. doi: 10.1038/s12276-018-0126-x.

Chen, C., Chen, L., Lin, L., Jin, D., Du, Y. & Lyu, J. (2021). Research progress on gut microbiota in patients with gastric cancer, esophageal cancer, and small intestine cancer. *Applied Microbiology and Biotechnology*, 105 (11): 4415-4425. doi: 10.1007/s00253-021-11358-z.

Chu, H. & Mazmanian, S. K. (2013). Innate immune recognition of the microbiota promotes host-microbial symbiosis. *Nat Immunol*, 14 (7): 668-75. doi: 10.1038/ni.2635.

Cleland, W. W. (1964). Dithiothreitol, a New Protective Reagent for SH Groups. *Biochemistry* 3(4): 480-482. doi: 10.1021/bi00892a002.

Coleman, O. I. & Haller, D. (2021). Microbe-Mucus Interface in the Pathogenesis of Colorectal Cancer. *Cancers (Basel)*, 13 (4). doi: 10.3390/cancers13040616.

De Pelsmaeker, N., Korslund, L. & Steifetten, Ø. (2020). Do bank voles (Myodes glareolus) trapped in live and lethal traps show differences in tick burden? *PLoS ONE*, 15. doi: 10.1371/journal.pone.0239029.

Dean, A., Voss, D. & Draguljić, D. (2017). *Design and Analysis of Experiments*. 2nd ed. Springer Texts in Statistics. USA: Springer.

Eckhardt, E. R., Witta, J., Zhong, J., Arsenescu, R., Arsenescu, V., Wang, Y., Ghoshal, S., De Beer, M. C., De Beer, F. C. & De Villiers, W. J. (2010). Intestinal Epithelial Serum Amyloid A Modulates Bacterial Growth In Vitro and Pro-Inflammatory Responses in Mouse Experimental Colitis. *BMC Gastroenterology*, 10 (1): 133. doi: 10.1186/1471-230x-10-133.

Ehrencrona, E., Van Der Post, S., Gallego, P., Recktenwald, C. V., Rodriguez-Pineiro, A. M., Garcia-Bonete, M.-J., Trillo-Muyo, S., Bäckström, M., Hansson, G. C. & Johansson, M. E. V. (2021). The IgGFc-binding protein FCGBP is secreted with all GDPH sequences cleaved but maintained by interfragment disulfide bonds. *Journal of Biological Chemistry*, 297 (1): 100871. doi: 10.1016/j.jbc.2021.100871.

Eissa, N., Kermarrec, L., Hussein, H., Bernstein, C. N. & Ghia, J.-E. (2017). Appropriateness of reference genes for normalizing messenger RNA in mouse 2,4-dinitrobenzene

sulfonic acid (DNBS)-induced colitis using quantitative real time PCR. *Scientific Reports*, 7 (1): 42427. doi: 10.1038/srep42427.

Eshleman, E. M. & Alenghat, T. (2021). Epithelial sensing of microbiota-derived signals. *Genes Immun*, 22 (5-6): 237-246. doi: 10.1038/s41435-021-00124-w.

Evstatiev, R., Cervenka, A., Austerlitz, T., Deim, G., Baumgartner, M., Beer, A., Krnjic, A., Gmainer, C., Lang, M., Frick, A., et al. (2011). The food additive EDTA aggravates colitis and colon carcinogenesis in mouse models. *Scientific reports*, 11 (1): 5188. doi: https://doi.org/10.1038/s41598-021-84571-5.

FELASA. (2015). Glossay of clinical signs in laboratory animals.

Fentener Van Vlissingen, J., Borrens, M., Girod, A., Lelovas, P., Morrison, F. & Torres, Y. S. (2015). The reporting of clinical signs in laboratory animals. *Laboratory Animals*, 49 (4): 267-283. doi: 10.1177/0023677215584249.

Fiege, J. K., Block, K. E., Pierson, M. J., Nanda, H., Shepherd, F. K., Mickelson, C. K., Stolley, J. M., Matchett, W. E., Wijeyesinghe, S., Meyerholz, D. K., et al. (2021). Mice with diverse microbial exposure histories as a model for preclinical vaccine testing. *Cell Host & Microbe*. doi: 10.1016/j.chom.2021.10.001.

Fluidigm. (2020). *D3 Assay Design User Guide. 100-6812 Rev 06.*

Fluidigm. (2021). *Real-Time PCR Analysis User Guide. 68000088 Rev 17.*

Frafjord, K. (2021a). *husmus*: Store norske leksikon. Available at: https://snl.no/husmus.

Frafjord, K. (2021b). *småskogmus*. Store norske leksikon. Available at: https://snl.no/sm%C3%A5skogmus.

Gerard, G. F., Potter, R. J., Smith, M. D., Rosenthal, K., Dhariwal, G., Lee, J. & Chatterjee, D. K. (2002). The role of template-primer in protection of reverse transcriptase from thermal inactivation. *Nucleic Acids Research*, 30 (14): 3118-3129. doi: 10.1093/nar/gkf417.

Gewirtz, A. T., Navas, T. A., Lyons, S., Godowski, P. J. & Madara, J. L. (2001). Cutting Edge: Bacterial Flagellin Activates Basolaterally Expressed TLR5 to Induce Epithelial Proinflammatory Gene Expression. *The Journal of Immunology*, 167 (4): 1882-1885. doi: 10.4049/jimmunol.167.4.1882.

Goodyear, A. W., Kumar, A., Dow, S. & Ryan, E. P. (2014). Optimization of murine small intestine leukocyte isolation for global immune phenotype analysis. *J Immunol Methods*, 405: 97-108. doi: 10.1016/j.jim.2014.01.014.

Graham, A. L. (2021). Naturalizing mouse models for immunology. *Nat Immunol*, 22 (2): 111-117. doi: 10.1038/s41590-020-00857-2.

Haber, A. L., Biton, M., Rogel, N., Herbst, R. H., Shekhar, K., Smillie, C., Burgin, G., Delorey, T. M., Howitt, M. R., Katz, Y., et al. (2017). A single-cell survey of the small intestinal epithelium. *Nature*, 551 (7680): 333-339. doi: 10.1038/nature24489.

Hamilton, S. E., Badovinac, V. P., Beura, L. K., Pierson, M., Jameson, S. C., Masopust, D. & Griffith, T. S. (2020). New Insights into the Immune System Using Dirty Mice. *Journal of Immunology*, 205 (1): 3-11. doi: 10.4049/jimmunol.2000171.

Heyworth, M. F. (2014). Immunological aspects of *Giardia* infections. *Parasite*, 21: 55. doi: https://doi.org/10.1051/parasite/2014056.

Hild, B., Dreier, M. S., Oh, J. H., McCulloch, J. A., Badger, J. H., Guo, J., Thefaine, C. E., Umarova, R., Hall, K. D., Gavrilova, O., et al. (2021). Neonatal exposure to a wild-derived microbiome protects mice against diet-induced obesity. *Nat Metab*, 3 (8): 1042-1057. doi: 10.1038/s42255-021-00439-y.

Hooper, L. V., Stappenbeck, T. S., Hong, C. V. & Gordon, J. I. (2003). Angiogenins: a new class of microbicidal proteins involved in innate immunity. *Nature Immunology*, 4 (3): 269-273. doi: 10.1038/ni888.

Hugenholtz, F. & de Vos, W. M. (2018). Mouse models for human intestinal microbiota research: a critical evaluation. *Cell Mol Life Sci*, 75 (1): 149-160. doi: 10.1007/s00018-017-2693-8.

Jakobsson, H. E., Abrahamsson, T. R., Jenmalm, M. C., Harris, K., Quince, C., Jernberg, C., Bjorksten, B., Engstrand, L. & Andersson, A. F. (2014). Decreased gut microbiota diversity, delayed Bacteroidetes colonisation and reduced Th1 responses in infants delivered by caesarean section. *Gut*, 63 (4): 559-66. doi: 10.1136/gutjnl-2012-303249.

Jakobsson, H. E., Rodríguez-Piñeiro, A. M., Schütte, A., Ermund, A., Boysen, P., Bemark, M., Sommer, F., Bäckhed, F., Hansson, G. C. & Johansson, M. E. (2015). The composition of the gut microbiota shapes the colon mucus barrier. *EMBO reports*, 16 (2): 164-177. doi: 10.15252/embr.201439263.

Jarquín-Díaz, V. H., Balard, A., Jost, J., Kraft, J., Dikmen, M. N., Kvičerová, J. & Heitlinger, E. (2019). Detection and quantification of house mouse Eimeria at the species level – Challenges and solutions for the assessment of coccidia in wildlife. *International Journal for Parasitology: Parasites and Wildlife*, 10: 29-40. doi: https://doi.org/10.1016/j.ijppaw.2019.07.004.

Jasper, H. (2020). Intestinal Stem Cell Aging: Origins and Interventions. *Annu Rev Physiol*, 82: 203-226. doi: 10.1146/annurev-physiol-021119-034359.

Johansen, F.-E., Pekna, M., Norderhaug, I. N., Haneberg, B., Hietala, M. A., Krajci, P., Betsholtz, C. & Brandtzaeg, P. (1999). Absence of Epithelial Immunoglobulin a Transport, with Increased Mucosal Leakiness, in Polymeric Immunoglobulin Receptor/Secretory Component–Deficient Mice. *Journal of Experimental Medicine*, 190 (7): 915-922. doi: 10.1084/jem.190.7.915.

Kayo, T., Maria, E. L., Pierre, L., Laura, E., Karl-Christian, N., Isabelle, B., Ewan, M., Aesun, S., Sue, P., Robert, T. G., et al. (2021). Cancer incidence in agricultural workers: Findings from an international consortium of agricultural cohort studies (AGRICOH). *Environment International*, 157: 106825. doi: https://doi.org/10.1016/j.envint.2021.106825.

Klein, D. (2002). Quantification using real-time PCR technology: applications and limitations. *Trends in Moleculat Medicine*, 8 (6). doi: https://doi.org/10.1016/S1471-4914(02)02355-9.

Koetsier, G. & Cantor, E. (2019). *A Practical Guide to Analyzing Nucleic Acid Concentration and Purity with Microvolume Spectrophotometers*, Technocal note.

Kominsky, D. J., Campbell, E. L., Ehrentraut, S. F., Wilson, K. E., Kelly, C. J., Glover, L. E., Collins, C. B., Bayless, A. J., Saeedi, B., Dobrinskikh, E., et al. (2014). IFN-γ–Mediated Induction of an Apical IL-10 Receptor on Polarized Intestinal Epithelia. *The Journal of Immunology*, 192 (3): 1267-1276. doi: 10.4049/jimmunol.1301757.

Korenková, V., Scott, J., Novosadová, V., Jindřichová, M., Langerová, L., Švec, D., Šídová, M. & Sjöback, R. (2015). Pre-amplification in the context of high-throughput qPCR gene expression experiment. *BMC Molecular Biology*, 16 (1): 5. doi: 10.1186/s12867-015-0033-9.

Koudela, B., Nohýnková, E., Vítovec, J., Pakandl, M. & Kulda, J. (1991). Giardia infection in pigs: detection and in vitro isolation of trophozoites of the Giardia intestinalis group. *Parasitology*, 102 Pt 2: 163-6. doi: 10.1017/s0031182000062442.

Kuriakose, T. & Kanneganti, T.-D. (2018). ZBP1: Innate Sensor Regulating Cell Death and Inflammation. *Trends in Immunology*, 39 (2): 123-134. doi: 10.1016/j.it.2017.11.002.

Latorre, E., Layunta, E., Grasa, L., Pardo, J., García, S., Alcalde, A. I. & Mesonero, J. E. (2018). Toll-like receptors 2 and 4 modulate intestinal IL-10 differently in ileum and colon. *United European Gastroenterology Journal*, 6 (3): 446-453. doi: 10.1177/2050640617727180.

Leung, J. M., Budischak, S. A., Chung The, H., Hansen, C., Bowcutt, R., Neill, R., Shellman, M., Loke, P. N. & Graham, A. L. (2018). Rapid environmental effects on gut nematode susceptibility in rewilded mice. *PLOS Biology*, 16 (3): e2004108. doi: 10.1371/journal.pbio.2004108.

Levy, M., Thaiss, C. A., Zeevi, D., Dohnalová, L., Zilberman-Schapira, G., Mahdi, J. A., David, E., Savidor, A., Korem, T., Herzig, Y., et al. (2015). Microbiota-Modulated Metabolites Shape the Intestinal Microenvironment by Regulating NLRP6 Inflammasome Signaling. *Cell*, 163 (6): 1428-1443. doi: https://doi.org/10.1016/j.cell.2015.10.048.

Li, K., Zhang, J., Cao, J., Li, X. & Tian, H. (2019). 1,4-Dithiothreitol treatment ameliorates hematopoietic and intestinal injury in irradiated mice: Potential application of a treatment for acute radiation syndrome. *International Immunopharmacology*, 76. doi: https://doi.org/10.1016/j.intimp.2019.105913.

Lin, J.-D., Devlin, J. C., Yeung, F., McCauley, C., Leung, J. M., Chen, Y.-H., Cronkite, A., Hansen, C., Drake-Dunn, C., Ruggles, K. V., et al. (2020). Rewilding Nod2 and Atg16l1 Mutant Mice Uncovers Genetic and Environmental Contributions to Microbial Responses and Immune Cell Composition. *Cell Host & Microbe*, 27 (5): 830-840.e4. doi: 10.1016/j.chom.2020.03.001.

Livak, K. J. & Schmittgen, T. D. (2001). Analysis of Relative Gene Expression Data Using Real-Time Quantitative PCR and the 2−ΔΔCT Method. *Methods*, 25 (4): 402-408. doi: https://doi.org/10.1006/meth.2001.1262.

Lu, F., Inoue, K., Kato, J., Minamishima, S. & Morisaki, H. (2019). Functions and regulation of lipocalin-2 in gut-origin sepsis: a narrative review. *Critical Care*, 23 (1). doi: 10.1186/s13054-019-2550-2.

Lundin, A., Bok, C. M., Aronsson, L., Bjorkholm, B., Gustafsson, J. A., Pott, S., Arulampalam, V., Hibberd, M., Rafter, J. & Pettersson, S. (2008). Gut flora, Toll-like receptors and nuclear receptors: a tripartite communication that tunes innate immunity in large intestine. *Cell Microbiol*, 10 (5): 1093-103. doi: 10.1111/j.1462-5822.2007.01108.x.

Maniatis, Sambrook & Fritsch. (1989). *Molecular Cloning: A Laboratory Manual*. 2nd ed.: Cold Spring Harbor Laboratory.

Masahata, K., Umemoto, E., Kayama, H., Kotani, M., Nakamura, S., Kurakawa, T., Kikuta, J., Gotoh, K., Motooka, D., Sato, S., et al. (2014). Generation of colonic IgA-secreting cells in the caecal patch. *Nat Commun*, 5: 3704. doi: 10.1038/ncomms4704.

Matziouridou, C., Rocha, S. D. C., Haabeth, O. A., Rudi, K., Carlsen, H. & Kielland, A. (2018). iNOS- and NOX1-dependent ROS production maintains bacterial homeostasis in the ileum of mice. *Mucosal Immunology*, 11 (3): 774-784. doi: 10.1038/mi.2017.106.

McAllister, T. A., Olson, M. E., Fletch, A., Wetzstein, M. & Entz, T. (2005). Prevalence of Giardia and Cryptosporidium in beef cows in southern Ontario and in beef calves in southern British Columbia. *Can Vet J*, 46 (1): 47-55. doi: 10.4141/cjas66-008.

McCafferty, J., Mühlbauer, M., Gharaibeh, R. Z., Arthur, J. C., Perez-Chanona, E., Sha, W., Jobin, C. & Fodor, A. A. (2013). Stochastic changes over time and not founder effects drive cage effects in microbial community assembly in a mouse model. *The ISME Journal*, 7 (11): 2116-2125. doi: 10.1038/ismej.2013.106.

Milani, C., Duranti, S., Bottacini, F., Casey, E., Turroni, F., Mahony, J., Belzer, C., Palacio, S. D., Montes, S. A., Mancabelli, L., et al. (2017). The First Microbial Colonizers of the Human Gut: Composition, Activities, and Health Implications of the Infant Gut Microbiota. *Microbiology and Molecular Biology Reviews*, 81 (4). doi: 10.1128/MMBR.00036-17.

Mo, Y., Wan, R. & Zhang, Q. (2012). Application of reverse transcription-PCR and real-time PCR in nanotoxicity research. *Methods Mol Biol*, 926: 99-112. doi: 10.1007/978-1-62703-002-1_7.

Mommaerts, K., Sanchez, I., Betsou, F. & Mathieson, W. (2015). Replacing β-mercaptoethanol in RNA extractions. *Analytical Biochemistry*, 479: 51-53. doi: https://doi.org/10.1016/j.ab.2015.03.027.

Motulsky, H. *Analysis checklist: One-way ANOVA*. Available at: https://www.graphpad.com/guides/prism/latest/statistics/stat_checklist_1wayanova.htm (accessed: 10.03.2022).

Motulsky, H. *How the Dunn method for nonparametric comparisons works*. Available at: https://www.graphpad.com/guides/prism/latest/statistics/stat_how_the_dunn_method_for_nonpar.htm (accessed: 10.03.2022).

Motulsky, H. *How the Dunnett T3, Games and Howell, and Tamhane T2 tests work*. Available at: https://www.graphpad.com/guides/prism/latest/statistics/stat_multiple-comparisons-without-a.htm (accessed: 10.03.2022).

Motulsky, H. *How the Tukey and Dunnett methods work*. Available at: https://www.graphpad.com/guides/prism/latest/statistics/stat_howprismcomputesmulcomparisons.htm (accessed: 10.03.2022).

Motulsky, H. *How to: Identify outliers*. Available at: https://www.graphpad.com/guides/prism/latest/statistics/stat_how_to_removing_outliers.htm (accessed: 10.03.2022).

Motulsky, H. *Interpreting results: Kruskal-Wallis test*. Available at: https://www.graphpad.com/guides/prism/latest/statistics/how_the_kruskal-wallis_test_works.htm (accessed: 10.03.2022).

Motulsky, H. *Interpreting results: Welch and Brown-Forsythe tests*. Available at: https://www.graphpad.com/guides/prism/latest/statistics/interpreting_welch_browne-forsythe_tests.htm (accessed: 10.03.2022).

Motulsky, H. *Options tab: Multiple comparisons: One-way ANOVA*. Available at: https://www.graphpad.com/guides/prism/latest/statistics/stat_options_tab_1wayanova.htm (accessed: 10.03.2022).

Motulsky, H. *What is a P value?* Available at: https://www.graphpad.com/guides/prism/latest/statistics/what_is_a_p_value.htm (accessed: 10.03.2022).

Mowat, A. M. & Agace, W. W. (2014). Regional specialization within the intestinal immune system. *Nat Rev Immunol*, 14 (10): 667-85. doi: 10.1038/nri3738.

Mueller, O., Lightfoot, S. & Schroeder, A. (2016). *RNA Integrity Number (RIN) – Standardization of RNA Quality Control*: Application note 5989-1165EN.

Mukherjee, S. & Hooper, L. V. (2015). Antimicrobial defense of the intestine. *Immunity*, 42 (1): 28-39. doi: 10.1016/j.immuni.2014.12.028.

Mähler, M., Berard, M., Feinstein, R., Gallagher, A., Illgen-Wilcke, B., Pritchett-Corning, K. & Raspa, M. (2014). FELASA recommendations for the health monitoring of mouse, rat, hamster, guinea pig and rabbit colonies in breeding and experimental units. *Lab Anim*, 48 (3): 178-192. doi: 10.1177/0023677213516312.

NEB. (NA). *Reverse Transcription (cDNA Synthesis)*: New England BioLabs Inc. Available at: https://international.neb.com/applications/cloning-and-synthetic-biology/dna-preparation/reverse-transcription-cdna-synthesis.

Nguyen, Q. P., Deng, T. Z., Witherden, D. A. & Goldrath, A. W. (2019). Origins of CD4+ circulating and tissue-resident memory T-cells. *Immunology*, 157 (1): 3-12. doi: 10.1111/imm.13059.

Niimi, K. & Morimoto, M. (2021). Cytokine elevation in the mouse small intestine at the early stage of infection with the gastrointestinal parasite Heligmosomoides polygyrus</i&gt. *Journal of Veterinary Medical Science*, 83 (4): 573-580. doi: 10.1292/jvms.20-0498.

Nonnecke, E. B., Castillo, P. A., Dugan, A. E., Almalki, F., Underwood, M. A., De La Motte, C. A., Yuan, W., Lu, W., Shen, B., Johansson, M. E. V., et al. (2021). Human intelectin-1 (ITLN1) genetic variation and intestinal expression. *Scientific Reports*, 11 (1): 12889. doi: 10.1038/s41598-021-92198-9.

NorwegianSequencingCentre. (2020). *SAMPLE REQUIREMENTS for Illumina Submission*. Available at: https://www.sequencing.uio.no/illumina-submission/1.%20General%20information/.

Nowarski, R., Jackson, R., Gagliani, N., Marcel, Noah, Bailis, W., Jun, Christian, Graham, M., Elinav, E., et al. (2015). Epithelial IL-18 Equilibrium Controls Barrier Function in Colitis. *Cell*, 163 (6): 1444-1456. doi: 10.1016/j.cell.2015.10.072.

Nyström, E. E. L., Arike, L., Ehrencrona, E., Hansson, G. C. & Johansson, M. E. V. (2019). Calcium-activated chloride channel regulator 1 (CLCA1) forms non-covalent oligomers in colonic mucus and has mucin 2-processing properties. *J Biol Chem*, 294 (45): 17075-17089. doi: 10.1074/jbc.RA119.009940.

Oemcke, L. A., Anderson, R. C., Altermann, E., Roy, N. C. & McNabb, W. C. (2021). The Role of Segmented Filamentous Bacteria in Immune Barrier Maturation of the Small Intestine at Weaning. *Frontiers in Nutrition*, 8. doi: 10.3389/fnut.2021.759137.

Otani, T. & Furuse, M. (2020). Tight Junction Structure and Function Revisited. *Trends Cell Biol*, 30 (10): 805-817. doi: 10.1016/j.tcb.2020.08.004.

Parham, P. (2015). *The Immune System*. Fourth ed. USA: Garland Science, Taylor & Francis Group.

Paruch, L. & Paruch, A. M. (2022). Molecular Identification of Infectious Enteropathogens in Faeces of Healthy Horses. *Microbiology Insights*, 15: 117863612210890. doi: 10.1177/11786361221089005.

Patankar, J. V. & Becker, C. (2020). Cell death in the gut epithelium and implications for chronic inflammation. *Nat Rev Gastroenterol Hepatol*, 17 (9): 543-556. doi: 10.1038/s41575-020-0326-4.

Peirson, S. N. & Butler, J. N. (2007). RNA Extraction From Mammalian Tissues. *Methods Mol Biol*, 362: 315-27. doi: 10.1007/978-1-59745-257-1_22.

Peters, L. L., Robledo, R. F., Bult, C. J., Churchill, G. A., Paigen, B. J. & Svenson, K. L. (2007). The mouse as a model for human biology: a resource guide for complex trait analysis. *Nature Reviews Genetics*, 8 (1): 58-69. doi: 10.1038/nrg2025.

Petersen, H. H., Jianmin, W., Katakam, K. K., Mejer, H., Thamsborg, S. M., Dalsgaard, A., Olsen, A. & Enemark, H. L. (2015). Cryptosporidium and Giardia in Danish organic pig farms: Seasonal and age-related variation in prevalence, infection intensity and species/genotypes. *Veterinary Parasitology*, 214 (1-2): 29-39. doi: 10.1016/j.vetpar.2015.09.020.

Phifer-Rixey, M. & Nachman, M. W. (2015). Insights into mammalian biology from the wild house mouse Mus musculus. *Elife*, 4. doi: 10.7554/eLife.05959.

Pineda, C. O., Leal, D. A. G., Fiuza, V. R. D. S., Jose, J., Borelli, G., Durigan, M., Pena, H. F. J. & Bueno Franco, R. M. (2020). *Toxoplasmagondii* oocysts, *Giardia* cysts and *Cryptosporidium* oocysts in outdoor swimming pools in Brazil. *Zoonoses and Public Health*, 67 (7): 785-795. doi: 10.1111/zph.12757.

Propheter, D. C., Chara, A. L., Harris, T. A., Ruhn, K. A. & Hooper, L. V. (2017). Resistin-like molecule beta is a bactericidal protein that promotes spatial segregation of the

microbiota and the colonic epithelium. *Proc Natl Acad Sci U S A*, 114 (42): 11027-11033. doi: 10.1073/pnas.1711395114.

Qin, J., Li, R., Raes, J., Arumugam, M., Burgdorf, K. S., Manichanh, C., Nielsen, T., Pons, N., Levenez, F., Yamada, T., et al. (2010). A human gut microbial gene catalogue established by metagenomic sequencing. *Nature*, 464 (7285): 59-65. doi: 10.1038/nature08821.

Qiu, Z. & Sheridan, B. S. (2018). Isolating Lymphocytes from the Mouse Small Intestinal Immune System. *J Vis Exp* (132). doi: 10.3791/57281.

Reikvam, D. H., Erofeev, A., Sandvik, A., Grcic, V., Jahnsen, F. L., Gaustad, P., McCoy, K. D., Macpherson, A. J., Meza-Zepeda, L. A. & Johansen, F.-E. (2011). Depletion of Murine Intestinal Microbiota: Effects on Gut Mucosa and Epithelial Gene Expression. *PLoS ONE*, 6 (3): e17996. doi: 10.1371/journal.pone.0017996.

Reikvam, D. H., Derrien, M., Islam, R., Erofeev, A., Grcic, V., Sandvik, A., Gaustad, P., Meza-Zepeda, L. A., Jahnsen, F. L., Smidt, H., et al. (2012). Epithelial-microbial crosstalk in polymeric Ig receptor deficient mice. *European Journal of Immunology*, 42 (11): 2959-2970. doi: 10.1002/eji.201242543.

Riccio, C. (2019). *RNA re-precipitation protocol V.2*. Available at: https://www.protocols.io/view/rna-re-precipitation-protocol-5qpvon11dl4o/v2?step=1 (accessed: 25.01).

Ringnér, M. (2008). What is principal component analysis? *Nature Biotechnology*, 26 (3): 303-304. doi: 10.1038/nbt0308-303.

Ririe, K. M., Rasmussen, R. P. & Wittwer, C. T. (1997). Product Differentiation by Analysis of DNA Melting Curves during the Polymerase Chain Reaction. *Analytical Biochemistry*, 245: 154-160. doi: 10.1006/abio.1996.9916.

Robertson, L. J. (2009). GiardiaandCryptosporidiuminfections in sheep and goats: a review of the potential for transmission to humans via environmental contamination. *Epidemiology and Infection*, 137 (7): 913-921. doi: 10.1017/s0950268809002295.

Rook, G. A. W. (2005). Microbes, immunoregulation, and the gut. *Gut*, 54 (3): 317-320. doi: 10.1136/gut.2004.053785.

Rook, G. A. W., Raison, C. L. & Lowry, C. A. (2014). Microbial 'old friends', immunoregulation and socioeconomic status. *Clinical and Experimental Immunology*, 177 (1): 1-12. doi: 10.1111/cei.12269.

Rosshart, S. P., Vassallo, B. G., Angeletti, D., Hutchinson, D. S., Morgan, A. P., Takeda, K., Hickman, H. D., McCulloch, J. A., Badger, J. H., Ajami, N. J., et al. (2017). Wild Mouse Gut Microbiota Promotes Host Fitness and Improves Disease Resistance. *Cell*, 171 (5): 1015-1028 e13. doi: 10.1016/j.cell.2017.09.016.

Rosshart, S. P., Herz, J., Vassallo, B. G., Hunter, A., Wall, M. K., Badger, J. H., McCulloch, J. A., Anastasakis, D. G., Sarshad, A. A., Leonardi, I., et al. (2019). Laboratory mice born to wild mice have natural microbiota and model human immune responses. *Science*, 365 (6452): eaaw4361. doi: 10.1126/science.aaw4361.

Royston, P. (1995). Remark AS R94: A Remark on Algorithm AS 181: The W-test for Normality. *Journal of the Royal Statistical Society*, 44 (4): 547-551. doi: https://doi.org/10.2307/2986146.

Ruijter, J. M., van der Velden, S. & Ilgun, A. *LinRegPCR (11.0) Analysis of quantitative RT-PCR data*.

Saez, A., Gomez-Bris, R., Herrero-Fernandez, B., Mingorance, C., Rius, C. & Gonzalez-Granado, J. M. (2021). Innate Lymphoid Cells in Intestinal Homeostasis and Inflammatory Bowel Disease. *International Journal of Molecular Sciences*, 22 (14): 7618. doi: 10.3390/ijms22147618.

Sandhu, K. S. & Acharya, K. K. (2005). ExPrimer: to design primers from exon--exon junctions. *Bioinformatics*, 21 (9): 2091-2. doi: 10.1093/bioinformatics/bti304.

Sano, T., Huang, W., Jason, Yang, Y., Chen, A., Samuel, Lee, J.-Y., Ziel, J. W., Emily, Ana, et al. (2015). An IL-23R/IL-22 Circuit Regulates Epithelial Serum Amyloid A to Promote Local Effector Th17 Responses. *Cell*, 163 (2): 381-393. doi: 10.1016/j.cell.2015.08.061.

Schnoor, M. (2015). E-cadherin Is Important for the Maintenance of Intestinal Epithelial Homeostasis Under Basal and Inflammatory Conditions. *Digestive Diseases and Sciences*, 60 (4): 816-818. doi: 10.1007/s10620-015-3622-z.

Scudellari, M. (2017). News Feature: Cleaning up the hygiene hypothesis. *Proc Natl Acad Sci U S A*, 114 (7): 1433-1436. doi: 10.1073/pnas.1700688114.

Sender, R., Fuchs, S. & Milo, R. (2016). Are We Really Vastly Outnumbered? Revisiting the Ratio of Bacterial to Host Cells in Humans. *Cell*, 164 (3): 337-340. doi: 10.1016/j.cell.2016.01.013.

Serrano-Gomez, S. J., Maziveyi, M. & Alahari, S. K. (2016). Regulation of epithelial-mesenchymal transition through epigenetic and post-translational modifications. *Molecular Cancer*, 15 (1). doi: 10.1186/s12943-016-0502-x.

Singh, V., Yeoh, B. S., Chassaing, B., Zhang, B., Saha, P., Xiao, X., Awasthi, D., Shashidharamurthy, R., Dikshit, M., Gewirtz, A., et al. (2016). Microbiota-inducible Innate Immune, Siderophore Binding Protein Lipocalin 2 is Critical for Intestinal Homeostasis. *Cell Mol Gastroenterol Hepatol*, 2 (4): 482-498.e6. doi: 10.1016/j.jcmgh.2016.03.007.

Soderholm, A. T. & Pedicord, V. A. (2019). Intestinal epithelial cells: at the interface of the microbiota and mucosal immunity. *Immunology*, 158 (4): 267-280. doi: 10.1111/imm.13117.

Sonnenburg, J. L., Chen, C. T. L. & Gordon, J. I. (2006). Genomic and Metabolic Studies of the Impact of Probiotics on a Model Gut Symbiont and Host. *PLoS Biology*, 4 (12): e413. doi: 10.1371/journal.pbio.0040413.

Spehlmann, M. E. & Eckmann, L. (2009). Nuclear factor-kappa B in intestinal protection and destruction. *Current Opinion in Gastroenterology*, 25 (2): 92-99. doi: 10.1097/MOG.0b013e328324f857.

Strachan, D. P. (1989). Hay fever, hygiene, and household size. *BMJ*, 299 (6710): 1259-1260. doi: 10.1136/bmj.299.6710.1259.

Sun, X. & Kaufman, P. D. (2018). Ki-67: more than a proliferation marker. *Chromosoma*, 127 (2): 175-186. doi: 10.1007/s00412-018-0659-8.

Thaiss, C. A., Zmora, N., Levy, M. & Elinav, E. (2016). The microbiome and innate immunity. *Nature*, 535 (7610): 65-74. doi: 10.1038/nature18847.

Tual, S., Lemarchand, C., Boulanger, M., Dalphin, J.-C., Rachet, B., Marcotullio, E., Velten, M., Guizard, A.-V., Clin, B., Baldi, I., et al. (2017). Exposure to Farm Animals and Risk of Lung Cancer in the AGRICAN Cohort. *American Journal of Epidemiology*, 186 (4): 463-472. doi: 10.1093/aje/kwx125.

van der Flier, L. G. & Clevers, H. (2009). Stem Cells, Self-Renewal, and Differentiation in the Intestinal Epithelium. *Annual Review of Physiology*, 71 (1): 241-260. doi: 10.1146/annurev.physiol.010908.163145.

Van der Sluis, M., De Koning, B. A., De Bruijn, A. C., Velcich, A., Meijerink, J. P., Van Goudoever, J. B., Büller, H. A., Dekker, J., Van Seuningen, I., Renes, I. B., et al. (2006). Muc2-deficient mice spontaneously develop colitis, indicating that MUC2 is critical for colonic protection. *Gastroenterology*, 131 (1): 117-29. doi: 10.1053/j.gastro.2006.04.020.

van Putten, J. P. M. & Strijbis, K. (2017). Transmembrane Mucins: Signaling Receptors at the Intersection of Inflammation and Cancer. *J Innate Immun*, 9 (3): 281-299. doi: 10.1159/000453594.

Vannella, K. M., Ramalingam, T. R., Hart, K. M., de Queiroz Prado, R., Sciurba, J., Barron, L., Borthwick, L. A., Smith, A. D., Mentink-Kane, M., White, S., et al. (2016). Acidic chitinase primes the protective immune response to gastrointestinal nematodes. *Nature Immunology*, 17 (5): 538-544. doi: 10.1038/ni.3417.

Velcich, A., Yang, W., Heyer, J., Fragale, A., Nicholas, C., Viani, S., Kucherlapati, R., Lipkin, M., Yang, K. & Augenlicht, L. (2002). Colorectal cancer in mice genetically deficient in the mucin Muc2. *Science*, 295 (5560): 1726-9. doi: 10.1126/science.1069094.

Viney, M., Lazarou, L. & Abolins, S. (2015). The laboratory mouse and wild immunology. *Parasite Immunology*, 37 (5): 267-273. doi: 10.1111/pim.12150.

Volk, N. & Lacy, B. (2017). Anatomy and Physiology of the Small Bowel. *Gastrointest Endosc Clin N Am*, 27 (1): 1-13. doi: 10.1016/j.giec.2016.08.001.

Wang, F., Scoville, D., He, X. C., Mahe, M. M., Box, A., Perry, J. M., Smith, N. R., Lei, N. Y., Davies, P. S., Fuller, M. K., et al. (2013). Isolation and Characterization of Intestinal Stem Cells Based on Surface Marker Combinations and Colony-Formation Assay. *Gastroenterology*, 145 (2): 383-395.e21. doi: 10.1053/j.gastro.2013.04.050.

Williams, J. M., Duckworth, C. A., Burkitt, M. D., Watson, A. J., Campbell, B. J. & Pritchard, D. M. (2015). Epithelial cell shedding and barrier function: a matter of life and death at the small intestinal villus tip. *Vet Pathol*, 52 (3): 445-55. doi: 10.1177/0300985814559404.

Williams, M. A., O'Callaghan, A. & Corr, S. C. (2019). IL-33 and IL-18 in Inflammatory Bowel Disease Etiology and Microbial Interactions. *Frontiers in Immunology*, 10. doi: 10.3389/fimmu.2019.01091.

Xi, R., Montague, J., Lin, X., Lu, C., Lei, W., Tanaka, K., Zhang, Y. V., Xu, X., Zheng, X., Zhou, X., et al. (2021). Up-regulation of gasdermin C in mouse small intestine is associated with lytic cell death in enterocytes in worm-induced type 2 immunity. *Proceedings of the National Academy of Sciences*, 118 (30): e2026307118. doi: doi:10.1073/pnas.2026307118.

Xu, F., Jiménez-González, A., Einarsson, E., Ástvaldsson, Á., Peirasmaki, D., Eckmann, L., Andersson, J. O., Svärd, S. G. & Jerlström-Hultqvist, J. (2020). The compact genome of *Giardia muris* reveals important steps in the evolution of intestinal protozoan parasites. *Microbial Genomics*, 6 (8). doi: 10.1099/mgen.0.000402.

Yan, J.-B., Luo, M.-M., Chen, Z.-Y. & He, B.-H. (2020). The Function and Role of the Th17/Treg Cell Balance in Inflammatory Bowel Disease. *Journal of Immunology Research*, 2020: 1-8. doi: 10.1155/2020/8813558.

Yazdanbakhsh, M., Kremsner, P. G. & van Ree, R. (2002). Allergy, Parasites, and the Hygiene Hypothesis. *Science*, 296. doi: 10.1126/science.296.5567.490.

Yu, S. & Gao, N. (2015). Compartmentalizing intestinal epithelial cell toll-like receptors for immune surveillance. *Cellular and Molecular Life Sciences*, 72 (17): 3343-3353. doi: 10.1007/s00018-015-1931-1.

Zheng, D., Liwinski, T. & Elinav, E. (2020). Interaction between microbiota and immunity in health and disease. *Cell Res*, 30 (6): 492-506. doi: 10.1038/s41422-020-0332-7.

Zheng, D., Kern, L. & Elinav, E. (2021). The NLRP6 inflammasome. *Immunology*, 162 (3): 281-289. doi: 10.1111/imm.13293.

Åhlgren, J. & Voikar, V. (2019). Housing mice in the individually ventilated or open cages—Does it matter for behavioral phenotype? *Genes, Brain and Behavior*, 18 (7): e12564. doi: https://doi.org/10.1111/gbb.12564.

APPENDICES

Appendix A – Equipment and instruments

Table A1 – Equipment. List of equipment used in this experiment.

Equipment	Supplier
Dynamic Array™ 48.48 GE IFC	Fluidigm Corporation, South San Francisco, CA USA https://store.fluidigm.com/Genomics/ConsumablesandReagentsGenomics/Reagents/GE%2048-48%20Dynamic%20Array%20Reagent%20Kit%20with%20Control%20Line%20Fluid%E2%80%9410%20IFCs?cclcl=en_US
Individual ventilated cages (IVCs) and racks	Innovive Inc., San Diego, CA, USA
Live traps	Ugglan Special No 1 live traps; Grahnab, Gnosjö, Sweden
Organic plant soil	Plantasjen, Norway
RM1 (E)	SDS; Special Diet Services, Witham, United Kingdom https://sdsdiets.com/wp-content/uploads/2021/02/rm1p-e-fg.pdf
Woodchips	Scanbur, Norway https://www.scanbur.com/products/consumables/bedding/tapvei-bedding

Table A2 – Instruments. List of instruments used in this experiment.

Instrument	Supplier
Bioanalyzer 2100	Agilent Technologies, CA, USA. https://www.agilent.com/en/product/automated-electrophoresis/bioanalyzer-systems/bioanalyzer-instrument/2100-bioanalyzer-instrument-228250
Biomark HD	Fluidigm Corporation, South San Francisco, CA, USA https://www.fluidigm.com/products-services/instruments/biomark-hd
CFX96 Touch Real-Time PCR Detection System	Bio-Rad Laboratories, Ink., Hercules, CA, USA. https://www.bio-rad.com/en-no/product/cfx96-touch-real-time-pcr-detection-system?ID=LJB1YU15
Countess 3 Automated cell counter	Invitrogen, Thermo Fischer Scientific, USA https://www.thermofisher.com/no/en/home/life-science/cell-analysis/cell-analysis-instruments/automated-cell-counters/models/countess-3.html
CytoFLEX LX Flow Cytometer	Beckman Coulter Ink. Indianapolis, IN, USA https://www.beckman.com/flow-cytometry/research-flow-cytometers/cytoflex-lx#f:@ftaz120xonomycategoriesselected24655=[CytoFLEX%20LX]
IFC Controller MX	Fluidigm Corporation, South San Francisco, CA USA
NanoDrop™ 2000	Thermo Fischer Scientific, CA, USA https://www.thermofisher.com/order/catalog/product/ND2000CLAPTOP
Veriti 96 Well Thermal Cycler	**applied**biosystems, Thermo Fischer Scientific, CA, USA. https://www.thermofisher.com/order/catalog/product/4375305

Appendix B – Chemicals and reagents

Table B1 – Chemicals and reagents. Comprehensive list of chemicals and reagents used in this experiment, including their supplier and catalog number.

Chemical/reagent product name	Cat. No.	Supplier
Alanyl-Glutamine, Glutamine-S (Ala-Gln) 200mM	G8541	Sigma-Aldrich, St. Louis, MO, USA
Dulbecco's phosphate-buffered saline (PBS)	L0615	Biowest, Nuaillé, France
Enrofloxacin	17849	Sigma-Aldrich, St. Louis, MO, USA
Ethylenediaminetetraacetic acid (EDTA)	03609	Sigma-Aldrich, St. Louis, MO, USA
Exonuclease I (Exo I)	EN0582	Thermo Fischer Scientific, Vilnius, Lithuania
Fetal bovine serum (FBS)	F7524	Sigma-Aldrich, non-US origin
Hank's Balanced Salt Solution (HBSS) w/o/$Mg^{2+}Ca^{2+}$	H9394	Sigma-Aldrich, St. Louis, MO, USA
HEPES	H3375	Sigma-Aldrich, St. Louis, MO, USA
MEM Non-essential Amino Acid (NEAA) Solution 100x	M7145	Sigma-Aldrich, St. Louis, MO, USA
Molecular biology grade water	MT46000CV	Mediatech, Inc., Manassas, VA, USA
Penicillin-Streptomycin Solution 100x	L0022	Biowest, Nuaillé, France
Polymyxin B sulfate salt	P4932	Sigma-Aldrich, St. Louis, MO, USA
RNA*later*™ solution	AM7021	Invitrogen™ by Thermo Fisher Scientific Baltics, Vilnius, Lithuania
RPMI-1640	R0883	Sigma-Aldrich, St. Louis, MO, USA
Sodium pyruvate solution 100mM	S8636	Sigma-Aldrich, St. Louis, MO, USA
SsoFast EvaGreen® Supermix with Low ROX	1725211	Bio-Rad Laboratories, CA, USA
TE-EF Redissolving Buffer	P64047	Macherey-Nagel, Düren, Germany
TruStain FcX™ anti-mouse CD16/32	101320	BioLegend Inc., San Diego, CA, USA
Trypan blue solution	T10282	Life Technologies, OR, USA
β-mercaptoethanol	M6250	Sigma-Aldrich, Bayern, Germany

Table B2 – Kits. Overview of the kits used in this experiment.

Kit	Supplier
eBioscience™ IC staining kit	Invitrogen™ Thermo Fischer Scientific, Waltham MA, USA
GE 48.48 Dynamic Array™ DNA Binding Dye Loading Reagent Kit	Fluidigm, CA, USA
NucleoSpin RNA, Mini kit for RNA purification	Macherey-Nagel, Düren, Germany
PreAmp and Reverse Transcription Master Mix Kit	Fluidigm, CA, USA
RNA 6000 Nano Assay kit	Agilent Technologies, CA, USA
Zombie NIR™ Fixable Viability Kit	BioLegend Inc., San Diego, CA, USA

Table B3 – Solutions composition. Composition of ZRF cocktail and solutions used in this experiment.

Solution	Substance	Quantity per mL
cRPMI	Ala-Gln	2 mM
	FBS	2%
	HEPES	25 mM in RPMI
	Non-essential amino acids	1 X
	PSEPx	Pen/Strep (100 units/ml Penicillin + 100 ug/ml Streptomycin) + 25 ug/ml Enrofloxacin + 100 units/ml polymyxin B
	RPMI-1640	
	Sodium pyruvate	1 mM
DTT	DTT	5 mM
	EDTA solution (as below)	
EDTA	EDTA	5 mM
	FBS	2%
	HBSS w/o/$Mg^{2+}Ca^{2+}$	
	HEPES	10 mM
	PSEPx	Same as in cRPMI
FACS buffer	EDTA	2 mM
	FCS	0.5%
	HEPES	10 mM
	PBS	w/o/ $Ca^{2+}Mg^{2+}$
ZRF cocktail	Fentanyl	2.6 µg
	Isotonic (0.9%) NaCl	1 mL
	Tiletamine (constituent of rompun)	3.2 mg
	Xylazine (constituent of rompun)	0.45 mg
	Zolazepam	3.2 mg

Table B4 – Flow cytometry antibody cocktail. Cell markers used for the epithelial cell suspension in this experiment.

Laser (nm)/name	Filter mean/width	Marker	Fluorochrome	Clone
405/Violet	450/45	CD45	VioBlue	90/CD38
405/Violet	525/40	CD103	BV510	2E7
405/Violet	660/10	CD4	BV650	RM4-5
488/Blue	525/40	TCRgd	FITC	GL3
488/Blue	690/50	CD8b	Percpcy5.5	YTS156.7.7
561/Yellow	585/42	EpCam	PE	Miltenyi
561/Yellow	763/43	Ki67	PE-Cy7	SolA15
638/Red	660/10	TCRb	APC	H57-597
638/Red	712/25	CD8a	Alexa700	53-6.7
638/Red	763/43	Zombie L/D	Near Infra Red	-

Appendix C – Software and websites

Table C1 – Software and websites. List of software and websites used in this experiment.

Software/website	Reference
Bioanalyzer 2100 Expert Software	Agilent Technologies, CA, USA. Software: *2100 Bioanalyzer Expert Software*. Available at: https://www.agilent.com/en/product/automated-electrophoresis/bioanalyzer-systems/bioanalyzer-software/2100-expert-software-228259
Biorender	BioRender (2021/2022). Website available at: https://app.biorender.com/
Fluidigm Biomark HD analysis software	Fluidigm Corporation, South San Francisco, CA USA (2022). Software: *Fluidigm Biomark HD analysis software* for Windows (version 4.8.1). Available at: https://www.fluidigm.com/products-services/software#biomark_hd-anchor (downloaded 16.03.2022)
Fluidigm D3 portal	Fluidigm Corporation, South San Francisco, CA USA (2021). Website available at https://d3.fluidigm.com/account/login
Graphpad	Graphpad software Inc. San Diego, CA USA (2022). Software: *Graphpad Prism 9* for Windows (version 9.3.1471). Available at: www.graphpad.com (downloaded 29.03.2022)
Kaluza Analysis Software	Beckman Coulter Inc. (2022). Software: *Kaluza Analysis Software* (version 2.1). Available at https://www.beckman.com/flow-cytometry/software/kaluza/downloads
LinRegPCR	Ruijter, J. M. (2022). Software: *LinRegPCR: analysis of quantitative PCR data* for Windows (version 2021.2).Available at: https://medischebiologie.nl/files/ (downloaded 19.03.2022)
Nanodrop 2000/2000c Operating Software	Thermo Scientific Inc (x) Software: *Nanodrop 2000/2000c*. Available at: https://www.thermofisher.com/no/en/home/industrial/spectroscopy-elemental-isotope-analysis/molecular-spectroscopy/ultraviolet-visible-visible-spectrophotometry-uv-vis-vis/uv-vis-vis-instruments/nanodrop-microvolume-spectrophotometers/nanodrop-software-download.html
RStudio	RStudio, PBC. Boston, MA USA (2022). Software: *RStudio Desktop* (version 2022.02.1+461). Available at: https://www.rstudio.com/products/rstudio/download/ (downloaded 25.04.2022)

Appendix D – Cell numbers

Table D1 – Total cell numbers. Given is the total number of cells/mL of RNAlater-cell suspension and the volume of this that gives five million cells. Included are the average volumes for colon and small intestine (SI).

Sample	Total number of cells/mL	µL that gives 5 x 10^6 cells
Colon	15 850 000	315.5
Colon	15 900 000	314.5
Colon	7 550 000	662.3
Colon	18 850 000	265.3
Colon	7 400 000	675.7
Colon	26 150 000	191.2
Colon	14 150 000	353.4
Colon	21 000 000	238.1
Colon	16 450 000	304.0
Colon	7 750 000	645.2

Colon	22 250 000	224.7
Colon	7 700 000	649.4
Average	**14 531 250**	**403**
SI	54 000 000	92.6
SI	79 250 000	63.1
SI	56 500 000	88.5
SI	69 000 000	72.5
SI	61 500 000	81.3
SI	69 500 000	71.9
SI	52 250 000	95.7
SI	85 000 000	58.8
SI	43 750 000	11.3
SI	52 000 000	96.2
SI	72 500 000	69.0
SI	26 750 000	186.9
Average	**60 166 667**	**91**

Appendix E – RNA purity and integrity

Table E1 – Nanodrop absorption ratios. Values represent RNA purity of samples included in the final gene expression analysis. 260/280 and 260/230 refers to the ratios of absorption values at 260 nm, 230 nm, and 280 nm.

	Colon			Small intestine	
Sample	**260/280**	**260/230**	**Sample**	**260/280**	**260/230**
Lab 1	2.11	2.17	Lab 1	2.12	2.21
Lab 3	2.09	2.06	Lab 3	2.12	2.15
Lab 4	1.94	1.83	Lab 4	2.05	2.07
Lab 5	2.13	1.86	Lab 5	2.13	2.18
Lab 6	1.80	2.37	Lab 6	2.13	2.14
Lab 7	2.11	2.12	Lab 7	2.12	2.22
Lab 8	2.12	2.19	Lab 8	2.13	2.01
Lab 10	2.12	2.09	Lab 9	2.11	2.20
Lab 11	2.11	2.07	Lab 10	2.14	2.21
Lab 12	1.77	2.38	Lab 11	2.13	2.18
Fer 1	2.07	2.09	Lab 12	2.12	2.20
Fer 2	2.12	1.95	Fer 1	2.12	2.18
Fer 3	1.78	2.33	Fer 2	2.11	2.16
Fer 4	1.90	2.09	Fer 3	1.96	1.86
Fer 6	1.87	2.34	Fer 4	1.83	2.56
Fer 7	2.11	2.18	Fer 5	2.14	2.20
Fer 8	2.12	2.15	Fer 6	2.12	2.23
Fer 9	2.11	2.08	Fer 7	2.14	2.15
Co 1	2.13	2.12	Fer 8	2.12	2.22
Co 2	2.10	1.98	Fer 9	2.12	2.23
Co 3	1.74	2.39	Co 1	2.12	2.17

Co 4	2.12	2.15	Co 2	2.13	2.20
Co 5	2.12	2.16	Co 3	2.11	2.17
Co 6	2.12	2.13	Co 5	2.13	2.18
Co 7	2.11	1.92	Co 7	2.12	2.24
Co 8	2.13	2.18	Co 8	2.13	2.17
Co 9	2.12	2.10	Co 9	2.13	2.22
Co 10	2.11	2.19	Co 10	2.13	2.21
Co 11	2.12	2.18	Co 11	2.13	2.18
Co 12	2.10	2.01	Co 12	2.11	2.20
Fer-Co 1	2.10	2.12	Fer-Co 1	2.11	2.19
Fer-Co 2	2.11	2.14	Fer-Co 2	2.11	2.20
Fer-Co 3	2.10	2.02	Fer-Co 3	2.14	2.03
Fer-Co 4	2.12	1.91	Fer-Co 5	2.13	2.23
Fer-Co 5	2.11	2.08	Fer-Co 6	2.13	2.22
Fer-Co 6	2.10	2.03	Fer-Co 7	2.13	2.04
Fer-Co 7	1.88	2.35	Fer-Co 8	2.13	2.13
Fer-Co 8	2.10	2.09	Fer-Co 9	2.13	2.20
Fer-Co 9	2.12	2.17	Fer-Co 10	2.08	2.17
Fer-Co 10	2.11	2.14	Fer-Co 11	2.12	2.22
Fer-Co 11	2.11	2.22	Fer-Co 12	2.12	2.22
Fer-Co 12	2.12	2.22			

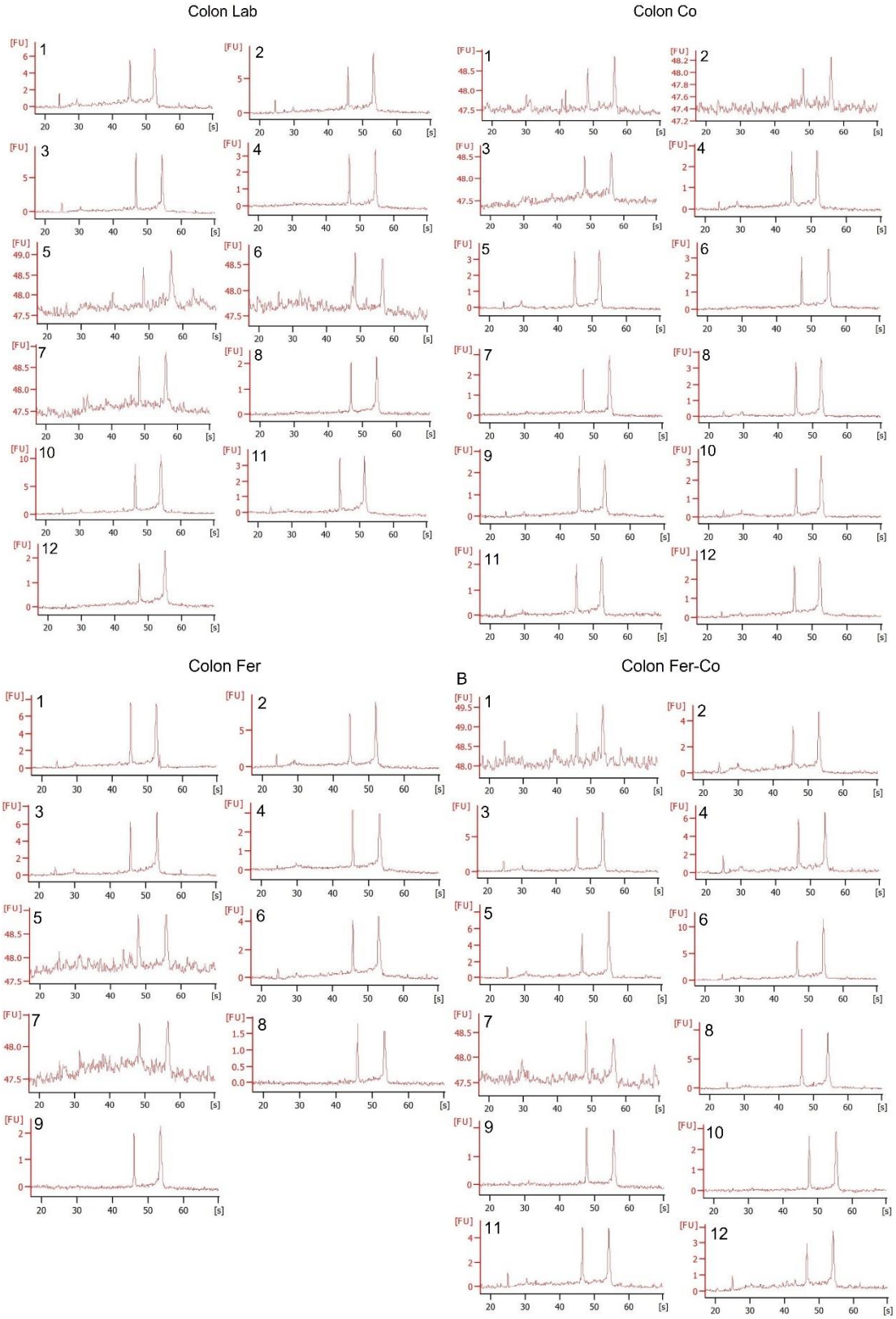

Figure E1 – Bioanalyzer electrographs of RNA samples from colonic IECs. Given are all four groups. Numbers represent sample number. FU=fluorescent units, s=seconds. The two peaks indicate the 18S (first) and 28S (second) ribosomal subunits used to assess RIN-value.

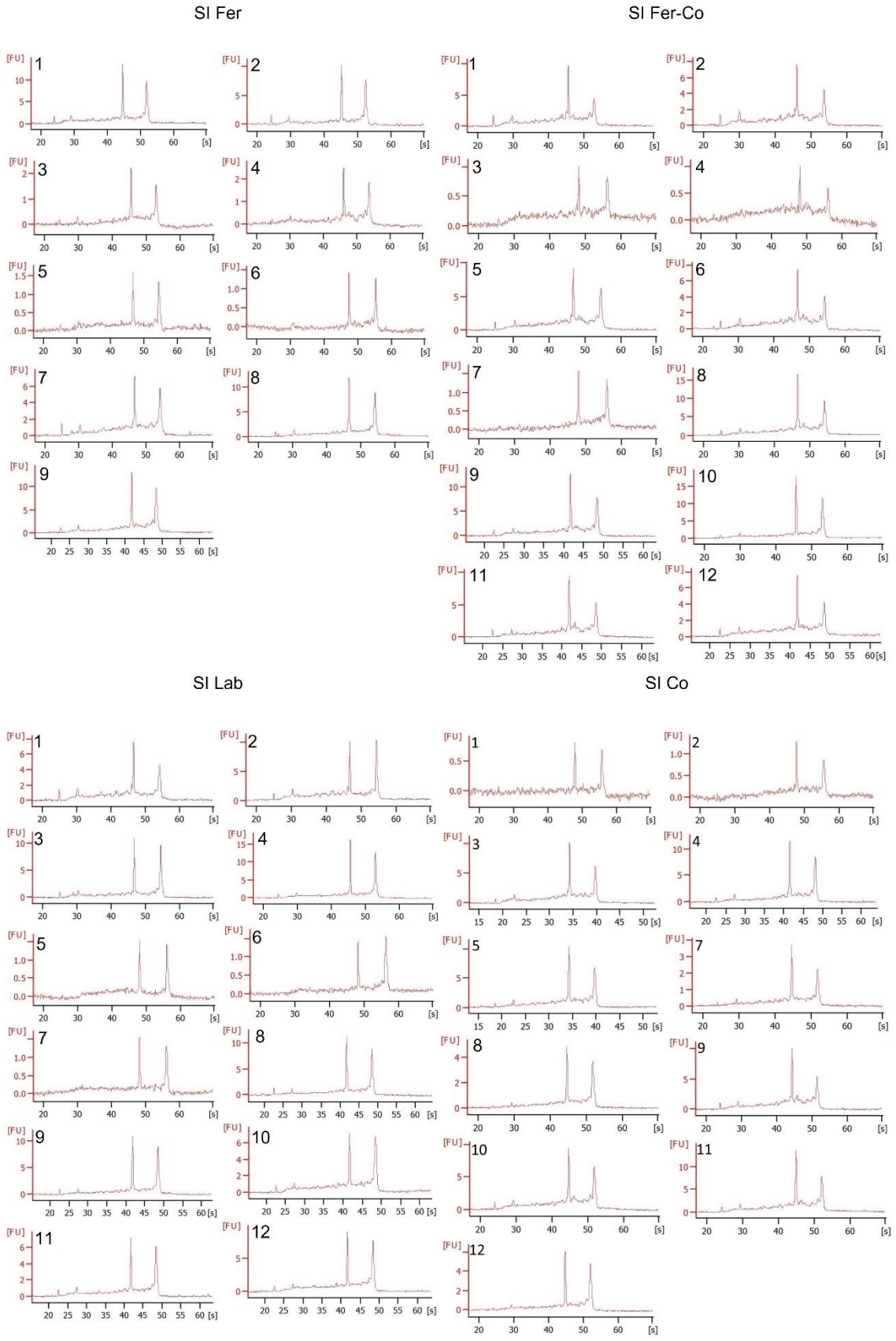

Figure E2 – Bioanalyzer electrographs of RNA samples from SI IECs. Given are all four groups. Numbers represent samples number. FU=fluorescent units, s=seconds. The two peaks indicate the 18S (first) and 28S (second) ribosomal subunits used to assess RIN-value.

Appendix F – Full list of target genes

Table F1 – Target gene function. List of genes and their general function in the intestines. Full name of protein they encode and the gene RefSeq number included.

Gene	RefSeq number	Protein encoded by gene	General function
Alpi	NM_001081082.2	Alkaline phosphatase, intestinal	Inflammation
Ang4	NM_177544.4	Angiogenin 4	Antimicrobial
Cdh1	NM_009864.3	E-cadherin/Cadherin 1	Barrier
Clca1	NM_017474.2	Calcium-activated chloride channel regulator 1	Barrier
Cldn1	NM_016674.4	Claudin	Barrier (tight junctions)
Cyp1A1	NM_009992.4	Cytochrome P4501 A1	AhR target
Defa24	NM_001024225.2	Defensin alpha 24	Antimicrobial
Defa3	NM_007850.2	Defensin alpha 3	Antimicrobial
Defb1	NM_007843.3	Defensin beta 1	Antimicrobial
Defb3	NM_013756.2	Defensin beta 3	Antimicrobial
Defb4	NM_019728.4	Defensin beta 4	Antimicrobial
Duox2	NM_001362755.1	Dual oxidase 2	ROS/RNS production
F11r	NM_172647.2	F11 receptor	Barrier (JAM)
Fcgbp	NM_001122603.1	Fc fragment of IgG binding protein	Barrier
Gapdh	NM_008084.3	Glyceraldehyde 3-phosphate dehydrogenase	Housekeeping
Gsdmc	NM_031378.3	Gasdermin C	Inflammation
Gsdmd	NM_026960.4	Gasdermin D	Inflammation
Hmox1	NM_010442.2	Heme oxygenase 1	ROS/RNS production
Il-10	NM_010548.2	Interleukin-10	Inflammation
Il-18	NM_001357221.1	Interleuki-18	Inflammation
Il-1b	NM_008361.4	Interleukin-1β	Inflammation
Il-25	NM_080729.3	Interleukin-25	Inflammation
Itln1	NM_010584.3	Intelectin 1	Antimicrobial
Lcn2	NM_008491.1	Lipocalin 2	Inflammation
Mir31	NR_029747.1	MicroRNA 31	Inflammation (proliferation)
Muc2	NM_023566.4	Mucin 2	Barrier
Muc3	NM_010843.2	Mucin 3	Barrier
Mylk	NM_139300.3	Myosin light chain kinase 3	Barrier (tight junctions)
Nlrp3	NM_145827.4	NLR Family Pyrin Domain-containing 3	Inflammation
Nlrp6	NM_133946.2	NLR Family Pyrin Domain Containing 6	Inflammation
Nod1	NM_172729.3	Nucleotide-binding oligomerization domain-containing protein 1	Immunosurveillance
Nod2	NM_145857.2	Nucleotide-binding oligomerization domain-containing protein 2	Immunosurveillance

Nos2	NM_010927.4	Inducible nitric oxide synthase (iNOS)	ROS/RNS production
Nox1	NM_172203.2	NADPH oxidase 1	ROS/RNS production
Nox4	NM_015760.5	NADPH oxidase 4	ROS/RNS production
Nqo1	NM_008706.5	NAD(P)H dehydrogenase, quinone 1	ROS/RNS production
Ocln	NM_001360536.1	Occludin	Barrier (tight junctions)
Reg3b	NM_011036.1	Regenerating islet-derived 3 beta	Antimicrobial
Reg3g	NM_011260.2	Regenerating islet-derived 3 gamma	Antimicrobial
Retnlb	NM_023881.4	Resistin like molecule beta	Antimicrobial
Saa1	NM_001357493.1	Serum amyloid A1	Inflammation
Tbp	NM_013684.3	TATA box binding protein	Housekeeping
Tgfb1	NM_011577.2	Tumor growth factor beta	Inflammation
Tjp1 (Zo1)	NM_001163574.1	Tight junction protein-1 (Zonula occludens-1)	Barrier (tight junctions)
Tlr2	NM_011905.3	Toll-like receptor 2	Immunosurveillance
Tlr4	NM_021297.3	Toll-like receptor 4	Immunosurveillance
Tlr5	NM_016928.4	Toll-like receptor 5	Immunosurveillance
Zbp1	NM_021394.2	Z-DNA-binding protein 1	Immunosurveillance

Table F2 – Primer sequences. Forward and reverse primer sequences used for gene expression analysis of target genes. Primers with no estimated E (Ê) were excluded from analysis. bp=base pairs, EEJ=exon-exon junction, R^2=coefficient of correlation, mp=melt peaks (number of), bt=below threshold.

Target	Primer	Sequence 5' → 3'	bp	EEJ?	Ê	R^2	mp
Alpi	Forward	TCGCCACTCAACTCATCTCC	80	Yes	2.02	0.998	1
	Reverse	AGTCCCCTTGGGAAACATGAA					
Ang4	Forward	CTCCAGGAGCACACAGCTA	116	Yes	2.05	0.999	1
	Reverse	CAGCACGAAGACCAACAACA					
Cdh1	Forward	ATTGCAAGTTCCTGCCATCC	76	Yes	2.03	0.997	1
	Reverse	CAGTAGGAGCAGCAGGATCA					
Clca1	Forward	ACAACCACTAAGGTGGCCTA	80	Yes	2.01	0.999	1
	Reverse	GAGCTCGCTTGAATGCTGTA					
Defa24	Forward	CAGAAGGCGCTTCTCTTCAA	71	Yes	2.09	0.998	1
	Reverse	TTTGCAGCCTCTTGCTCTAC					
Duox2	Forward	GGCAGCCAGATGCTCTGTAA	80	Yes	2.01	0.998	1
	Reverse	ATGTCAGCCAGCCACTCAAA					
F11r	Forward	TGGAGTGGAAGTTCGTCCAA	87	Yes	2.01	0.998	1
	Reverse	AGGTGACTCGGTCCGCATA					
Fcgbp	Forward	ATCGAGCAATGTGGCTGCTA	83	Yes	2.06	0.998	1
	Reverse	CAATGCTGCTGGCAGTTTTCA					
Gapdh	Forward	CAAGGTCATCCCAGAGCTGAA	82	No	2.01	0.999	1
	Reverse	CAGATCCACGACGGACACA					
Gsdmc	Forward	AGGTTCAGAGTAAGAGCATCCC	78	Yes	2.04	0.998	1
	Reverse	ATGTGGGCAACTGATCCAAC					

Gsdmd	Forward	GAGCCCAGTGCTCCAGAA	73	Yes	2.01	0.998	1
	Reverse	TGTTCCCATCGACGACATCA					
Hmox1	Forward	TCAAGCACAGGGTGACAGAA	76	Yes	1.98	0.998	1
	Reverse	ATCACCTGCAGCTCCTCAAA					
Il10	Forward	AAAGGACCAGCTGGACAACA	79	Yes	2.00	0.999	1
	Reverse	TAAGGCTTGGCAACCCAAGTA					
Il18	Forward	CAAAGAAAGCCGCCTCAAAC	82	Yes	2.04	0.999	1
	Reverse	GACGCAAGAGTCTTCTGACA					
Il1b	Forward	TGGCAACTGTTCCTGAACTCA	83	Yes	2.00	0.999	1
	Reverse	GGGTCCGTCAACTTCAAAGAAC					
Il25	Forward	CTCTCTCAGAAGGCCTGTCA	97	Yes	1.98	0.999	1
	Reverse	CCCACGATCATTGCCAAGAA					
Itln1	Forward	TCTTTTCCTCTCTGCCCAGAA	82	Yes	2.10	0.997	1
	Reverse	GTGCGCAGGAAATAGAGACC					
Lcn2	Forward	GCTACAATGTCACCTCCATCC	84	Yes	1.97	0.999	1
	Reverse	CCCTGGAGCTTGGAACAAA					
Mir31	Forward	AACTGGAGAGGAGGCAAGAT	83	No	2.03	0.998	1
	Reverse	GTCAGACAGGAAAGATGGCAAT					
Muc2	Forward	CAGCACACCAACCAAAACCA	81	Yes	2.04	0.997	1
	Reverse	CACAGCCACCAGGTCTCATTA					
Muc3	Forward	CCGGAGTATGAAGGGGTTATCA	82	Yes	2.09	0.996	1
	Reverse	ACTTGGCCTTCAGGATGACA					
Mylk	Forward	TTCAACAGGGTCACCAACCA	78	Yes	2.05	0.998	1
	Reverse	TCCAGGAAAGCTTGGGAGAC					
Nlrp6	Forward	CACCTCGGTGCTTCTCTCC	78	Yes	2.05	0.998	1
	Reverse	TTCACCTTAGCATGCTGTCGTA					
Nod1	Forward	GTGGCTTTGGCTGTGAAGAA	80	Yes	1.99	0.999	1
	Reverse	TTTGCCCCTTCGTCTCCAA					
Nod2	Forward	AAGCCCTGGCTGAAGTTGTA	77	Yes	2.01	0.997	1
	Reverse	CATGCTGCCAATGTTGTTTCC					
Nos2	Forward	GAGGAGCAGGTGGAAGACTA	81	Yes	1.96	0.999	1
	Reverse	GGAAAAGACTGCACCGAAGATA					
Nox1	Forward	GTGCCGACAACAAGCTCAAA	70	Yes	1.94	0.999	1
	Reverse	GCAAAGGCACCTGTCTCTCTA					
Nqo1	Forward	AAGCTGCAGACCTGGTGATA	88	Yes	1.98	0.999	1
	Reverse	ACGAGCACTCTCTCAAACCA					
Ocln	Forward	GAATGGCAAGCGATCATACCC	74	Yes	1.97	0.998	1
	Reverse	GAATCTCCTGGGCCACTTCA					
Reg3b	Forward	CTTTCTGTGGCAGCTTGTCA	76	Yes	1.99	0.998	1
	Reverse	TAGGGCAACTTCACCTCACA					
Reg3g	Forward	GTATGGATTGGGCTCCATGAC	76	Yes	1.98	0.999	1
	Reverse	CATCAGCATTGCTCCACTCC					
Retnlb	Forward	CCTAAGACGATCTCCTGCACTA	84	Yes	2.02	0.998	1
	Reverse	AGCACATCCAGTGACAACCA					
Saa1	Forward	ATCTCTCATGTGTGTATCCCACAA	79	No	2.02	0.998	1
	Reverse	TACCCTCTCCTCCTCAAGCA					
Tbp	Forward	ACCAGAACAACAGCCTTCCA	80	Yes	1.92	0.999	1
	Reverse	AAAGATGGGAATTCCAGGAGTCA					

Tgfb1	Forward	GCTGCGCTTGCAGAGATTAA	82	Yes	1.91	0.998	1
	Reverse	GTAACGCCAGGAATTGTTGCTA					
Tjp1	Forward	TCTGGCATCATTCGCCTTCA	86	Yes	2.01	0.999	1
	Reverse	TCAACCGCATTTGGCGTTAC					
Tlr2	Forward	TGCATCACCGGTCAGAAAAC	80	Yes	1.96	0.999	1
	Reverse	AGCCAAAGAGCTCGTAGCA					
Tlr4	Forward	GTTCTTCTCCTGCCTGACAC	91	Yes	2.01	0.998	1
	Reverse	GCTGAGTTTCTGATCCATGCA					
Tlr5	Forward	ATGGATGGATGCTGAGTTCCC	93	Yes	1.91	0.998	1
	Reverse	CTGGCCATGAAGATCACACCTA					
Zbp1	Forward	TGGCAGAAGCTCCTGTTGAC	102	Yes	1.98	0.998	1
	Reverse	CCAGCTGGCCAATCTTCACA					
		(Not included in gene expression analysis)					
Cldn1	Forward	GCCACAGCATGGTATGGAAAC	89	Yes	-	-	1 bt
	Reverse	AGGGCCTGGCCAAATTCA					
Cyp1a1	Forward	TCATCCTTCGTCCCCTTCAC	83	Yes	-	-	1 bt
	Reverse	CAGCACCCCTTGGGGATATA					
*Defa3**	Forward	CCCAGAAGGCTCTTCTCTTCA	106	Yes	2.05	0.999	1
	Reverse	CTTTCTGCAGGTCCCATTCA					
Defb1	Forward	TGGCTGCCACCACTATGAAAA	100	Yes	-	-	1 bt
	Reverse	CCAAGACTTGTGAGAATGCCAAC					
*Defb3**	Forward	GAATCGGTGCATTGGCAACA	65	No	1.96	0.999	1 bt
	Reverse	TGCAGCATTTGAGGAAAGGAAC					
Defb4	Forward	CTGGTGCTGCTGTCTCCA	78	Yes	-	-	1 bt
	Reverse	TATGGCTCCATTGGTCATGCA					
Nlrp3	Forward	TGCTCTGCAACCTCCAGAAA	77	Yes	-	-	1 bt
	Reverse	AACCAATGCGAGATCCTGACA					
Nox4	Forward	CGTCCTCGGTGGAAACTTTTA	79	Yes	-	-	None
	Reverse	GTCCACAGCAGAAAACTCCA					

*Excluded because mp>1 in Fluidigm qPCR reaction melt curve analysis.

Appendix G – R-script

Appendix G1 - PCA of colonic fold change values

```
##prepare file
library(readxl)
library(tidyverse)
library(ggrepel)

file <- read_xlsx(path)

vector <- sapply(file[-c(1:2)], sd)
sort(vector)

##PCA
pca <- prcomp(file[-c(1:2)], scale=TRUE, center = TRUE)
sort(pca$rotation[,2])
plot(pca)
pca$sdev
summary(pca)

##plot
PCplot <- file %>%
  mutate(PC1 = pca$x[,1],
         PC2 = pca$x[,2],
         PC3 = pca$x[,3],
         PC4 = pca$x[,4],
         PC5 = pca$x[,5],
         PC6 = pca$x[,6],
         PC7 = pca$x[,7],
         PC8 = pca$x[,8],
         PC9 = pca$x[,9],)

scatterplot <- PCplot %>%
  ggplot(mapping = aes(x=PC1, y=PC2)) +
  geom_point(mapping=aes(color=Group), size=4)
  geom_text_repel(aes(label = file$IFC)) ##alternative: for adding run number

windowsFonts(Calibri=windowsFont("Calibri"))

scatterplot+scale_color_manual(values=c("#7D5300", "#00AC38",
"khaki3","lightblue"))+theme_bw()+theme(text=element_text(family="Calibri"))
```

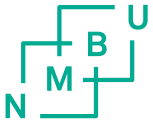

Norges miljø- og biovitenskapelige universitet
Noregs miljø- og biovitskapelege universitet
Norwegian University of Life Sciences

Postboks 5003
NO-1432 Ås
Norway